

INFORMATION TO USERS

This manuscript has been reproduced from the microfilm master. UMI films the text directly from the original or copy submitted. Thus, some thesis and dissertation copies are in typewriter face, while others may be from any type of computer printer.

The quality of this reproduction is dependent upon the quality of the copy submitted. Broken or indistinct print, colored or poor quality illustrations and photographs, print bleedthrough, substandard margins, and improper alignment can adversely affect reproduction.

In the unlikely event that the author did not send UMI a complete manuscript and there are missing pages, these will be noted. Also, if unauthorized copyright material had to be removed, a note will indicate the deletion.

Oversize materials (e.g., maps, drawings, charts) are reproduced by sectioning the original, beginning at the upper left-hand corner and continuing from left to right in equal sections with small overlaps. Each original is also photographed in one exposure and is included in reduced form at the back of the book.

Photographs included in the original manuscript have been reproduced xerographically in this copy. Higher quality 6" x 9" black and white photographic prints are available for any photographs or illustrations appearing in this copy for an additional charge. Contact UMI directly to order.

UMI

**A Bell & Howell Information Company
300 North Zeeb Road, Ann Arbor MI 48106-1346 USA
313/761-4700 800/521-0600**

Configuration Mixing of Quark States in Nucleons and Other Baryons in the MIT Bag Model

by

William Donald Hazelton

A dissertation submitted in partial fulfillment
of the requirements for the degree of

Doctor of Philosophy

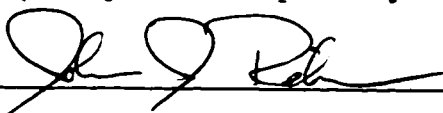
University of Washington

1997

Approved by



(Chairperson of Supervisory Committee)



Program Authorized

to Offer Degree

Physics

Date

July 30, 1997

UMI Number: 9806980

UMI Microform 9806980
Copyright 1997, by UMI Company. All rights reserved.

**This microform edition is protected against unauthorized
copying under Title 17, United States Code.**

UMI
300 North Zeeb Road
Ann Arbor, MI 48103

In presenting this dissertation in partial fulfillment of the requirements for the Doctoral degree at the University of Washington, I agree that the Library shall make its copies freely available for inspection. I further agree that extensive copying of this dissertation is allowable only for scholarly purposes, consistent with "fair use" as prescribed in the U.S. Copyright Law. Requests for copying or reproduction of this dissertation may be referred to University Microfilms, 1490 Eisenhower Place, P.O. Box 975, Ann Arbor, MI 48106, to whom the author has granted "the right to reproduce and sell (a) copies of the manuscript in microform and/or (b) printed copies of the manuscript made from microform."

Signature William O. Hutton

Date 7-30-91

University of Washington

Abstract

Configuration Mixing of Quark States in Nucleons and Other Baryons in the MIT Bag Model

by William Donald Hazelton

Chairperson of Supervisory Committee: *Professor Lawrence Wilets*
Department of Physics

The MIT bag model incorporates two of the main features of Quantum Chromodynamics (QCD), confinement of quarks in color singlet states, and asymptotic freedom. Most prior studies using this model have been perturbative, and have considered limited subsets of possible excitations, such as pair creation from the three quark ground state. However, there are many three quark excitations lower in energy than the five particle states. We calculate the ground state configuration of baryons, including all quark states up to a consistent energy cutoff, using the one gluon exchange (OGE) interaction. We study the p , n , Σ^+ , Σ^- , Ξ^- , and Ξ^0 in a spherical bag with a Fock space truncated at a succession of cutoffs, with the maximum cutoff at 1.5 GeV above the three quark ground state. This allows many qqq (three quark) and $qqqq\bar{q}$ (four quark plus anti-quark) states in the basis. As we raise the cutoff, the strength of the strong coupling constant necessary to fit the $\Delta - N$ splitting decreases from a value of $\alpha_s = 2.2$ with three valence quarks to a value of about $\alpha_s = 1.4$ at the 1.5 GeV cutoff. We require a positive Casimir energy for stability, in agreement with theoretical studies. This is opposite to the sign assumed for the original MIT bag model.

Part of the motivation for this study stems from experiments at the Electron Muon Collaboration (EMC), Stanford Linear Accelerator (SLAC), and the Spin Muon Collaboration (SMC) that indicate the nucleon spin attributable to the spin of quarks is small. We find that configuration mixing may provide a partial explanation. Configuration mixing leads to substantial probabilities for states with two $p_{3/2}$ quark

excitations, as well as for various other basis states. This allows much of the nucleon spin to be carried by quark orbital angular momentum. We calculate the spin fractions carried by u , d , and s quarks. We find reasonable agreement with the experimental measurements of the nucleon spin structure functions and the Bjorken sum rule. For the MIT bag with configuration mixing, we find $\Gamma_1^p \approx 0.141 - 0.148$ and $\Gamma_1^p - \Gamma_1^n \approx 0.141 - 0.147$.

TABLE OF CONTENTS

List of Figures	iv
Chapter 1: Introduction	1
1.0.1 Overview of this study	2
1.1 Historical overview	5
1.1.1 Origins of QCD	5
1.1.2 Confinement	8
1.1.3 Confined QCD models of hadrons	9
Chapter 2: Quarks, Gluons, and the MIT Bag Model	19
2.1 Introduction	19
2.1.1 QCD Lagrangian for quarks and gluons	19
2.1.2 SU(3)	20
2.1.3 Symmetries and conserved currents	21
2.2 Static spherical MIT bag model	22
2.2.1 Dirac equation—spherical solutions for quarks	23
2.2.2 Anti-quarks	27
2.2.3 Quark and antiquark currents	29
2.3 Confined gluons in Coulomb gauge	29
2.3.1 Longitudinal gluon modes	29
2.3.2 Transverse gluon modes	30
2.3.3 Color and spin sums	32
Chapter 3: Multi-quark states	34
3.1 Introduction	34
3.1.1 States below cutoff	37
3.1.2 Symmetries	38

Chapter 4:	Nucleon Configuration Mixing and Ground State Energies	42
4.1	Assembly of the OGE interaction matrix	42
4.2	Model assumptions	46
4.2.1	Quark masses, bag constant, and self-energy prescriptions . . .	47
4.2.2	Adjustment of α_s to maintain $\Delta - N$ splitting	48
4.2.3	Confinement in the spherical bag and the MIT Casimir term .	50
4.3	Configuration mixing	54
4.3.1	Why is less than half of the nucleon probability accounted for by three $s_{1/2}$ quarks?	55
4.3.2	Why are excitations higher than $J = 1/2$ allowed in a spherical MIT bag?	56
4.3.3	Why are three quark states much more probable than states with an extra quark pair?	56
4.3.4	What enhances probabilities for states with two identical excitations?	57
4.3.5	Why do $p_{3/2}$ excitations dominate over $p_{1/2}$ excitations?	57
4.3.6	Why are u pairs more probable than d , and d more probable than s pairs in our proton ground state?	58
4.3.7	Why are quark-antiquark sea probabilities much smaller than those calculated previously by perturbative methods?	61
4.3.8	Why are some energy levels unused?	62
4.3.9	What about interactions of higher multipole?	62
4.3.10	What states would enter if we continued to raise our cutoff? .	62
4.3.11	Summary	63
Chapter 5:	Fits to the octet baryon masses	71
5.1	Mass splitting of the neutron and proton	71
5.2	Mass splitting of the N and Δ	75
5.3	Octet mass splittings as functions of m_s and B and the self-energy . .	76
5.4	Best fits to the baryon mass spectrum	78

Chapter 6: Nucleon observables	85
6.1 Charge radii of the baryons	86
6.2 Magnetic moments	88
6.3 Axial currents and the baryon spin fraction carried by quarks	90
Chapter 7: Conclusion	98
Bibliography	100
Appendix A: Non-color quark and anti-quark configurations contributing to proton	110
Appendix B: Ground state configuration mixing for the Delta	114
Appendix C: Examples of matrix element calculations	117
Appendix D: Perturbative dipole overlap between valence proton state and five particle states involving one $p_{1/2}$ excitation showing interference effects.	120
Appendix E: Configuration mixing for different parameter sets and several self-energy prescriptions	122

LIST OF FIGURES

4.1	Color sums for quark-quark and quark-antiquark OGE interactions .	44
4.2	$\Delta - N$ splitting vs. energy cutoff with $\alpha_s = 2.2$ (grey) and $\alpha_s = 1.3636$ (black).	64
4.3	Neutron configuration mixing energy vs. cutoff with two forms for the self-energy.	65
4.4	Composition of neutron ground state for $\alpha_s = 1.3636$ (Part 1 of 2). The basis states are combined into categories, with probabilities for each category shown in the upper part of the figure.	66
4.5	Composition of neutron ground state for $\alpha_s = 1.3636$ (Part 2 of 2). The basis states are combined into categories, with probabilities for each category shown in the upper part of the figure.	67
4.6	Perturbative neutron ground state for $\alpha_s = 1.3636$ (Part 1 of 2). The basis states are combined into categories, with perturbative probabilities for each category shown in the upper part of the figure.	68
4.7	Perturbative neutron ground state for $\alpha_s = 1.3636$ (Part 2 of 2). The basis states are combined into categories, with perturbative probabilities for each category shown in the upper part of the figure.	69
4.8	Density of color singlet basis states vs basis state energy. As the cutoff is raised, more basis states can mix into the configuration. The density of states is plotted using an arbitrary Gaussian weighting of width 100 MeV to smooth rapid variations.	70
B.1	Composition of Δ^+ ground state for $\alpha_s = 1.3636$ (Part 1 of 2). The basis states are combined into categories, with probabilities for each category shown in the upper part of the figure.	115

B.2	Composition of Δ^+ ground state for $\alpha_s = 1.3636$ (Part 2 of 2). The basis states are combined into categories, with probabilities for each category shown in the upper part of the figure.	116
-----	--	-----

ACKNOWLEDGMENTS

I want to express my sincere appreciation to my advisor, Lawrence Wilets. His keen insight and gentle guidance has been an inspiration to me, and has helped me to broaden my understanding of physics. I also want to express my sincere thanks to Ernest Henley, Mary Alberg and John Rehr for stimulating discussions, for reading this thesis, and for their many helpful suggestions.

DEDICATION

I dedicate this thesis to my family. I worked for a number of years in the family machine shop business with my parents, Lloyd and Carolyn Hazelton. We share many interesting memories from those days. My sister, Anne Anholm, received Masters of Nursing, Nurse Practitioners, and M.D. degrees from the University of Washington. I appreciate the hard work and exceptional care she devotes to all she does. Lowell Hazelton, my older brother, and I took a number of undergraduate physics courses together. He received a Ph.D. in Physics from Caltech, and has been a continual inspiration to me. On many occasions we have discussed physics and other topics long into the night. My younger brother, Douglas Hazelton, studied engineering and has been involved in several business ventures. I appreciate the independent attitude with which he approaches life.

Chapter 1

INTRODUCTION

The textbook picture of a nucleon¹ portrays a simple combination of three ground state ($s_{1/2}$) quarks. One d - (down) and two u - (up) flavor quarks make a proton, or one u - and two d -flavor quarks make a neutron. The quarks carry spin and color and combine to make an antisymmetric wave function that is invariant under any rotation of color variables—the wave function must be a color singlet. Quantum Chromodynamics, (QCD), the theory behind the strong interaction, describes gluons as the carriers of force between quarks. The strong interaction prevents separation of any single quark from a color singlet state. This leads to well defined nucleon ground states². However, there are an infinite number of other configurations made of quarks, antiquarks, and gluons that can form color singlet states with the same quantum numbers as the nucleon. These states should mix to some extent with the three $s_{1/2}$ quark state to form the nucleon ground state. Contributions from excited quark states generally decrease as their energy increases, but the density of states tends to increase with energy. This leaves open the question of how many basis configurations should be included to get a reasonable approximation to the nucleon ground state, or whether this is possible.

One way to address this question is to use a quark model to construct all confined

¹ Protons and neutrons are called nucleons. They are building blocks of nuclei at the center of atoms. The nucleons are examples of baryons—half integral spin particles (Fermions) that interact primarily by the strong interaction. (They also interact through the electromagnetic and weak interactions, and by gravity.) Baryons are made primarily of three quarks. The other particles that interact strongly are mesons (like the pion or kaon). Mesons are integral spin particles (Bosons) and each is made primarily of a quark and an antiquark. Together the mesons and baryons are classified as hadrons.

² The neutron does decay by the weak interaction to the proton with a lifetime of $\tau = 882 \pm 2$ seconds. The possible supersymmetric decay of the proton has not been observed: $\tau > 1.6 \times 10^{25}$ years.[1]

quark configurations below some energy cutoff (a truncated Fock space). Use of a model is necessary to enforce confinement, since confinement based on QCD presumably involves a multiplicity of graphs involving gluon loops. Direct calculation of confinement by this type of expansion has not been demonstrated, and is probably not currently feasible. When using artificial means to confine quarks to a region (a bag), care must be taken to avoid duplication of effort when adding gluons. If two or more gluons are introduced within the bag at one time, they can combine as a color singlet. But the bag confinement mechanism also carries no color, so it is difficult to separate these overlapping contributions. Perhaps the simplest way to avoid this type of double counting is to restrict interactions to the one-gluon exchange (OGE) approximation and to build basis states from quarks and antiquarks only. Once a model is chosen, one constructs all orthonormal color-singlet states below some energy cutoff. The interaction Hamiltonian acting between these states is diagonalized to study configuration mixing. This is repeated for different cutoffs to study convergence of the ground state wave function.

1.0.1 Overview of this study

In this study, we use the static spherical MIT bag model, with (current) quarks and antiquarks coupled by the OGE interaction. The spherical MIT bag utilizes solutions to the Dirac equation for a spherical cavity with hard boundary conditions. Interactions are calculated by doing a sum over gluon modes in the cavity. We work in Coulomb gauge, so there are transverse electric and magnetic (TE and TM) and Coulomb-type contributions. We diagonalize the interaction for successive cutoffs up to 1.5 GeV above the qqq (three quark) ground state (2.725 GeV above the energy zero).

There are many excited qqq configurations, and $qqqq\bar{q}$ configurations reached through pair creation, that contribute below our highest cutoff. The qqq sector includes combinations of quark excitations ranging up to $f_{7/2}$, as well as some radial excitations up to $n = 3$. There are 2727 normal ordered qqq configurations which combine to make 467 orthonormal color-singlet states. The $qqqq\bar{q}$ configurations below this cutoff include up, down, and strange pairs where a single quark or antiquark is excited to a $p_{1/2}$ or $p_{3/2}$ level to conserve parity. In this sector, 3828 normal ordered configurations form 392 color-singlet states. Taken together, 6555 normal ordered

configurations form a basis of 859 color-singlet states (below the maximum cutoff) with the same quantum numbers as the nucleon.

The OGE graphs are effectively four-point interactions involving two quark-gluon vertices. At each vertex, the gluon may interact with a quark or antiquark, or it may create or annihilate a quark pair. Our maximum cutoff allows at most one quark pair in addition to the three initial quarks. Thus we have forward and backward diagrams of four types. These types are: a) gluon exchange between quarks and/or antiquarks, b) quark-gluon interaction followed by pair creation, c) quark-gluon interaction followed by pair annihilation, and d) pair annihilation to a gluon followed by pair creation.

In the OGE approximation, the QCD equations are linear in the gluon field strength. Thus, other than carrying color indices, the equations are identical with Maxwell's equations. It is possible to solve for magnetic and electric fields from the quark wave functions, and to use these to calculate interaction energies[5]. Working in Coulomb gauge, we achieve the same results by calculating Coulomb (zero frequency) terms and adding to them a mode sum[2, 71, 4] over TE and TM cavity modes. In calculating the transverse OGE contributions, we consistently sum over the lowest five gluon modes. A product of two quark-gluon vertex integrals is divided by an energy denominator for each transverse gluon mode, and for each time ordering. This mode sum converges rapidly, generally to better than one part in ten thousand. We calculate $L = 1 - 4$ (dipole through hexadecapole) TM and TE couplings between states within our basis. The Coulomb terms couple for $L = 0 - 4$, with monopole interactions making the most significant contribution. The Coulomb terms require a six dimensional $(r_<, r_>)$ integral over combinations of four quark wave functions along with the Coulomb propagator. We include all couplings that link states within our basis. But we also do several diagonalizations, including successive multipoles, to further examine convergence.

Our approach to studying the nucleon ground state is model-dependent. Thus we are unable to draw definitive conclusions about the true ground state of the nucleon. Some of the model limitations include the rigid boundary conditions of the MIT bag, the use of a spherical bag rather than one with a dynamical surface, use of the (Coulomb gauge) OGE approximation, a Fock space truncated 1.5 GeV above the qqq ground state, restriction of basis states to those built from quarks and antiquarks

(but not gluons, interacting mesons, instantons, or ghosts), use of a shell model approach which introduces spurious states (we do not do momentum projection), and uncertainties in the choice of parameters and self-energy to use with the MIT bag model. A further limitation will become apparent in our inability to carry the energy cutoff as high as necessary to demonstrate fully convergent results.

We attempt to determine the sensitivity of our calculations to variation in parameters and to some model assumptions. We use two different choices for bag radii so that ground state energies for other radii may be approximated by a linear fit. We calculate results for $m_u = 0$ MeV and $m_d = 5$ MeV. We also examine the effect of including different amounts of the self-energy. The two approximations we try are: 1) the ‘minimal’ MIT bag prescription including only longitudinal electric (Coulomb) self-energy terms where the quark remains in the same space-spin-color state, 2) and a self-energy built from all Coulomb, magnetic, and electric graphs contributing to OGE interactions below our cutoff.

Much of our motivation in conducting this study was to calculate the contribution of the strange sea to the nucleon spin and to other observables. But that is only one small subset of excitations, and should not be considered in isolation. For this reason, we chose to diagonalize the interaction over all possible quark states (within the context of our model) below each cutoff. Our results indicate minimal contribution from strange quarks to ground state properties for this model. However, we are in reasonable agreement with experimental results for the proton and neutron integrated structure functions, Γ_1^p and Γ_1^n , and with the Bjorken sum rule. As discussed in Ch. 6, we make two least squares fits to bag parameters and find values for the MIT bag with configuration mixing of $\Gamma_1^p - \Gamma_1^n = 0.141$ or 0.147 .

There are several observations that may be drawn from this study. There is significant configuration mixing. This means that conclusions drawn from perturbation theory are suspect. Previous perturbative fits to the mass spectra for baryons and mesons required an uncomfortably large value for the strength of the strong coupling constant $\alpha_s = g_s^2/4\pi$. The value $\alpha_s = 2.2$ was needed to reproduce the proper $\Delta - N$ splitting. Our results for diagonalizing over the full model space indicate a value of about $\alpha_s = 1.4$ is needed to achieve the proper splitting. In addition we find a depression of the nucleon ground state energy of about -580 MeV with the minimal MIT self-energy, and about -437 MeV with the self-energy built from all vertices used

below cutoff. This is more negative than the Casimir contribution[54] $E_C = -Z_0/R$ introduced in earlier fits to the mass spectra. There is reason to question the inclusion of a Casimir term with negative sign on more fundamental grounds. The contribution was based on Casimir's calculation[7] of vacuum fluctuations for a parallel plate capacitor. A number of calculations[111, 115, 116, 117, 118] have shown the Casimir term for spherical and rectangular cavities is positive rather than negative. The contribution from quarks is small and negative, while the gluons make a much larger positive contribution. Thus the sign utilized in the MIT bag model appears to be incorrect[8]. Another problem with the Casimir term is that it makes the vacuum unstable to decay. The traditional MIT Casimir energy for an empty bag is negative and unbounded from below as the bag radius decreases. Thus an alternative mechanism for lowering the nucleon ground state energy (necessary to achieve a proper fit to the mass spectra) is welcome.

1.1 Historical overview

1.1.1 *Origins of QCD*

Electron beam experiments at SLAC[9] in the 1960's showed excess hard scattering events from protons as one would expect for discrete scattering centers within the proton. The scattering distribution as a function of angle and energy was scale invariant, indicating the scattering centers were point-like[13, 14] (at least to the resolution of the experiment). This was reminiscent of the 1897 discovery of the electron by J. J. Thomson[10], and of the nucleus by Rutherford[11] in 1911. However, smaller constituents were not seen from proton scattering even when bombarded at high energies. The final states consisted of combinations of photons, leptons (members of the electron family), and more hadrons. There seemed to be an endless supply of new hadrons waiting to be discovered. One view of the situation was that perhaps there were no elementary particles—each particle might be a composite of every other particle[12]. An alternative interpretation was offered by Bjorken[15] and Richard Feynman[16]. They described hadrons as being built from unknown constituents called partons. Electrodynamics processes were well understood to high energies, so interactions between electrons and hadrons could be described in terms of virtual photon interactions with partons. The early parton models assumed the par-

ton transverse momentum was bounded. The probability to observe high transverse momentum fell exponentially with momentum.

In the 1960's, Murray Gell-Mann[17, 18] and George Zweig[19] argued for the existence of a few fundamental particles related by simple forces. The hadrons could be arranged into families, called multiplets. They interpreted this as an approximate realization of an $SU(3)_{\text{FLAVOR}}$ [21, 22] symmetry³ and proposed new particles, called quarks by Gell Mann (and aces by Zweig), with flavors u , d , and s (up, down and strange). Combining flavor and spin, essentially all the mesons and baryons could be arranged into a few $SU(6)$ multiplets[23, 24]. The u and d quarks have almost no current⁴ mass. The s quark is moderately heavy (see Table 1.1).

Table 1.1: Light quark quantum numbers and current masses.

flavor	charge	$I(J^P)$	I_z	strangeness	current mass[1]
u	$\frac{2}{3} e$	$\frac{1}{2}(\frac{1}{2}^+)$	$+\frac{1}{2}$	0	2 to 8 MeV
d	$-\frac{1}{3} e$	$\frac{1}{2}(\frac{1}{2}^+)$	$-\frac{1}{2}$	0	5 to 15 MeV
s	$-\frac{1}{3} e$	$0(\frac{1}{2}^+)$	0	-1	100 to 300 MeV
\bar{u}	$-\frac{2}{3} e$	$\frac{1}{2}(\frac{1}{2}^-)$	$-\frac{1}{2}$	0	2 to 8 MeV
\bar{d}	$\frac{1}{3} e$	$\frac{1}{2}(\frac{1}{2}^-)$	$\frac{1}{2}$	0	5 to 15 MeV
\bar{s}	$\frac{1}{3} e$	$0(\frac{1}{2}^-)$	0	+1	100 to 300 MeV

During this same time period, there was rapid progress in the study of non-Abelian field theories. Together these developments led to the birth of Quantum Chromodynamics, or QCD[17, 18, 19]. It was modeled after Quantum Electrodynamics (QED)[25, 26], the eminently successful quantum field theory of electrodynamics. But QCD had a long incubation. Non-Abelian theories were first introduced by Yang and Mills in 1954[27]. There were problems in understanding quantization, renormal-

³ Three much heavier flavors of quarks were later discovered: c , t , and b (charm, top and bottom)[1]. The c , t , and b quarks are not as well described within a flavor symmetry because of the large differences in their masses.

⁴ Quark current masses are the masses of the renormalized QCD Lagrangian. They are not directly measurable (and are somewhat model dependent) since quarks are confined within hadrons. We utilize current masses defined in the context of the relativistic MIT bag model in this study. Constituent masses are effective masses determined from non-relativistic model fits to particle spectra. They are model dependent quantities, and have no direct relation to the masses in the Lagrangian[20].

ization, and in finding approximate solutions to the field equations. QCD is a theory of elementary particles (quarks and gluons), and it provided a natural explanation for the scattering centers seen in the nucleon. This led to reinterpretation and modification of the parton model[28]. QCD predicted the parton transverse momentum would not fall exponentially, but as a power law. This introduced important logarithmic corrections to the parton model. This was tested experimentally, demonstrating that QCD was predicting correct results. Many of the scaling relations developed in the study of partons remain useful, with quarks and gluons accepted as the partons.

QCD is a Yang-Mills type of gauge theory invariant under $SU(3)_{\text{COLOR}}$ [29, 30] group transformations. (It was patterned after QED, which is invariant under a change of phase—a $U(1)$ symmetry.) The $SU(3)_{\text{COLOR}}$ group describes an exact symmetry under interchange among three values of a new quantum number, called color by Gell-Mann. The existence of a symmetry in the Lagrangian[31] leads to conservation of color charges carried by the spin-1/2 quarks. The three quark colors don't mix with the three anti-colors carried by antiquarks. These symmetries are classified respectively as $SU(3)$ triplet, or $\mathbf{3}$, and anti-triplet, or $\bar{\mathbf{3}}$, because of their dimensions. The quarks are Fermions like the electrons of QED. As with photons in electrodynamics, gauge invariance requires vector particles to couple to the Fermions. The gluons in QCD are the analog of the vector photons of QED. Unlike photons, (which carry no electric charge), the $SU(3)$ coupling requires gluons to carry color charge. A gluon interacting with a quark can change the quark color. Three colors can be created, and three destroyed, but the interaction is traceless. The gluon charge is classified in an $SU(3)$ octet, or $\mathbf{8}$, representation because of the $(3^2 - 1)$ values it can assume.

It was difficult to understand the structure of hadrons. How could quarks be totally trapped in a hadron, yet behave as essentially free point particles when probed at high energy? These properties were called confinement and asymptotic freedom respectively. Confinement requires a much stronger coupling constant than the coupling of electromagnetism at large distances. But it changes to a relatively weak coupling for short distances or high momenta. In QED, the small (essentially constant) value of the coupling constant, $\alpha \simeq 1/137$, allows accurate calculations to be made by perturbation expansion. QCD is quite successful for scattering predictions at high energies (but doesn't come close to the accuracies of QED). However, the

perturbative approach is essentially useless when considering processes dominated by confinement at low energy. The coupling strength is of order one, so perturbative expansions don't converge for low-energy processes.

Renormalization group[32, 33] methods proved useful in studying the strong coupling regime inaccessible to perturbation theory. Renormalization group theory involves looking at the behavior of theories under a change of scale. For QCD, in rescaling the momentum $p \rightarrow \lambda p$, one can remove the λ from λp and put it inside a dimensionless effective coupling constant $g_s(\lambda)$. The coupling constant becomes scale-dependent. 't Hooft[34], Politzer[35], Gross and Wilczek[36, 37] found that QCD became asymptotically free at large momenta, $g_s(\lambda \rightarrow \infty) \sim O(\ln \lambda)^{-1} \rightarrow 0$. This running of the coupling constant is another confirmation of QCD as the correct theory of the strong interaction.

1.1.2 Confinement

Confinement proved more difficult to demonstrate explicitly. In 1962, Schwinger[39] showed that vector mesons could get a nonzero mass if the gauge theory had its charges totally screened by vacuum polarization. In 1974 Kenneth Wilson[38] used a similar mechanism to show soft (long-time-scale) confinement for strongly coupled gauge fields quantized on a 4-d Euclidean lattice. He also showed there was a weak coupling phase for small g_s . He argued these behaviors should be separated by a phase transition, and that this should generalize in a straight-forward manner to non-Abelian theories. The mechanism preserved exact gauge invariance and treated the gauge fields as angular variables. However, the lattice theory was not covariant, and the cutoff precluded free point-like behavior for quarks.

Nielsen and Olesen[40] and Nambu[41] explained the confinement of quarks by drawing attention to the parallel situation of lines of flux linking charges within a superconductor. This requires associating the electric-type color fields of non-Abelian SU(3) with the magnetic lines of flux which can not penetrate superconducting matter. As in a superconductor, flux is concentrated into tubes that carry energy proportional to their length, and quarks form the analog of magnetic monopoles. Mandelstam[42] showed that low energy quark states would be more or less spherical as in bag models, whereas states of high angular momentum would form elongated cavities as if connected by strings. This would provide a natural explanation for

Regge-trajectory behavior of hadronic excitations. This is where energy is asymptotically proportional to the square of angular momentum of the states. Unlike Abelian fields, non-Abelian fields can interact to shield a color charge using several other color charges, instead of drawing an anti-color charge closer. This leads to anti-screening—a color fluctuation seen at a distance may have vanishing imbalance at the center. This leads to asymptotic freedom rather than the singular behavior of ordinary screened charges at short distances.

Migdal[43] and Kadanoff[44] developed lattice-renormalization techniques for gauge theories. Their bond-moving scheme allows recursive summation over bonds that are decimated to generate successively coarser lattices. Each step involves changes in the effective coupling constant(s). To the degree the Migdal approximation is accurate, recursion in $d/2$ dimensions for nearest neighbor couplings behaves as recursion in d dimensions for gauge theories. The 4-d gauge theory of strings and quarks where couplings are strong can be studied in terms of the simpler 2-d nearest neighbor problem if one assumes the gauge fields (and not the quarks) determine the phase transitions of the system. (This is not necessarily a good assumption, as both strings and quarks are near a phase transition as the lattice constant is taken to zero. Interference can occur for phase transitions that occur essentially together, as in the Baxter system where two Ising systems interact[44].)

Kadanoff studied the flow of the coupling of gauge theories during renormalization. He demonstrated that confinement at large distances, and asymptotic freedom at short distances are possible behaviors of a single theory. This occurs when the coupling constant g_s flows from infinity (confinement) to zero (asymptotic freedom) as the lattice constant decreases. Any value of g_s other than zero exhibits quark confinement, so there is no phase change for the 4-d system of quarks and links. Gross and Wilczek[36, 37], and also Politzer[35], showed there would be no phase transition in 4-d QCD if there are fewer than 17 flavors, and they derived a formula for running of the QCD coupling constant.

1.1.3 Confined QCD models of hadrons

In 1967, Bogoliubov[45] introduced quarks within a spherical infinite square well potential using spherical solutions to the (relativistic) Dirac equation[46, 47, 48]. The square well was described as a ‘self-consistent’ approximation to the inter-quark po-

tential. Although this model is perhaps over-simplified, it embodies features required in a successful model of hadrons. Inside the bag, particles are free, consistent with asymptotic freedom. The hard scalar potential determines the quark boundary conditions and provides total quark confinement.

The MIT bag model

Later, without knowledge of Bogoliubov's work, the MIT bag model was developed. The MIT bag[49, 53, 51, 52] is similar to Bogoliubov's bag except that a constant, B (with units of energy density) parameterizes a bag pressure. The bag is like a bubble in the strongly coupled vacuum. The bag size and shape is determined by demanding dynamical balance between bag pressure and quark and gluon field pressures. When introducing the MIT bag model in 1974, Chodos, Jaffe, Johnson, Thorn and Weisskopf proposed that "a strongly interacting particle is a finite region of space to which fields are confined". By adding the energy density B to the stress-energy tensor, they claimed they achieved confinement in a Lorentz-invariant (but somewhat artificial) way. The bag surface has no dynamical degrees of freedom, but they considered classical shape deformations and oscillations including fission of bags. The color fields carried by quarks requires the quarks to be arranged in color singlets within the bags—anything else gives rise to infinite energy because of the effectively vanishing dielectric constant outside the bag. Confinement leads to an unbounded spectrum of quark modes and an infinitely rising Regge trajectory for the hadron spectrum.

DeGrand, Jaffe, Johnson, and Kiskis[54] used the MIT bag model to fit the mass spectrum of ground state hadrons. In the process, they added several features to the MIT model. A 'Casimer' term was added to include effects of zero-point fluctuations. As noted previously, the sign of this term is controversial[8] because calculations show the net contribution from quarks and gluons is positive. The term also makes the vacuum unstable to decay in the presence of an empty bag unless a cutoff is employed. (An empty bag could be created by surface fluctuations leading to pinching off of a piece of a bag containing quarks and gluons.) However the Casimir term fulfilled the need for a large negative energy contribution to get a good fit for the MIT bag model to the hadron mass spectra. With configuration mixing, we find the need for a negative Casimir term is eliminated.

The MIT bag had been shown to confine colored quarks, but interacting gluons

had not been included previously. DeGrand *et al.* incorporated gluons by taking the first order (α_s) approximation to the QCD field equations. This one-gluon exchange (OGE) approximation is linear in the gluon field strength. It includes a spin-spin and color-color interaction between the quark currents. This approximation simplifies the complexity arising from non-commutativity of the color fields, and also removes three-gluon and four-gluon interactions which arise in the full theory. This hyperfine type of interaction was first proposed as a mechanism for mass splitting between hadrons by De Rujula, Georgi, and Glashow[73], breaking the $SU(6)$ symmetry of spin and flavor. With these simplifications, each color field satisfies Maxwell's equations. The electric and magnetic fields must satisfy boundary conditions at the surface of the bag. It is necessary to add a piece of the self-energy to satisfy the electric field boundary condition and to preserve gauge invariance for the gluon. The approach taken was to include only the part of the self-energy needed to meet these requirements. This self-energy piece involves the longitudinal (radial) electric field contributions where the quark remains in the initial state inside the self-energy loop. The full self-energy includes a sum over all intermediate states within the gluon loop. The other self-energy terms are considered to be included in renormalized values for the mass and Casimir term. They tried including more self-energy terms, and found similar final results (but it required major changes to the quark masses and Casimir term). The non-Abelian group structure of the theory is not totally erased. All the color fields are coupled by Gell-Mann's eight $SU(3)$ color matrices (the λ matrices). The gluons carry this octet color, and must also be confined to the bag because of the vanishing value of the vacuum dielectric. This is accomplished by adopting standard solutions[56] for electromagnetic modes in a cavity, except that the fields carry color indices.

DeGrand, *et al.* made two separate (four parameter) fits to the masses of light hadrons. Then they looked at predictions for magnetic moments, weak decay constants, and charge radii. The first fit assumed zero mass for the u and d quark, whereas the second fit assumed a value of 108 MeV for the u and d (current) masses. They quote values of $\alpha_c = 0.55$ for the first fit, and $\alpha_c = 0.75$ for the second fit. However, their definition for coupling constant was not standard, as they used the color interaction $(\lambda)^2$, rather than $(\frac{\lambda}{2})^2$. Their numbers must be multiplied by four to conform to current usage[70, 71]. Thus their first fit has $\alpha_s = 4\alpha_c = 2.2$, and the second fit has $\alpha_s = 4\alpha_c = 3.0$. Although the coupling does run[36, 37, 35, 34],

growing as the relevant energy decreases, their couplings are uncomfortably large[72].

The equilibrium bag radius R_0 for each particle was found by minimizing the energy, with the minimum energy being the mass of the particle. Mesons and baryons were modeled together using the same sets of parameters. In both fits, B , Z , and α_s , (bag constant, Casimir coefficient, and strong coupling constant) were adjusted to fit masses of the ω meson, the proton, and the Δ . Then the s quark mass was adjusted to fit the energy of the Ω . This involves $SU(3)_{FLAVOR}$ symmetry breaking in making the s mass heavier than the u and d masses. If α_s was set to zero, the masses of mesons would differ from baryons because they are made of two rather than three quarks. However, the nucleon and Δ would be degenerate, and also the π and ρ . Making α_s non-zero (turning on the color magnetic interaction) splits these energies. Since the same mass was assumed for the u and d quark, there was no splitting between neutron and proton.

Both fits gave quite good results for the ten hadron masses that they did not use in setting parameters. The baryon decuplet fit was good, with equal spacing between rows of the multiplet. The baryon octet has equal spacing, but the Ξ mass is approximately 30 MeV too small, and the $\Sigma - \Lambda$ splitting is half what it should be. In the meson sector, the ω and ρ are degenerate (they should differ by 13 MeV), and the ϕ mass is 50 MeV too large. There are difficulties in the pseudo-scalar meson sector. In the first fit, the $K - \pi$ mass difference is about 210 MeV, (it should be 350 MeV). A small part of this arises because the K is about 2 MeV high, but the π mass is 280 MeV (experimentally it is 139 MeV). Recoil effects would lower the π mass, but the MIT bag model does not allow one to correct for recoil effects. For the second fit with the masses of u and d at 108 MeV, there was no solution for the π with $R > 0$. This was considered encouraging because the Goldstone nature of the π makes it difficult to reconcile the π with the quark model. Although the mass fits are slightly better with the first set of parameters, the average magnetic moments of the octet baryons and g_A/g_V are worse. The prediction for the magnetic moments for zero mass u and d is too small: $2M_p\mu_p = 1.9$ vs. 2.6 experimentally. This is the most serious discrepancy in the model predictions. The axial to vector coupling is also small, with the first fit predicting $g_A/g_V = 1.09$ vs. 1.25 experimentally. Larger masses improve this value, with of $g_A/g_V = 1.25$ for $mR \sim 1$ [57, 58].

DeGrand and Jaffe[59] used the parameters derived from the first fit with $\alpha_s = 2.2$

to calculate low-lying excitations of quarks and gluons in the MIT bag. There were no free parameters left to fit in this study, so all results were predictions. The states they considered had one quark excited to a $p_{1/2}$ state, with the others in the $s_{1/2}$ ground state. Using $Spin^{Parity}$ notation, the hadrons they modeled were $\frac{1}{2}^-$ and $\frac{3}{2}^-$ baryons as well as 0^+ and 1^- mesons. The spectrum they calculated suffered from two defects: the states were too low in energy on average, and there were too many states. In particular, excited non-strange baryon states were on average ~ 150 MeV too low. Further modification of these results would be expected from inclusion of higher-order gluon interactions. They attributed the extra states to excitation of the center of mass of the system. In models using two body forces, such states are spurious and need to be projected out. However in the MIT bag, confinement involves interaction of the quarks with the bag, which acts as an external object. Thus there was no reason to exclude these states. However surface oscillations include translational modes[60] which are spurious. The present wave functions should be orthogonalized against those spurious states. This would tend to push up the energy of the states. (It is difficult in a relativistic theory to isolate the center of mass coordinates[61, 8]. The center-of-energy operator is quite intractable[62, 63], although various approximate momentum projection methods have been developed[64, 65, 66].)

Bowler, Hey, and Walters[67, 68] considered radial excitation of baryons formed from three quarks in $s_{1/2}$ states. They interpreted their results as a prediction of the $NP11$ Roper resonances. Their masses were in fairly good agreement with πN phase-shift analyses for these resonances. They also considered breathing modes for the bag, concluding that their effect is small.

In the meson sector, Jaffe[69] used the MIT bag model to calculate effects of extra quark pairs. The spectra and dominant decay modes of 'cryptoexotic' $qq\bar{q}\bar{q}$ mesons were calculated, with all quarks in $s_{1/2}$ states. The lowest cryptoexotic particle was correlated with known 0^+ meson resonances. Higher resonances were predicted to be broad, but it was suggested some other states might be observable.

Donoghue and Golowich[70] used the same OGE mechanism to perturbatively calculate effects of pair creation for the proton ground state. Transitions from the $s_{1/2}$ 'valence' qqq state to $qqqq\bar{q}$ states were calculated. They called the contribution from additional pairs $q\bar{q}$ 'sea' states. Anti-quarks have opposite intrinsic parity as quarks. Adding a pair requires compensating this by changing the orbital angular

momentum of at least one quark (for example changing an $s_{1/2}$ quark or antiquark state to a $p_{1/2}$ or $p_{3/2}$ state). In that study, only $s_{1/2}$ and $p_{1/2}$ states were considered, but radial excitations of quarks were calculated. Four flavors of pairs were considered, u , d , s , and c (charm). The same parameters were used as found by DeGrand *et al.* in their first fit with zero mass for the u and d quarks, and 279 MeV for the s quark. In addition they used a value of 1.55 GeV for the c quark. Their use of the coupling $\alpha_s = 2.2$ led to prediction of large values for sea contributions. Their perturbative probabilities for $u\bar{u}$, $d\bar{d}$, $s\bar{s}$, and $c\bar{c}$ sea configurations were respectively 0.360, 0.271, 0.167 and 0.020. They calculated the effects of the sea on hadron properties to be 20-30 %. However the gluon propagator they started with gave several huge contributions due to near cancelation of energies in the denominators for some gluon and quark modes. (One term alone contributed -1.26×10^5). They removed this behavior in a rather ad hoc way by a modification to the bag boundary condition for the gluons.

In a similar study, Maciel and Paton[74] used confined perturbation theory[2, 71, 4] (see below) and found values for the $q\bar{q}$ sea roughly six times smaller. They attributed the difference to the ad hoc propagator choice of Donoghue and Golowich, and also to a missing interference term in the prior work. They also considered the effects of a b (bottom) quark with a mass of 4 GeV, and also the mixing if there were an (unknown) 'o quark' with zero mass. Their parameters differed only slightly from Donoghue and Golowich, with the s mass at 0.3 GeV and the c mass at 1.5 GeV. Their probabilities for $q\bar{q}$ contributions for $u\bar{u}$, $d\bar{d}$, $o\bar{o}$, $s\bar{s}$, $c\bar{c}$, and $b\bar{b}$ were respectively 0.056, 0.040, 0.045, 0.045, 0.74×10^{-2} , and 0.85×10^{-3} .

Donoghue and Golowich tabulated (in their Table II.) the perturbative probability for a proton to include five particle states as a function of quark modes (including spin) and flavor. They summed these expressions over all states to arrive at their final results. They found that there was enhancement of probability where there were other quarks in the $qqqq\bar{q}$ sector with the same flavor as the flavor of the $q\bar{q}$ pair. This arises from interference between amplitudes for pairing the \bar{q} with any of the other q of the same flavor. This results in a significant decrease in $s\bar{s}$ or $c\bar{c}$ scattering relative to $u\bar{u}$ or $d\bar{d}$, in addition to suppression from the larger energy denominators. The calculation by Maciel and Paton shows similar results, taking into account differences in their normalization and their correction to the work of Donoghue and Golowich. However both studies leave out some interference terms, as

they apparently squared terms before summing over all links to the qqq state. Pair creation amplitudes involving an OGE exchange with a qqq quark having the same flavor as others in the bag should interfere. This effect will be demonstrated in the present study. This enhances the probability for emission of a gluon that creates a pair from the u quark relative to the d quark in the proton. This effect can be seen to be missing from Table II. of Donoghue and Golowich and from Table I. of Maciel and Paton.

In 1979, Lee[2] introduced Feynman rules for QCD confined to a finite volume. This is called confined perturbation theory[71, 4]. His theory is applicable to any of the Friedberg-Lee bag models (see below), as well as to the MIT bag. The Feynman rules depend on the bag radius R (and on the dielectric constant of the vacuum, which is effectively zero outside the MIT bag). At high four-momentum, this theory reduces to ordinary QCD with no dependence on the bag radius. In Coulomb gauge, the theory gives a prescription for perturbative calculation of gluon exchange between quarks.

Close and Horgan[71, 4] developed and applied Lee's confined perturbation theory to the MIT bag model. This approach provides an alternative to calculating the electric and magnetic field energies from the quark wave functions as was done previously for OGE. (A third alternative is to calculate interactions using a confined-tensor Green's function for transverse modes and a scalar Green's function for longitudinal modes[8, 75, 76].) In the confined perturbation approach, one first calculates quark wave functions and then the currents. One solves for the transverse electric and magnetic (TE and TM) gluon modes that exist as discrete solutions in the bag. The vector potential from these modes is expanded in vector-spherical harmonics. Depending on time-ordering, the vector potential (or its complex conjugate) is integrated with a quark current to get a vertex integral. The product of two vertex integrals is divided by an energy denominator to calculate the contribution of one mode to a time-ordered OGE graph. These terms are summed over gluon modes until adequate convergence is reached. Typically the sum converges rapidly (to better than a part in 10^4 with five modes). Finally, the longitudinal or Coulomb terms must be included. Lee calculated the scalar Green's function appropriate for the confined longitudinal gluon field. This Green function must be integrated with four quark wave functions over six ($r_<, r_>$) dimensions.

Close and Monaghan used this technique to calculate (dipole) results for arbitrary mass $s_{1/2}$ and $p_{1/2}$ quarks and antiquarks. They found agreement with the earlier MIT bag[54] results. In addition to magnetic and electric types of quark-gluon vertices, they also calculated three and four gluon vertices.

In 1984, Wroldsen and Myhrer[5] calculated more extensive tables for OGE interactions of $s_{1/2}$, $p_{3/2}$, and $p_{1/2}$ quarks in the MIT bag. They used the older approach, calculating magnetic and electric fields. They presented numerical results for the whole OGE graph, which are multiplied by α_s/R and spin and color sums. (They also calculated results for a chiral bag model. The chiral bag model assumes a pion field is present in addition to the quarks in the MIT bag. Conservation of the axial current determines the strength of the quark-pion coupling.) Wroldsen and Myhrer's MIT bag results (as corrected by Umino and Myhrer[83]) have been useful in comparison to the results of this study, which were done by a different technique (using confined perturbation theory).

In the mid '80s, Ushio and Konashi[77] and Ushio[78, 79] used confined perturbation theory to calculate OGE corrections to g_A/g_V for weak semileptonic decay processes. They found adjustments of 1% - 30%, depending on the decay process considered. Experimentally[1], the value of $g_A/g_V = 1.2573 \pm 0.0028$ for decay of the neutron, but the zeroth order MIT bag prediction is 1.09. There are problems in matching g_A/g_V for decays of many hadrons. Calculations were done for both sets of parameters of DeGrand *et al.*, except differences in bag radii were neglected between particles. They found only about a 3% correction to the g_A/g_V ratio for $n \rightarrow p$ decay. However the magnitude of g_A/g_V for $\Sigma^- \rightarrow n$ decay was increased by OGE effects to agree with experiment[77].

In 1988, Myhrer and Thomas[81] examined the OGE corrections to the integrated spin structure functions of the nucleons in the Bjorken sum rule[146]. They used intermediate $J = \frac{1}{2}$ and $\frac{3}{2}$ quark and antiquark states. They found a negative contribution to the Bjorken sum rule for the neutron of less than 2%. This was about the same size as the pionic correction in the chiral or cloudy bag model[82].

Other bag models

Umino and Myhrer[83], calculated masses of low-lying negative-parity excited Λ^* and Σ^* using the chiral bag model. They diagonalized the interaction for $J = \frac{1}{2}$ and

$\frac{3}{2}$ states. They also tested a prescription to project out translational modes and compared their results to the results of non-relativistic models[84].

Høgaasen and Myhrer[151, 86] used confined perturbation theory to look at SU(6) violations and corrections to magnetic moments as calculated in the chiral bag model. Without correction, the pionic contributions added to the chiral bag create a problem for the ratio of proton and neutron magnetic moments. Experimentally $\mu_p/\mu_n = -1.46$ [1]. SU(6) additive quark models and the MIT bag predict a value of $\mu_p/\mu_n = -3/2$, which is good. However, the chiral bag with pionic (isovector) contributions destroys the good match. A fit indicates there should be a very small pion contribution compared to the chiral bag prediction. Høgaasen and Myhrer show that this ratio can be restored to $-3/2$ for the chiral bag by including intermediate excited states in the calculation of the nucleon magnetic moments. Inclusion of intermediate states also helped explain why the magnetic moment of the Ξ^- is more negative than the Λ .

Friedberg and Lee[87, 2] suggested physical properties of the vacuum were responsible for confinement. They developed a new class of models to achieve confinement. Their renormalizable-Lagrangian-based approach uses a scalar field interacting with quarks in three spatial dimensions to create ‘nontopological soliton’ solutions for hadrons. The quasiclassical soliton behaves much as a gas bubble in a medium with surface tension, pressure of the medium and gas, and a ‘thermodynamical’ gas energy. They demonstrated that the quasiclassical solution is a good approximation to the quantum solution over a wide range of coupling constants. In limiting cases, their model reduces to the Creutz version of the MIT bag model[51, 52] or the SLAC bag model[88] developed by Bardeen and his collaborators. The hard-wall boundary condition of the MIT bag, in this picture, is the limiting case of a bag with a smooth transition from inside to outside. The scalar field attains its vacuum value outside the bag. Quarks are excluded from the vacuum by a potential that depends on the scalar field. The quark, gluon, and scalar fields are solved self-consistently.

One problem with the Friedberg Lee model is that the quark-scalar coupling breaks chiral invariance (the coupling acts as an effective quark mass)[89, 8]. Chiral symmetry is not exact, but it exerts an important influence on low energy hadron properties. (Non-zero masses in the Lagrangian break Chiral symmetry. Thus small u and d quark masses are required to achieve a good fit to nucleon properties).

The chromodielectric model[90, 91, 89] (CDM) is related to the Friedberg-Lee

soliton model. There is no direct quark-scalar coupling, so the (massless) CDM Lagrangian is chirally invariant. The CDM Lagrangian is a combination of the QCD Lagrangian supplemented by a scalar field governing dielectric properties of the medium. The scalar field is identified with the gluon condensate. Quarks acquire a self-energy when they interact with gluons in the dielectric. This effective mass increases without limit in the vacuum region. This leads to quark spatial confinement. The equations have been solved numerically in the mean field approximation. Chiral invariance is dynamically broken and this was interpreted as evidence of a Nambu-Goldstone pion[89]. Color confinement is due to the self-energy and mutual-interactions of quarks through one-gluon exchange. The self-consistent solutions that have been found are illuminating. In addition to modeling individual hadrons, the soliton bag has been used to model interactions between bags[92], nuclear and quark matter[93, 94], and hadron dynamics[95] including color flux tubes[96]. For individual bags, the confining scalar potential which results from this self consistent approach is similar to the infinite step function of the MIT model[8]. This helps justify using the simpler MIT model to explore hadron properties.

Chapter 2

QUARKS, GLUONS, AND THE MIT BAG MODEL

2.1 Introduction

It is generally accepted that QCD is the fundamental theory of the strong interaction. QCD is a non-Abelian gauge field theory that describes interactions between quarks and gluons. At low energies, the strong coupling becomes large, making a non-perturbative approach necessary when confinement is the dominant feature of the system of interest. We are studying nucleon ground state energies, where quarks and gluons are confined to a region of space within a radius $r_n \sim 1 \text{ fm}$ (10^{-15} m). The non-perturbative approach we take is to utilize the static spherical MIT bag model[49, 51, 52, 53] to confine quarks, and then diagonalize over all basis states below some energy cutoff to find the ground state configuration mixing. The static spherical MIT bag model is similar to Bogliubov's original model[45], where solutions of the Dirac equation are found for a spherical cavity. We use confined perturbation theory[2] to calculate the OGE[54] interaction in Coulomb gauge. This includes a color-charge interaction based on SU(3), a traceless unitary Lie group of three-dimensions, where the group generators T_a act as color charges.

2.1.1 QCD Lagrangian for quarks and gluons

Quark and gluon fields interact via the SU(3) color group as specified by the QCD Lagrangian. Let q be the wave function for a quark with mass m , which we may think of as a three-component column vector indicating (red, green, or blue) color. (Anti-quarks are described by a charge-conjugate wave function carrying three values of anti-color.) We suppress indices for type of quark or antiquark. (The type includes flavor, mode, and spin). The gluon gauge field, A_μ^a has octet color, so the color label a is summed over eight values corresponding to the eight 3×3 λ matrices. We will also suppress the gluon-mode indices.

The QCD Lagrangian[97, 98] describing interaction between quarks and gluons is

$$\mathcal{L} = \sum_{types} (i \bar{q} \not{D} q - m \bar{q} q) - \frac{1}{4} G_a^{\mu\nu} G_{a\mu\nu}, \quad (2.1)$$

where local gauge invariance requires the covariant derivative to be

$$\not{D} = (\partial^\mu + i g_s T_a A_a^\mu) \gamma^\mu, \quad (2.2)$$

where $\bar{q} = q^\dagger \gamma^0$ is the spinor adjoint, γ^μ are the Dirac matrices and g_s is the quark-gluon coupling strength. We use the standard representation,

$$\gamma^0 = \begin{pmatrix} 1 & 0 \\ 0 & -1 \end{pmatrix}, \quad \gamma = \begin{pmatrix} 0 & \boldsymbol{\sigma} \\ -\boldsymbol{\sigma} & 0 \end{pmatrix}, \quad (2.3)$$

where $\mathbf{1}$ is the 2x2 unit matrix and $\boldsymbol{\sigma}$ are the Pauli matrices. The gluon field strength tensor is

$$G_a^{\mu\nu} = \partial^\mu A_a^\nu - \partial^\nu A_a^\mu - g_s f_{abc} A_b^\mu A_c^\nu. \quad (2.4)$$

The T_a are the group generators of SU(3).

2.1.2 SU(3)

A non-Abelian Lie group with generators T_a obeys

$$[T_a, T_b] = i f_{abc} T_c, \quad (2.5)$$

with normalization $\text{tr} (T_a T_b) = \frac{1}{2} \delta_{ab}$. The f_{abc} are real numbers called the structure constants of the group. SU(3) has eight generators, with

$$T_a = \frac{\lambda_a}{2},$$

$$\begin{aligned}
\lambda_1 &= \begin{pmatrix} 0 & 1 & 0 \\ 1 & 0 & 0 \\ 0 & 0 & 0 \end{pmatrix}, & \lambda_2 &= \begin{pmatrix} 0 & -i & 0 \\ i & 0 & 0 \\ 0 & 0 & 0 \end{pmatrix}, & \lambda_3 &= \begin{pmatrix} 1 & 0 & 0 \\ 0 & -1 & 0 \\ 0 & 0 & 0 \end{pmatrix}, \\
\lambda_4 &= \begin{pmatrix} 0 & 0 & 1 \\ 0 & 0 & 0 \\ 1 & 0 & 0 \end{pmatrix}, & \lambda_5 &= \begin{pmatrix} 0 & 0 & -i \\ 0 & 0 & 0 \\ i & 0 & 0 \end{pmatrix}, & \lambda_6 &= \begin{pmatrix} 0 & 0 & 0 \\ 0 & 0 & 1 \\ 0 & 1 & 0 \end{pmatrix}, \\
\lambda_7 &= \begin{pmatrix} 0 & 0 & 0 \\ 0 & 0 & -i \\ 0 & i & 0 \end{pmatrix}, & \lambda_8 &= \begin{pmatrix} 1 & 0 & 0 \\ 0 & 1 & 0 \\ 0 & 0 & -2 \end{pmatrix} \frac{1}{\sqrt{3}}.
\end{aligned} \tag{2.6}$$

The eight λ_a are 3x3 traceless Hermitian matrices often called the Gell-Mann matrices.

2.1.3 Symmetries and conserved currents

In 1918, Emmy Noether[31, 97] showed that for every symmetry of a Lagrangian, there is a conserved current. Consider a Lagrangian that depends only on fields $\phi_r(x)$ and their first derivatives. Its equations of motion are:

$$\partial_\mu \frac{\delta \mathcal{L}}{\delta(\partial_\mu \phi_r)} = \frac{\delta \mathcal{L}}{\delta \phi_r}. \tag{2.7}$$

If the Lagrangian has a symmetry so that it doesn't change under an infinitesimal variation $\delta\phi_s(x)$,

$$\delta \mathcal{L}(\phi_s) = \mathcal{L}(\phi_s + \delta\phi_s) - \mathcal{L}(\phi_s) = \frac{\delta \mathcal{L}}{\delta \phi_s} \delta\phi_s + \frac{\delta \mathcal{L}}{\delta(\partial_\mu \phi_s)} \delta(\partial_\mu \phi_s) = 0. \tag{2.8}$$

Using the equations of motion and simplifying,

$$0 = \partial_\mu \left[\frac{\delta \mathcal{L}}{\delta(\partial_\mu \phi_s)} \delta\phi_s \right]. \tag{2.9}$$

The piece within square brackets must be constant. It is called a conserved current.

$$j^\mu = \frac{\delta \mathcal{L}}{\delta(\partial_\mu \phi_s)} \delta\phi_s \tag{2.10}$$

For QCD, invariance under rotation in color space leads to conserved color currents for the quarks:

$$j_a^\mu = \bar{q}\gamma^\mu T_a q = \bar{q}\gamma_\mu \frac{\lambda_a}{2} q. \quad (2.11)$$

The coupling of the quark field to the gluon field through the covariant derivative is unavoidable if one demands that invariance under a color rotation holds as a local symmetry. With this assumption, the color current is conserved under arbitrary (space-time dependent) color gauge rotations.

2.2 Static spherical MIT bag model

The OGE interaction we use is an approximation to the QCD Lagrangian where only terms linear in the gluon field strength are kept. We utilize the fixed spherical MIT bag model to study quarks and gluons interacting within a finite volume. The MIT bag model used by DeGrand *et al.*[54] to fit the hadron mass spectrum has four free parameters, B , α_s ¹, Z_0 , and m_s . The bag constant, B , is an energy density representing the pressure of the vacuum. The strong coupling constant, $\alpha_s = g_s^2/4\pi$, is adjusted to give the correct $\Delta - N$ splitting. The coefficient of the ‘Casimir’ term, Z_0 , was introduced to lower the ground state energy of the hadrons, and was justified as representing a piece of the zero point energy. We find a significant depression of the ground state energy with the introduction of a larger basis set of states than used by DeGrand, *et al.*, making a negative Casimir term unnecessary. This will be discussed in more detail later. DeGrand *et al.* set the u and d quark masses, m_u and m_d , equal to zero, and treated the s mass, m_s , as a parameter. We make calculations using a similar parameter set, but allow α_s to change to keep the proper $\Delta - N$ splitting. We include many more basis states than considered by DeGrand *et al.*, and the value for α_s decreases significantly. In addition, we allow the u and d quark masses to differ by five MeV. We also calculate results for several different choices of the self-energy, and for several values of B , implying different bag radii R .

The bag radius, R , is not an independent parameter. It is found by balancing the field pressure of quarks and gluons against the bag pressure. A larger choice for B results in a smaller value for R .

¹ DeGrand *et al.* used $(\lambda)^2$ rather than $(\frac{\lambda}{2})^2$ as their color coupling, so their coupling constant, α_c , must be multiplied by four to equal our α_s , $\alpha_s = 4\alpha_c$.

The MIT bag energy (or particle mass) is

$$E = \frac{4}{3}\pi BR^3 - Z_0/R + \sum \omega_q + E_{OGE}, \quad (2.12)$$

where ω_q are the frequencies of the quark modes in the bag. E_{OGE} is the one-gluon exchange energy including TE, TM, and instantaneous Coulomb contributions. It is a hyperfine type of interaction between two quark currents which together introduce spin-spin and color-color factors. Quark or antiquark wave functions can contribute to the current, propagating forward or backward in time. Thus each vertex represents a gluon scattering from a quark or an antiquark, or a gluon creating or destroying a quark—antiquark pair. Different time orderings of the two quark-gluon vertices correspond to forward or backward propagation of the gluon. (See figure 1.)

2.2.1 Dirac equation—spherical solutions for quarks

The Dirac equation is the equation of motion for independent relativistic spin-1/2 point-like particles. We use natural units where $\hbar = c = 1$.

The equation for quarks of current mass m is

$$i \partial q / \partial t = Hq = [\alpha \cdot p + \beta m] q = \omega_q q, \quad (2.13)$$

where ω_q is the energy of a quark stationary state. α and β are a set of four anti-commuting Hermitian matrices that form their own inverse (they are unitary). They may be written as

$$\alpha = \begin{pmatrix} 0 & \sigma \\ \sigma & 0 \end{pmatrix}, \quad \beta = \begin{pmatrix} 1 & 0 \\ 0 & -1 \end{pmatrix}. \quad (2.14)$$

The β and α matrices are related to the γ matrices by

$$\gamma^0 = \beta, \quad \gamma = \beta \alpha. \quad (2.15)$$

We need centrally symmetric solutions of the Dirac equation for quarks to satisfy the spherical boundary conditions. We write the Dirac equation in spherical coordinates,

$$\omega_q q = Hq = \left[-i \alpha_r \left(\frac{\partial}{\partial r} + \frac{1}{r} - \frac{\beta}{r} K \right) + \beta S(r) + \beta m \right] q. \quad (2.16)$$

where we introduce the Dirac quantum number κ , with

$$\kappa = \begin{cases} +(j + \frac{1}{2}) = l & \text{if } j = l - \frac{1}{2}, \\ -(j + \frac{1}{2}) = -(l + 1) & \text{if } j = l + \frac{1}{2}. \end{cases} \quad (2.17)$$

The operators \mathbf{j}^2 , j_z , and K all commute with the Hamiltonian, with eigenvalues $j(j+1)$, μ , and $-\kappa$, respectively. The orbital angular momentum and spin are not separately conserved. We have included a spherically symmetric scalar potential, $S(r)$. For the spherical MIT bag of radius R ,

$$S(r) = \begin{cases} 0 & \text{for } r < R, \\ M \rightarrow \infty & \text{for } r \geq R. \end{cases} \quad (2.18)$$

This is equivalent to the boundary condition

$$-i \vec{\gamma} \cdot \hat{r} q = q, \quad \text{at } r = R. \quad (2.19)$$

This boundary condition may be derived as the $(M \rightarrow \infty)$ limit of the matching condition for a field with mass m inside the bag, and a field of mass M outside the bag[49].

The wave function for a quark may be written as a column vector of two-component spinors, a bi-spinor;

$$q = \begin{pmatrix} q^u \\ q^l \end{pmatrix}. \quad (2.20)$$

For the wave function to satisfy the eigenvalue equation for K ,

$$(\boldsymbol{\sigma} \cdot \mathbf{l} + 1) q^u = -\kappa q^u, \quad (\boldsymbol{\sigma} \cdot \mathbf{l} + 1) q^l = \kappa q^l. \quad (2.21)$$

We introduce indices for κ and the z-component of angular momentum, μ . The eigenvalue requirements for κ are satisfied by making the upper and lower components proportional to \mathcal{Y}_κ^μ , and $\mathcal{Y}_{-\kappa}^\mu$ respectively, where the spinor

$$\mathcal{Y}_\kappa^\mu = \sum_m \langle l \mu - m \frac{1}{2} m \mid l \frac{1}{2} j \mu \rangle Y_l^{\mu-m} \chi^m. \quad (2.22)$$

The $\langle l \mu - m \frac{1}{2} m \mid l \frac{1}{2} j \mu \rangle$ are Clebsch-Gordan coefficients[99], and χ^m are two-component Pauli spinors. The $\mathcal{Y}_{\pm\kappa}^\mu$ spinors combine spin and angular information to satisfy

$$(\boldsymbol{\sigma} \cdot \mathbf{l} + 1) \mathcal{Y}_\kappa^\mu = -\kappa \mathcal{Y}_\kappa^\mu. \quad (2.23)$$

We can now write the upper and lower parts of the single particle wave function in terms of these spin-angular functions times radial functions. Thus we write

$$q_{\kappa}^{\mu}(\mathbf{r}) = \begin{pmatrix} f(r) \mathcal{Y}_{\kappa}^{\mu} \\ ig(r) \mathcal{Y}_{-\kappa}^{\mu} \end{pmatrix}, \quad (2.24)$$

where $f(r)$ and $g(r)$ are the radial functions (which also depend on κ). The factor i will allow $f(r)$ and $g(r)$ to be expressed as real functions.

Substituting this wave function into the spherical form of the Dirac equation, and using[46] $\sigma_r \mathcal{Y}_{\kappa}^{\mu} = -\kappa \mathcal{Y}_{\kappa}^{\mu}$,

$$\begin{aligned} (\omega_q - S(r) - m) f(r) \mathcal{Y}_{\kappa}^{\mu} &= \left[-\left(\frac{d g(r)}{dr} + \frac{g(r)}{r} \right) + \frac{\kappa g(r)}{r} \right] \mathcal{Y}_{\kappa}^{\mu} \\ (\omega_q - S(r) + m) g(r) \mathcal{Y}_{-\kappa}^{\mu} &= \left[\frac{d f(r)}{dr} + \frac{f(r)}{r} + \frac{\kappa f(r)}{r} \right] \mathcal{Y}_{-\kappa}^{\mu} \end{aligned} \quad (2.25)$$

We separate radial from angular variables, which gives the coupled radial equations for $f(r)$ and $g(r)$,

$$\begin{aligned} \frac{df(r)}{dr} + \frac{1+\kappa}{r} f(r) - (\omega_q - S(r) + m) g(r) &= 0, \\ \frac{dg(r)}{dr} + \frac{1-\kappa}{r} g(r) + (\omega_q - S(r) - m) f(r) &= 0. \end{aligned} \quad (2.26)$$

Defining functions

$$u_1 = r f(r), \quad \text{and} \quad u_2 = r g(r), \quad (2.27)$$

the radial equations are combined to eliminate u_2 ,

$$\begin{aligned} 0 &= \frac{d^2 u_1}{dr^2} + \frac{dS(r)/dr}{\omega_q - S(r) + m} \frac{du_1}{dr} + \\ &\quad \left[(\omega_q - S(r) - m)^2 - \frac{\kappa(\kappa+1)}{r^2} + \frac{\kappa}{r} \frac{dS(r)/dr}{\omega_q - S(r) + m} \right] u_1. \end{aligned} \quad (2.28)$$

For $r \leq R$, $S(r) = 0$, and the equation for u_1 simplifies to

$$\frac{d^2 u_1}{dr^2} + \left[(\omega_q^2 - m^2) - \frac{\kappa(\kappa+1)}{r^2} \right] u_1 = 0. \quad (2.29)$$

The solution that is finite at $r = 0$ is

$$u_1 = N r j_l \left(\sqrt{\omega_q^2 - m^2} r \right), \quad (2.30)$$

where $j_l(z)$ are spherical Bessel functions. From the coupled radial equations for u_1 and u_2 , we solve for u_2 ,

$$u_2 = \frac{1}{\omega_q + 1} \left(\frac{d}{dr} + \frac{\kappa}{r} \right) u_1. \quad (2.31)$$

Using the recurrence relations[101, 56] for spherical Bessel functions,

$$\frac{d}{dz} j_l(z) = \frac{1}{z} j_l(z) - j_{l+1}(z) = -\frac{l+1}{z} j_l(z) + j_{l-1}(z), \quad (2.32)$$

we define $\bar{l} = l - \kappa/|\kappa|$. Then

$$u_2 = N \frac{\kappa}{|\kappa|} \frac{\sqrt{\omega_q^2 - m^2} r}{\omega_q + m} j_{\bar{l}} \left(\sqrt{\omega_q^2 - m^2} r \right). \quad (2.33)$$

Defining dimensionless variables

$$\omega_q = R \omega_q, \quad \text{and} \quad x_q = R \sqrt{\omega_q^2 - m^2} = \sqrt{\omega_q^2 - (m R)^2}, \quad (2.34)$$

we find solutions regular at $r = 0$ that satisfy the boundary equation at $r = R$. The radial solutions are

$$\begin{aligned} f(r) &:= f_\kappa(r) = N j_l(x_q r/R), \\ g(r) &:= g_\kappa(r) = N \frac{\kappa}{|\kappa|} \frac{x_q}{(\omega_q + m R)} j_{\bar{l}}(x_q r/R), \end{aligned} \quad (2.35)$$

where l is specified by κ . For given R and m , these solutions form a tower of radial modes for each value of κ . The mode eigenvalues, x_q , are found numerically as solutions to the transcendental equation[59],

$$(\omega_q + m R) f_\kappa(x_q) + x_q f_{\kappa-1}(x_q) = 0. \quad (2.36)$$

The normalization, determined by $\int_{b_{ag}} d^3r \psi_\kappa^\dagger(\vec{r}) \psi_\kappa(\vec{r}) = 1$, is

$$N = \frac{x_q}{j_l(x_q) R^{3/2} \sqrt{2 \omega_q (\omega_q + \kappa) + m R}}. \quad (2.37)$$

Values for x_q and ω_q for $R=0.005 \text{ MeV}^{-1}$ and quark masses of 0, 5, and 279 MeV are listed in Table 2.1.

Table 2.1: Eigenvalues and frequencies for light quarks with $R=0.005 \text{ MeV}^{-1}$ and with the cutoff at 1.5 GeV above the qqq ground state. Some energy levels are not used because they can not be combined with other quark states, conserving parity and angular momentum, to generate multi-particle states below our cutoff (see Sec 4.3.8).

energy						m=0 MeV		m=5 MeV		m=279 MeV	
level	κ	J	l	n	x	ω	x	ω	x	ω	
1	-1	$\frac{1}{2}$	0	1	2.0428	2.0428	2.0547	2.0548	2.4878	2.8523	
2	-2	$\frac{3}{2}$	1	1	3.2039	3.2039	3.2142	3.2143	3.6340	3.8926	
3	1	$\frac{1}{2}$	1	1	3.8115	3.8115	3.8141	3.8142	3.9471	4.1864	
4	-3	$\frac{5}{2}$	2	1	4.3273	4.3273	4.3367	4.3367	4.7407	4.9417	
5	2	$\frac{3}{2}$	2	1	5.1231	5.1231	5.1249	5.1249	5.1276	5.4009	
6	-1	$\frac{1}{2}$	0	2	5.3960	5.3960	5.3989	5.3989	5.5464	5.7192	
7	-4	$\frac{7}{2}$	3	1	5.4295	5.4295	5.4382	5.4383	5.8276	5.9923	
8	3	$\frac{5}{2}$	3	1	6.3711	6.3711	6.3725	6.3725	6.4439	6.5932	
9	-5	$\frac{9}{2}$	4	1	not used						
10	-2	$\frac{3}{2}$	1	2	6.7578	6.7578	6.7604	6.7605	6.8985	7.0381	
11	1	$\frac{1}{2}$	1	2	7.0020	7.0020	7.0036	7.0036	7.0872	7.2232	
12	4	$\frac{7}{2}$	4	1	not used						
13	-6	$\frac{11}{2}$	5	1	not used						
14	-3	$\frac{5}{2}$	2	2	not used						
15	2	$\frac{3}{2}$	2	2	8.4076	8.4076	8.4088	8.4088	8.4736	8.5877	
16	-1	$\frac{1}{2}$	0	3	8.5776	8.5776	8.5792	8.5792	8.6678	8.7793	

2.2.2 Anti-quarks

Quarks time-evolve according to a frequency given by their energy, whereas antiquarks time-evolve with a negative frequency,

$$i \partial q^c(\mathbf{r}, t) / \partial t = -\omega_q q^c(\mathbf{r}, t). \quad (2.38)$$

A charge conjugate wave function is formed by having the charge conjugation operator act on a time dependent quark wave function. This is given by

$$q^c(\mathbf{r}) = (q_\kappa^\mu)^c(\mathbf{r}) = i \gamma_2 (q_\kappa^\mu(\mathbf{r}))^* = \begin{pmatrix} -g^c(r) \sigma_2 \mathcal{Y}_{-\kappa}^{\mu*} \\ i f^c(r) \sigma_2 \mathcal{Y}_{\kappa}^{\mu*} \end{pmatrix}, \quad (2.39)$$

where

$$\sigma_2 \mathcal{Y}_{\kappa}^{\mu*} = \sum_m \langle l \mu - m \frac{1}{2} m | l \frac{1}{2} j \mu \rangle \sigma_2 (-1)^{\mu-m} Y_l^{m-\mu} \chi^m, \quad (2.40)$$

and

$$\sigma_2 \chi^m = i(-1)^{m-1/2} \chi^{-m}. \quad (2.41)$$

Thus

$$\sigma_2 \mathcal{Y}_{\kappa}^{\mu*} = i(-1)^{\mu-1/2} \sum_m \langle l \mu - m \frac{1}{2} m | l \frac{1}{2} j \mu \rangle Y_l^{m-\mu} \chi^{-m}. \quad (2.42)$$

Replacing m by $-m$ in the sum, we use[46]

$$\langle l -\mu - m \frac{1}{2} m | l \frac{1}{2} j \mu \rangle = (-1)^{l+1/2-j} \langle l \mu + m \frac{1}{2} -m | l \frac{1}{2} j \mu \rangle. \quad (2.43)$$

The result of this is that

$$\sigma_2 \mathcal{Y}_{\kappa}^{\mu*} = i(-1)^{l-j+\mu} \mathcal{Y}_{\kappa}^{-\mu}. \quad (2.44)$$

Since $f(r)$ and $g(r)$ are defined so that they are real, this makes the conjugate wave function

$$(q_\kappa^\mu)^c(\mathbf{r}) = (-1)^{l-j+\mu+1} \begin{pmatrix} -ig^c(r) \mathcal{Y}_{-\kappa}^{-\mu} \\ f^c(r) \mathcal{Y}_{\kappa}^{-\mu} \end{pmatrix}. \quad (2.45)$$

Up to a phase, the charge conjugate antiquark wave functions may be formed by replacing $-if$ for g , $-ig$ for f , $-\kappa$ for κ and $-\mu$ for μ in the quark wave functions.

The opposite time evolution makes the radial equations for the antiquark become

$$\begin{aligned} \frac{dg^c(r)}{dr} + \frac{1-\kappa}{r} g^c(r) + (\omega_q + S(r) - m) f^c(r) &= 0, \\ \frac{df^c(r)}{dr} + \frac{1+\kappa}{r} f^c(r) - (\omega_q + S(r) + m) g^c(r) &= 0. \end{aligned} \quad (2.46)$$

Thus the radial functions have the same regular solutions found previously, but with the opposite sign for $\omega = \omega_q R$. ($S(r)$ also changes sign, but it is zero inside the bag, so this has no effect.)

2.2.3 Quark and antiquark currents

If we let $q_2(x)$ and $q_1(x)$ represent wave functions of either quark or antiquark of type 1 and 2 at space-time point x , the color current is

$$j_{a21}^\mu(x) = \bar{q}_2(x) \gamma^\mu \frac{\lambda_a}{2} q_1(x). \quad (2.47)$$

The wave functions labeled 1 and 2 in the current may have different values of κ , μ , radial mode x_q , and color, and may be any combination of quark or antiquark, but the initial and final flavor remains the same. Two currents and a gluon propagator are integrated (over all space-time locations for each vertex) to calculate an OGE interactions.

2.3 Confined gluons in Coulomb gauge

The gluon propagator couples one quark current at the space-time point x to another current at the space-time point x' . The gluon propagator in Coulomb gauge[2] may be separated into longitudinal and transverse parts.

2.3.1 Longitudinal gluon modes

The longitudinal propagator couples the two points at the same instant in time.

$$D_{ab}^{long}(x, x') = \delta(t - t') \delta_{ab} G(\mathbf{r}, \mathbf{r}'), \quad (2.48)$$

where a and b are octet color indices. $G(\mathbf{r}, \mathbf{r}')$ must be symmetrical in \mathbf{r} and \mathbf{r}' . The Green's function satisfies $-\nabla^2 G(\mathbf{r}, \mathbf{r}') = \delta^3(\mathbf{r}, \mathbf{r}')$ inside the sphere, and the inhomogeneous Neumann boundary condition is

$$-\hat{n} \cdot \nabla G(\mathbf{r}, \mathbf{r}') = A^{-1} \quad (2.49)$$

for \mathbf{r} on the surface and \mathbf{r}' inside the bag, where \hat{n} is normal to the surface and A is the surface area of the bag. These conditions specify $G(\mathbf{r}, \mathbf{r}')$ up to an additive constant. (Adding a constant would not change the results for a color singlet hadron[2].) For a fixed spherical bag of radius R , the instantaneous confined Green's function is

$$G(\mathbf{r}, \mathbf{r}') = (4\pi)^{-1} \left[\frac{1}{|\mathbf{r} - \mathbf{r}'|} + \sum_{l=1}^{\infty} \frac{l+1}{lR} \left(\frac{r r'}{R^2} \right)^l P_l(\cos \theta) \right], \quad (2.50)$$

where θ is the angle subtended by \mathbf{r} and \mathbf{r}' as viewed from the origin.

The multipole expansion for the Green's function inside the bag is

$$G(\mathbf{r}, \mathbf{r}') = \frac{1}{r_{>}} Y_{00}(\Omega') Y_{00}(\Omega) + \sum_{l=1}^{\infty} \sum_{m=-l}^l (-1)^m \frac{1}{2l+1} \left[\frac{r_{<}^l}{r_{>}^{l+1}} + \frac{l+1}{lR} \left(\frac{rr'}{R^2} \right)^l \right] Y_{l,-m}(\Omega') Y_{lm}(\Omega), \quad (2.51)$$

where the first term is the monopole part, and the l -sum is over higher multipoles. We include terms through $l = 4$ (hexadecapole) in our calculations. The monopole terms give the largest contribution, with contributions from higher multipoles decreasing rapidly with l .

2.3.2 Transverse gluon modes

The transverse part of the gluon propagator is calculated by doing a mode sum over transverse quantum modes. The solution for magnetic and electric modes in a fixed rigid spherical cavity may be expressed in terms of a scalar field satisfying the Hemholtz wave equation[2, 100],

$$\nabla^2 \Phi^r + k^2 \Phi^r = 0. \quad (2.52)$$

Solutions of this scalar equation are given by

$$\Phi_{klm}^r(\mathbf{r}) = N^r j_l(kr) Y_{lm}(\Omega). \quad (2.53)$$

The TE modes are given by

$$A_{klm}^{\text{TE}}(\mathbf{r}) = \nabla \times (\mathbf{r} \Phi_{klm}^{\text{TE}}), \quad (2.54)$$

which satisfies the boundary condition

$$\frac{d}{dr} \left[r j_l(kr) \right]_{r=R} = 0. \quad (2.55)$$

The TM modes are given by

$$A_{klm}^{\text{TM}}(\mathbf{r}) = \nabla \times [\nabla \times (\mathbf{r} \Phi_{klm}^{\text{TM}})]. \quad (2.56)$$

with boundary condition

$$j_l(kr)|_{r=R} = 0. \quad (2.57)$$

The normalization constant N^τ for τ representing TE or TM is chosen so that

$$\int_0^R d^3\mathbf{r} |A_{klm}^\tau|^2 = 1. \quad (2.58)$$

The transverse Feynman propagator is

$$D_{ab}^{tran}(x, x') = \delta_{ab} \sum_{\tau klm} (2k)^{-1} \begin{cases} A_{klm}^\tau(\mathbf{r}) A_{klm}^{\tau*}(\mathbf{r}') e^{-i k(t-t')} & \text{for } t > t' \\ A_{klm}^{\tau*}(\mathbf{r}) A_{klm}^\tau(\mathbf{r}') e^{-i k(t'-t)} & \text{for } t < t' \end{cases} \quad (2.59)$$

To evaluate the TE and TM gluon vector potentials, we express $\mathbf{r}\phi$ in terms of vector spherical harmonics, using the formula[102]

$$\hat{\mathbf{r}}Y_{lm} = -\sqrt{\frac{l+1}{2l+1}} \mathbf{Y}_{l+1\ l\ m}(\theta, \phi) + \sqrt{\frac{l}{2l+1}} \mathbf{Y}_{l-1\ l\ m}(\theta, \phi). \quad (2.60)$$

The vector spherical harmonics are defined by

$$\mathbf{Y}_{J\ l\ M}(\theta, \phi) = \sum_{m, q} \langle l m\ 1 q | l\ 1\ J M \rangle Y_l^m(\theta, \phi) \mathbf{e}_q, \quad (2.61)$$

where the spherical unit vectors are defined in terms of Cartesian unit vectors,

$$\mathbf{e}_{+1} = -\frac{1}{\sqrt{2}}(\mathbf{e}_x + i\mathbf{e}_y), \quad \mathbf{e}_0 = \mathbf{e}_z, \quad \text{and} \quad \mathbf{e}_{-1} = \frac{1}{\sqrt{2}}(\mathbf{e}_x - i\mathbf{e}_y). \quad (2.62)$$

The vector spherical harmonics are orthonormal in J , l , and M , with

$$\int_0^{2\pi} \int_0^\pi \mathbf{Y}_{J\ l\ M}^*(\theta, \phi) \mathbf{Y}_{J'\ l'\ M'}(\theta, \phi) \sin(\theta) d\theta d\phi = \delta_{JJ'} \delta_{ll'} \delta_{MM'}. \quad (2.63)$$

We use the curl formulae[102]

$$\begin{aligned} \nabla \times (\Phi(r) \mathbf{Y}_{l+1\ l\ m}(\theta, \phi)) &= i\left(\frac{d}{dr} + \frac{l+2}{r}\right) \Phi \sqrt{\frac{l}{2l+1}} \mathbf{Y}_{l\ l\ m}, \\ \nabla \times (\Phi(r) \mathbf{Y}_{l\ l\ m}(\theta, \phi)) &= \\ i\left(\frac{d}{dr} - \frac{l}{r}\right) \Phi \sqrt{\frac{l}{2l+1}} \mathbf{Y}_{l+1\ l\ m} &+ i\left(\frac{d}{dr} + \frac{l+1}{r}\right) \Phi \sqrt{\frac{l+1}{2l+1}} \mathbf{Y}_{l-1\ l\ m}, \\ \nabla \times (\Phi(r) \mathbf{Y}_{l-1\ l\ m}(\theta, \phi)) &= i\left(\frac{d}{dr} - \frac{l-1}{r}\right) \Phi \sqrt{\frac{l+1}{2l+1}} \mathbf{Y}_{l\ l\ m}. \end{aligned} \quad (2.64)$$

and the spherical Bessel function recursion relation[56]

$$\frac{d}{dz} j_l(z) = \frac{1}{2l+1} [l j_{l-1}(z) - (l+1) j_{l+1}(z)]. \quad (2.65)$$

to substitute these in the expressions for the TE and TM gluon vector potential.

After lengthy but straight-forward simplification, the TE modes are found to be[103, 4]

$$A_{klm}^{\text{TE}}(\mathbf{r}) = -i N^{\text{TE}} j_l(kr) \sqrt{l(l+1)} Y_{llm}, \quad (2.66)$$

with k for TE modes determined by the boundary condition of equation 2.54. The TM modes are

$$A_{klm}^{\text{TM}}(\mathbf{r}) = N^{\text{TM}} k l \sqrt{\frac{l+1}{2l+1}} \left(\sqrt{\frac{l+1}{l}} j_{l-1}(kr) Y_{l-1\ l-1\ m} - j_{l+1}(kr) Y_{l+1\ l+1\ m} \right), \quad (2.67)$$

with k for TM modes given by equation 2.57. The TE and TM radial equations have discrete solutions rising without limit. We calculate the transverse modes by doing a sum over the first five gluon eigenmodes in the cavity. This typically gives convergence to better than one part in a thousand. With the transverse quark-gluon vertex interaction given by $\hat{j} \cdot \hat{A}^T$, the transverse one-gluon exchange energy contribution to the ground state ϕ in perturbation theory is

$$\Delta E = \sum_n \langle \phi | H_I | n \rangle \frac{1}{E_\phi - E_n} \langle n | H_I | \phi \rangle. \quad (2.68)$$

The intermediate states $|n\rangle$ include each of the multi-quark states up to our energy cutoff plus one TE or TM gluon. This sum includes forward and backward propagating gluons, up to the fifth radial gluon mode. The interaction between two quarks (and/or antiquarks) p and q , involving states 1, 2, 3, and 4 (with i, j spatial indices) is

$$\Delta E_{1234}^{pq} = g_s^2 \int dx dx' j_a^p i_2(x) \sum_{\tau, k} \frac{\delta_{ab}}{2k} \left(\frac{A_k^{\tau i*}(x) A_k^{\tau j}(x')}{\omega_1 + k - \omega_2} + \frac{A_k^{\tau i}(x) A_k^{\tau j*}(x')}{\omega_3 + k - \omega_4} \right) j_b^q j_{34}(x'). \quad (2.69)$$

2.3.3 Color and spin sums

The longitudinal and transverse energy shift expressions include a sum over octet colors a of $\langle \lambda_a | \lambda_a \rangle$, since each current includes a λ matrix. Letting c_m be the color

of particle q_m , the color sum is

$$\langle \lambda_a | \lambda_a \rangle = \langle c_4 | \lambda_a | c_3 \rangle \langle c_2 | \lambda_a | c_1 \rangle = \begin{cases} 4/3 & \text{if } c_4 = c_3 = c_2 = c_1, \\ -2/3 & \text{if } c_4 = c_3 \neq c_2 = c_1, \\ 2 & \text{if } c_4 = c_1 \neq c_3 = c_2, \\ 0 & \text{otherwise.} \end{cases} \quad (2.70)$$

Each current also carries angular momentum, resulting in a spin sum for each OGE interaction. For transitions between $J = 1/2$ states, the spin sum is just the expectation of $\langle \sigma_i | \sigma_i \rangle$. For higher angular momenta, we construct a $(2J + 1)$ by $(2J' + 1)$ table for each gluon multipole in the $\hat{j} \cdot \hat{A}$ interaction. We calculate these spin sum tables by explicitly doing the angular integrals for each J_z value for initial and final (anti-)quark with each multipole of the vector potential. We then repeat the calculations with the complex conjugate vector potential. One table entry is used for each quark-gluon vertex in calculating the OGE interaction. Our approach gives results equivalent to the multipole transition matrix (MTM) approach of Wroldsen and Myhrer[5].

We compare our energy shift, ΔE , from our mode sums to the $\mathbf{E}^2 - \mathbf{B}^2$ energies calculated by Wroldsen and Myhrer[5], as corrected by Umino and Myhrer[83]. We get the same results for the OGE interactions as they do, although our calculational approach is quite different. We also agree with the vertex integrals calculated by Close and Monaghan[4], where they used the mode sum approach that we adopt.

Chapter 3

MULTI-QUARK STATES

3.1 Introduction

We build our many-body basis states from the product of independent single confined quark and antiquark wave functions. The OGE interaction involves pair-wise coupling of quark and/or antiquark currents, as discussed in the previous chapter. This includes a sum over time orderings of the two vertices in the interaction. The many-body OGE interaction between basis states involves the sum over all pairings of currents, with one current taken from each basis state.

There are several approximations implicit in this procedure. The interaction in principle should act to distort the single particle wave functions. It is also an approximation to take the many-body interaction as a sum of two-body interactions. (Perturbative QCD includes three and four gluon vertices which are ignored in the OGE approximation.) The OGE interaction assumes only one gluon is in the bag at any time, which truncates the full theory, as does the assumption of an energy cutoff, and also the use of a finite number of gluon modes in the mode sum.

If two or more gluons were included as part of the basis, they could combine as a color singlet and would in principle be inseparable from the confinement mechanism we already have assumed by imposing the bag boundary conditions. There is no double counting if single gluons are allowed, since gluons carry octet color, and the bag boundary condition is colorless. Our assumption that basis states are made only of quarks and antiquarks is consistent with having at most one gluon in the bag at a time, but it further restricts the theory. Before we turn on the gluon interaction, the quark energies are given by the Dirac equation, with H_0 given by Eq. 2.16. The interaction of gluons with quarks is given by $\hat{H}_I = \hat{j} \cdot \hat{A}$. This includes gluon scattering off quarks, quark pair creation, and pair annihilation diagrams. Beginning with a three-quark state with quantum numbers of a baryon, we have a Fock space

that only includes states with odd numbers of particles.

$$\psi = qqq + qqqq\bar{q} + qqqqq\bar{q}\bar{q} \cdots \quad (3.1)$$

The OGE interaction links the three-particle sector to itself and with the five-particle sector, but not directly to the seven-particle sector.

The Goldstone formula[104] gives the ground-state energy shift of a many body system. He showed that disconnected diagrams cancel to all orders, and that the energy shift is given by the sum over connected diagrams,

$$E - E_0 = \langle \Phi_0 | \hat{H}_I \sum_{n=0}^{\infty} \left(\frac{1}{E_0 - \hat{H}_0} \hat{H}_I \right)^n | \Phi_0 \rangle_{\text{connected}}, \quad (3.2)$$

where \hat{H}_0 and \hat{H}_I are time-independent operators in the Schrödinger representation, and E_0 is the unperturbed multi-quark ground state energy. The even powers of \hat{H}_I corresponding to odd n are included in diagonalization of the OGE interaction. However, odd powers of $\hat{H}_I = \hat{j} \cdot \hat{A}$ (for n even) lead to no overlap with the ground state if the ground state is not allowed to contain gluons as well as quarks.

Our multi-quark states are like shell-model states built from localized single particle wave functions. This gives rise to problems with spurious center-of-mass energy and spurious states in the excitation spectrum. It is difficult to provide a proper correction for the MIT bag center-of-mass energy, as the expectation $\langle \hat{p}^2 \rangle$ in the bag is infinite since the upper and lower components of the Dirac equation are nonzero just inside the bag boundary, and zero outside. Also, the center-of-mass operator is not tractable in a relativistic theory[8]. Approximate methods using momentum projection and boosts have been used quite successfully in soliton bag models[8, 65], where the boundary conditions are not as abrupt as with the MIT model.

In 1980, Donoghue and Johnson[125] introduced an “improved static bag model” which identifies a specific form of momentum-space wave packet, associated with a superposition of bag states, which allows first order center-of-mass corrections to be made for the MIT model. The corrections were most significant in lowering the mass of the bag model pion, but are smaller for the heavier baryons. To derive the wave packet, they started with the vacuum to π matrix element,

$$\langle 0 | \bar{u}(x) \gamma^\mu \gamma_5 d(x) | \pi(p) \rangle = i\sqrt{2} F_\pi p^\mu e^{ip \cdot x}. \quad (3.3)$$

They identified the unknown bag model pion wave packet $\phi(p)$ as responsible for (the time component of) this matrix element.

$$\langle 0 | \bar{u}(x) \gamma^0 \gamma_5 d(x) | \pi(p) \rangle_B = i \frac{F_\pi}{\sqrt{2}} \int d^3 p e^{ip \cdot x} \phi(p). \quad (3.4)$$

Using static bag wave functions, the left hand side is

$$\langle 0 | \bar{u}(x) \gamma^0 \gamma_5 d(x) | \pi(p) \rangle_B = i \sqrt{6} [u^2(x) - l^2(x)], \quad (3.5)$$

where $u(x)$ and $l(x)$ represent the upper and lower wave function components respectively. Thus

$$\phi(p) = \frac{2\sqrt{3}}{F_\pi} \int \frac{d^3 x}{(2\pi)^3} e^{-ip \cdot x} (u^2(x) - l^2(x)), \quad (3.6)$$

where F_π is determined by normalization of $\phi(p)$,

$$\int \frac{d^3 p}{2\omega_p} (2\pi)^3 |\phi(p)|^2 = 1. \quad (3.7)$$

In the limit $m_\pi \rightarrow 0$, $F_\pi = 0.501/R$. With a pion bag radius $R_\pi = 0.7$ fm, this would make $F_\pi = 141$ MeV, reasonably close to the experimental values[1] of $f_{\pi^+} = 130.7$ MeV and $f_{\pi^0} = 119$ MeV.

The wave packet $\phi(p)$ has the desirable feature of no discontinuity at the boundary, since $u^2(x) - l^2(x) \rightarrow 0$ as the bag surface is approached, making the $\langle p^2 \rangle$ expectation finite. This expression for $\phi(p)$ was also utilized for baryons, with corrections to g_A , μ , and $\langle r^2 \rangle$ calculated. However, we question the justification for extension of this form of wave packet to the baryons, other than the convenience of making a finite $\langle p^2 \rangle$ expectation, as the baryons are not linked to the vacuum by pseudo-scalar matrix elements. However, in Ch. 6, we will discuss approximate corrections to observables this model would imply if this form of wave packet was utilized.

Our goal is to diagonalize the OGE interaction among all many-body basis states with quantum numbers of the proton, below some energy cutoff. The maximum cutoff we consider is 1.5 GeV above the qqq ground state (where all quarks are in the $s_{1/2}$ state). Diagonalization effectively includes all iterations of the interaction. The lowest eigenvalue corresponds to the shifted ground state energy in the presence of the interaction. The associated eigenvector gives the configuration mixing. If we

interpret \hat{H}_I in the Goldstone formula to be the full OGE interaction, then the sum in the Goldstone formula is equivalent to diagonalizing the matrix.

We want to construct orthonormal many-body basis states. To do this, we first classify states by their symmetries. We use Young tableaux to construct template wave functions corresponding to each symmetry type. In the qqq sector, each symmetry corresponds to a single template basis state. But in the $qqqq\bar{q}$ sector, up to three distinct template basis states are possible for each symmetry. The template basis states are orthogonalized exactly using a Gramm-Schmidt approach. These orthonormal templates for the different symmetry types are utilized to rapidly construct all orthonormal quark (and antiquark) basis states. This is done by finding the symmetry type of each multi-particle quark configuration, and plugging these configurations into the corresponding types of templates for the wave functions to generate the orthonormal states.

3.1.1 States below cutoff

To diagonalize the OGE interaction, we construct a complete set of orthonormal states which preserves the nucleon quantum numbers, subject to our energy cutoff. The cutoff determines the states we allow in our basis. We start with the nucleon, and allow all multi-quark states with the nucleon quantum numbers up to the energy of our cutoff. For other baryons, these same states (with one quark flavor and mass substituted for another) are included, even though this makes a small increase in the energy of the cutoff for these particles. The states must be color singlet with overall Fermionic anti-symmetry. The z-components of angular momentum (μ) of the quarks forming each basis state must add to $1/2$ and be aligned with the ground state nucleon spin, and the parity of the state must be even. The parity of single-quark states is $(-1)^l$, so a qqq state must have an even number of odd- l excitations. An antiquark has odd intrinsic parity, so a $qqqq\bar{q}$ state requires an odd number of odd- l excitations if it is to mix with the nucleon ground state. Quark flavors are conserved—pair creation or annihilation must involve quark and antiquark of the same flavor. The energy cutoff constrains the maximum quark excitation in the qqq sector to be $f_{7/2}$. Radial excitations up to $n = 3$ are allowed for $s_{1/2}$ quarks, and $n = 2$ excitations for $p_{3/2}$, $p_{1/2}$, and $d_{3/2}$ quarks with this cutoff. In the $qqqq\bar{q}$ sector, a single quark or antiquark must be excited to a $p_{3/2}$ or $p_{1/2}$ level to conserve parity, and these are the

highest excitations allowed by the cutoff.

Considering these constraints, there are 467 ways that three quark energies, μ 's and flavors may be combined to form qqq (non-color) basis configurations below the 1.5 GeV cutoff. This includes 442 cases where all three quarks have distinct non-color quantum numbers (type 1), and 25 cases where two of the three quarks have the same quantum numbers, except for color (type 2). In addition, there are 168 non-color basis configurations in the $qqqq\bar{q}$ sector. Of these, there are 69 cases where all four quarks are distinct (type 3), 86 cases where two quarks are identical except for color (type 4), 8 cases where three quarks are identical except for color (type 5), and 5 cases where there are two pairs of identical quarks, except for color (type 6). The configurations which contribute significantly to the neutron ground state are listed in Tables A.1-A.3, along with the energies of each configuration in units of $1/R = 200$ MeV. (This table is based on quark masses of $m_u = 0$, $m_d = 5$ MeV, and $m_s = 279$ MeV.)

We work in the m - (or μ)-representation, and our basis states can also be used to construct states with angular momentum (J) and isospin (I) different from the nucleon. Thus the H matrix is in principle reducible to block diagonal form. However, the eigenvectors found by diagonalizing the matrix do not mix states of different J or I . Thus when we diagonalize the Hamiltonian acting on our basis states, some of the eigenvectors correspond to nucleons, and some to Δ states. This allows us to easily determine the $\Delta - N$ splitting. The Δ energy found by this method is not quite correct as it exists in a bag with a bag radius R optimized for the nucleon rather than the Δ . We will introduce an R -dependent linear correction to the Δ energy to achieve a better estimate of the $\Delta - N$ splitting. To calculate the correction, we calculate and diagonalize the matrix elements for two values of R . This allows us to interpolate to a new radius for the Δ where it is in equilibrium with the same bag constant B as used for the nucleon.

3.1.2 Symmetries

Quarks, being Fermions, must be antisymmetric under interchange. To form a baryon from quarks (and antiquarks) as an antisymmetric singlet state, the color symmetry and the symmetry of all other quantum numbers combined must correspond to conjugate Young diagrams[105]. We will make use of quite rigorous experimental evidence

that hadrons are only found as color singlets.

We first examine the case of three-quark configurations. There is only one independent way to arrange three colors in an $SU(3)$ singlet. The antisymmetric singlet is represented by a Young diagram with three boxes arranged vertically. If we arrange the colors in a definite order, introducing a minus sign for each color interchange, the six antisymmetric terms collapse to a single normal-ordered term.

The Young diagram conjugate to three vertical boxes has three boxes arranged horizontally. The other quantum numbers must combine symmetrically, corresponding to the three horizontal boxes. These non-color quantum numbers are specified in our spherically symmetric system by flavor, energy level and the z -component of angular momentum, μ , for each quark and/or antiquark. The energy level includes information on the radial excitation, n , the Dirac quantum number, κ , and it also depends on the quark mass and bag radius.

The non-color symmetrization involves fewer configurations if more than one quark has identical non-color quantum numbers. For example, with three objects, the symmetric combination of different objects involves six terms. But if two or three objects are identical, the symmetric combination has three or one term respectively. Thus we group quark configurations into symmetry types based on the number of identical quarks (without respect to color).

We generate the wave functions symbolically by placing three different symbols to represent colors into the color Young diagram, then expand by symmetrizing between rows, followed by antisymmetrization on columns. The same type of procedure is followed for the non-color variables, using as many symbols as there are particles with different non-color quantum numbers. Then we take the direct product of color and non-color symmetries to find the wave function. Many terms cancel and combine when we bring all the terms into normal order. This procedure is repeated for all standard and non-standard arrangements of variables in the Young diagram boxes. Many of the states formed by this procedure are duplicates, but soon one finds states that span the whole space for each choice of non-color symmetries. We then use Gram-Schmidt orthogonalization to generate orthonormal template states. By replacing the template variables with the actual quark quantum numbers corresponding to configurations of the same symmetry type, we generate all the orthonormal quark states.

In the qqq sector, a single template orthonormal state is found for each possible symmetry type of non-color quantum numbers. For example, if all three quarks have different quantum numbers, the template may be written as the normalized symmetrization of variables (a,b,c). As described above, these templates are derived by taking the direct product of color and non-color symmetries for each symmetry type—all three quarks having different non-color quantum numbers, or two quarks the same. The expansion is simplified by normal ordering in color, with a minus sign for each quark exchange. For three quarks with distinct non-color quantum numbers (type 1), the template state includes six normal-ordered configurations. If two quarks have identical non-color quantum numbers (type 2), the template state is built from three normal-ordered configurations. Only one configuration would describe the state of three quarks with identical non-color quantum numbers. However, this is not a possibility for hadrons where two quark flavors contribute to the wave function, as in the case of the nucleon.

By similar construction, four quarks may be combined with an antiquark to form a $qqqq\bar{q}$ color singlet, with a conjugate symmetry for the non-color quantum numbers. As before, each quark color is mapped to a single box. The anti-color is expressed in the color space as two boxes arranged vertically representing antisymmetrization of the two colors complementary to the anti-color. These six boxes may be arranged as a color singlet only by forming boxes two columns wide by three boxes high. Three standard arrangements for this color Young diagram may be formed by numbering the boxes in standard order. If this was the only wave function symmetry, there would be $3^2 = 9$ ways[106] to construct the color wave function for four quarks and one antiquark. However, the non-color symmetries place constraints on the form of the wave function. We must take the direct product of color and non-color symmetries to define the possible wave functions, and we find there are 1-3 wave functions for each $qqqq\bar{q}$ configuration, depending on symmetry type.

For $qqqq\bar{q}$ configurations, the conjugate Young diagram for non-color symmetries is given by boxes three wide by two high. Taking the direct product of color and non-color symmetries, the number of orthonormal states that are generated depends on the symmetry type of the non-color quantum numbers. Three template orthonormal states may be formed if all four quarks are distinct in the non-color quantum numbers (type 3). These three states are built from 36 normal-ordered configurations.

There are two template orthonormal states when two of the four quarks are identical (type 4). These two states are built from 15 normal-ordered configurations. One template state is built from three normal-ordered configurations if three of the four quarks are identical (type 5). If there are two pairs of quarks with identical non-color quantum numbers (type 6), a single template state is built from six normal-ordered configurations. This exhausts the possibilities consistent with the Pauli exclusion principle.

Normal ordering still involves a sign change for every quark exchange. The color, being anti-symmetric, introduces a sign change for interchanges between quarks of different color, but not for quarks of the same color. But the conjugate non-color symmetry has an anti-symmetric column for every symmetric color row representing quarks of the same color. This brings in the sign changes where necessary to make all quarks odd under interchange.

Applying the templates described above to the list of qqq and $qqqq\bar{q}$ non-color configurations, we find a total of 859 orthonormal states involving 6555 normal ordered configurations within the Fock space truncated 1.5 GeV above the qqq ground state.

Chapter 4

NUCLEON CONFIGURATION MIXING AND GROUND STATE ENERGIES

We diagonalize the matrix of OGE interactions between ortho-normal basis states to calculate the non-perturbative ground-state energy and configuration mixing for the proton and neutron. We do this for various choices of model parameters, beginning with the first parameter set of DeGrand *et al.*[54], who made several fits to the hadron mass spectra using the MIT bag model. We examine the effect of varying the quark masses, the bag radii, the self-energy prescription, and the energy cutoff, which determines the number of basis states in our matrix. We also examine other parameter cuts, where we vary the maximum gluon multipole in the OGE interactions, and we examine the errors in truncating the mode sum after different numbers of terms.

4.1 Assembly of the OGE interaction matrix

Much of our computation is done symbolically so we can verify that our OGE interactions (which include color and spin sums) are coming out correctly, and to allow for substitution of interactions using different parameters without having to start from the beginning. We also use our symbolic intermediate results as a starting point to calculate ground state properties of other baryons besides the nucleons. To do this, we substitute one quark flavor for another in the symbolic expressions to calculate results for the p , n , Σ^+ , Σ^- , Ξ^0 and Ξ^- . All these particles are built from two quarks of one flavor, and a third quark of a different flavor. These results will be presented in a subsequent chapter. We do not calculate mass and mixing for Σ^0 and Λ particles in this study, as their wave functions have different structures. They contain u , d , and s flavors, so they would require different sets of basis states patterned only after types 1, 3, and 4 template wave functions, where at most two quarks could have identical non-color quantum numbers in the $qqqq\bar{q}$ sector.

Although our matrix is ultimately formed from OGE matrix elements between orthonormal color-singlet states, it is expedient to first calculate the OGE interactions

between all normal-ordered (non-color-singlet) multi-quark configurations. This eliminates redundant calculations where the same multi-quark configuration contribute to as many as three different orthonormal states. After finding all multi-quark configurations, we organize them by type. (The most important configurations are listed in Tables A.1 - A.3). We only have to calculate the normal ordered configurations that are in the union of configurations making up the orthonormal quark template states of each type. For example, each type 5 $qqqq\bar{q}$ configuration forms three orthonormal color-singlet states, built respectively from 30, 30, and 18 normal-ordered configurations. Taking the union of these configurations, there are 36 normal-ordered configurations to calculate. These 36 configurations exhaust all possible color assignments of four quarks (with distinct non-color quantum numbers) and one antiquark to make configurations with no net color. (In this case, all possible assignments are trivially consistent with the Pauli principle). We label each antiquark by the two colors complementary to its anti-color, just as we used the two color representation for an anti-color when considering the Young symmetries. Each $qqqq\bar{q}$ configuration fills a 3 by 2 table (two positions for each of three colors), where the two positions labeling the antiquark must have different colors. The configurations are arranged in normal order by sorting the six positions into normal color order, then by sorting the entries within each color, introducing a minus sign for every quark exchange. All configurations where two quarks have the same quantum numbers including color are automatically excluded.

We represent each OGE interaction between two configurations by four symbols, a color factor, and a sign. The first symbol is a character string representing the gluon parity (combining information about the gluon type and multipole), the first quark's flavor and time path, along with its initial and final energy levels, and the second quark's flavor and time path, with its initial and final energy levels. The time path information tells if the gluon couples to a quark, an antiquark, or creates or destroys a pair. The second and third symbols represent spin-sum values, which depend on the gluon angular momentum and the angular momentum changes for the two quark currents, respectively. Each spin sum symbol is a character string indicating emission or absorption of the gluon (which depends on the time ordering), the particle/anti-particle character of initial and final quark, the initial and final angular momenta of the quark current, and the initial and final z-components (μ 's) of angular momentum.

The fourth symbol and sign represent the normal-ordered multi-quark configuration which results from normal ordering the quarks after two of them are subjected to the interaction. This symbol includes the type of non-color configuration (ranging from 1-5), the number of the non-color multi-quark configuration within that type (ranging from 1-442), and the number of the color configuration for that type (ranging from 1-36). Finally, the color sum is determined by the initial and final colors of the two quark currents. It is calculated by summing over the eight λ matrices sandwiched between these colors, as given in Eq. 2.70.

$$\begin{array}{c}
 \text{qq} \\
 \hline
 \begin{array}{c} b \quad r \\ | \quad | \\ \text{---} \\ | \quad | \\ r \quad b \\ 2 \end{array} \quad - \quad \begin{array}{c} b \quad \bar{b} \\ | \quad | \\ \text{---} \\ | \quad | \\ r \quad \bar{r} \\ -2 \end{array} \quad (-1) = \begin{array}{c} b \quad gr \\ | \quad | \\ \text{---} \\ | \quad | \\ \bar{r} \quad bg \\ 2 \end{array} (-1) \quad \text{From exchange.}
 \end{array}$$

$$\begin{array}{c}
 \begin{array}{c} b \quad b \\ | \quad | \\ \text{---} \\ | \quad | \\ b \quad b \\ 4/3 \end{array} \quad - \quad \begin{array}{c} b \quad \bar{b} \\ | \quad | \\ \text{---} \\ | \quad | \\ b \quad \bar{b} \\ -4/3 \end{array} \quad (-1) = \begin{array}{c} b \quad gr \\ | \quad | \\ \text{---} \\ | \quad | \\ b \quad gr \\ -2/3 \end{array} + \begin{array}{c} b \quad gr \\ | \quad | \\ \text{---} \\ | \quad | \\ b \quad gr \\ -2/3 \end{array}
 \end{array}$$

$$\begin{array}{c}
 \begin{array}{c} b \quad r \\ | \quad | \\ \text{---} \\ | \quad | \\ b \quad r \\ -2/3 \end{array} \quad - \quad \begin{array}{c} b \quad \bar{r} \\ | \quad | \\ \text{---} \\ | \quad | \\ b \quad \bar{r} \\ 2/3 \end{array} \quad (-1) = \begin{array}{c} b \quad bg \\ | \quad | \\ \text{---} \\ | \quad | \\ b \quad bg \\ 4/3 \end{array} + \begin{array}{c} b \quad bg \\ | \quad | \\ \text{---} \\ | \quad | \\ b \quad bg \\ -2/3 \end{array}
 \end{array}$$

Figure 4.1: Color sums for quark-quark and quark-antiquark OGE interactions

Color interactions involving antiquarks can be calculated in several equivalent ways. In the anti-color representation, the color factors of Eq. 2.70 can be used for each vertex except that a minus sign is introduced at each anti-particle vertex[98]. This is like the substitution $e \rightarrow -e$ used when calculating a vertex involving a positron rather than an electron in QED. Equivalent results are achieved by sum-

ming over all interactions involving the two colors complementary to the anti-color, using Eq. 2.70 without the minus sign. We use a sign convention where the two complementary colors which are substituted for the anti-color are arranged in cyclic order before normal ordering (which may introduce a minus sign). See Figure 4.1. This allows simple calculation of interactions in the $qqqq\bar{q}$ sector where quarks and antiquarks are normal ordered into six slots, two slots for each color. The antiquark takes up two slots of different color, with each entry treated as an interacting color. However, interactions between the two antiquark entries are self-interactions, which we calculate separately.

We next calculate numerical values for the vertex integrals, spin sums, and Coulomb Green's functions integrated between quark currents. We do the angular integrations by expanding the quark currents and gluon vector potentials in spherical harmonics. We use standard expressions[102] for the angular integrals over three Y_{lm} 's, evaluating them in terms of three-j symbols. For each multipole and time ordering of the TE and TM vector potential, we do the angular integrals, substituting all values for μ (the z-component of angular momentum) for each wave function contributing to the currents. We extract the spin sum tables, indexed by the angular momenta, μ 's and time orderings from the ratio of these vertex integrals integrated over the angular variables. This reduces the number of numerical radial integrals required for different combinations of μ 's that enter into the two currents for each OGE interaction. In doing the numerical radial part of the vertex integrals, we set $\mu = 1/2$, and use the spin-sum factors to account for the angular-momentum changes.

To calculate the radial integrals, we first find the eigenvalues and normalizations for the gluons (Eqs. 2.58, 2.57, and 2.54) and quark modes (Eqs. 2.37, 2.36, and 2.34) for all combinations of quark mass, bag radius, and allowed κ . These are substituted in the equations for the currents and vector potentials to calculate the TM and TE $\int j \cdot A$ vertex integrals and in the integrals over the currents with the Coulomb propagator, using Eqs. 2.48 and 2.51. The Coulomb terms are four-point functions, so require iteration through all combinations of the wave functions on four legs consistent with conservation of the quantum numbers, as well as iteration over mass combinations and Coulomb multipoles. The vertex integrals require less work as each one involves only two wave functions, TE or TM multipoles from 1-4, and a single quark mass for each flavor.

These pieces are combined and substituted for each symbolic expression in the calculation of the OGE interaction between quark configurations. The symbolic expressions are used repeatedly for each multipole order, but have different entries in each case. If the parity changes between initial and final wave functions in each quark current, the vertex symbol represents a TM mode sum of gluons if the multipole is odd, or a TE mode sum if the multipole is even (and vice versa if the parity does not change). Given a multipole, the spin sums are looked up from tables we calculated for each gluon time ordering, indexed by the μ 's of initial and final quarks for each current. There are different spin sum tables for the different graphs having different time ordering of the quark lines. The spin sums multiply the vertex element symbol which also depends on time ordering through the energy denominators. For each multipole, the vertex element symbol equals a Coulomb term added to a sum (over five gluon modes) of the product of two vertex integrals, each with different energy denominators. This is done separately for forward and backward time-ordered graphs. Energies in the denominators are measured from the qqq ground state energy. (See Appendix C for an example of how matrix elements are calculated.) Symbols representing the final configurations are utilized to avoid huge sparse matrices, as there are 6555 normal ordered configurations. For each projection of a configuration onto a final color-singlet state, these symbols are assigned the weights derived from generating the orthonormal template wave functions. Then weighted combinations of initial configurations allow generation of all OGE interactions between orthonormal color-singlet states.

The four graphs corresponding to interactions between quarks or antiquarks, pair creation, pair annihilation, and annihilation followed by creation are combined one multipole at a time. This is done so that we can examine the effect of truncating as a function of multipole. The multipoles are then summed together. The self-energy (using one of several prescriptions) is added to the energy of each color-singlet state for each diagonal matrix element. Finally this matrix is diagonalized to find the energies and configuration mixing of the lowest states.

4.2 Model assumptions

We examine the sensitivity of our calculations to different model assumptions. The model parameters are the bag constant B , strong coupling constant α_s , the coefficient

Z_0 of the Casimir term $E_C = Z_0/R$ (we assume a positive sign for Z_0), and the quark masses. We will use $m_u = 0$, $m_d = 5$ MeV, and $m_s = 279$ MeV or 300 MeV. We fit the bag parameters to reproduce experimental values for the neutron mass and the $\Delta - N$ splitting for several values of the bag constant and strange quark mass. This allows us to see what range of predictions are possible from the MIT bag model. We predict masses of other ground and excited state octet baryons. We also look at predictions for magnetic moments, g_A/g_V , charge radius, and other particle properties. The configuration mixing we find also has implications for observables that have not been measured. We make a fit to the Casimir energy term, which turns out to be positive rather than negative as in the MIT model. Thus we agree with theoretical calculations[111, 116, 117] for the sign, but not the magnitude, of the Casimir term, as discussed below. These calculations include a quadratic divergence that can only be canceled by a contact term of the form $\sim FR$, where F is a constant and R is the bag radius. We make a second fit to the hadron mass spectrum assuming Z_0 fixed at the theoretical (positive) value for the Casimir energy, allowing the new parameter F to vary. This turns out to be unsuccessful, as a negative value for B is required, making the bag unstable.

4.2.1 Quark masses, bag constant, and self-energy prescriptions

We diagonalize the OGE interaction with several choices for quark masses, bag radii and self-energy prescriptions, as well as with different energy cutoffs. By doing calculations for several bag radii, we can interpolate to a suitable bag radius for each particle to make them all consistent with a given value of B . Our first parameter set is similar to the parameters found in the first fit to hadron masses by DeGrand *et al.*[54], with $m_u = 0$, $m_d = 5$ MeV (rather than DeGrand's $m_d = 0$), $m_s = 279$ MeV, and $B^{1/4} = 145$ MeV (which makes the nucleon bag radius $R = .005$ MeV⁻¹). We start with their value for the strong coupling, $\alpha_s = 2.2$, which they found gave the correct $\Delta - N$ splitting. However, they only included $s_{1/2}$ qqq quark states in their basis. When we truncate our Fock space to include only $s_{1/2}$ qqq quark states, our results agree with the $\Delta - N$ splitting they found. However, as we raise the cutoff to include more states in our basis, we find the $\Delta - N$ splitting increases rapidly at first, then tends to level off as the energy cutoff is raised to 1.5 GeV above the qqq ground state. The $\Delta - N$ splitting is increased by about 50%. The value is somewhat uncertain

because of dependence on precisely where the energy cut is made (See figure 4.2).

The self-energy would be infinite if all quark and gluon modes were included in the self-energy diagrams. Traditionally[54, 59], MIT calculations have only included a small subset of these diagrams. These previous papers included only the self-energy diagrams necessary to satisfy the MIT boundary conditions (Coulomb contributions to make the electric field tangential at the bag surface), and then only diagrams where the quark remained in the same state. It was argued that a substantial fraction of the self-energy was absorbed in renormalization of the quark masses. However, DeGrand *et al.* stated that a more consistent procedure would be to calculate the whole self-energy and perform the required renormalization. We call including only the diagrams necessary to meet the boundary conditions the minimal MIT prescription. We find that with this prescription, the ground-state energy does not appear to converge as the energy cutoff is raised and more states are added to the bag. Thus we are motivated to consider a more self-consistent approach to the self-energy. We repeat our calculations including a self-energy constructed from all vertices used in the OGE diagrams up to a given cutoff. We find that this does not solve the problem with convergence of the ground-state energy. It does reduce the size of the (positive) Casimir term toward the theoretical value, and reduces the value for m_s , but has little effect on the fits to the hadron mass spectrum.

4.2.2 Adjustment of α_s to maintain $\Delta - N$ splitting

With three valence $s_{1/2}$ quarks, the OGE interaction requires a large value for the strong coupling constant, $\alpha_s = 2.2$, to account for the $\Delta - N$ splitting. By including more states in our basis, we have to reduce the value of the strong coupling constant to keep the $\Delta - N$ splitting at the proper value. We find a value for $\alpha_s = 1.3636$ with the cutoff at 1.5 GeV above the qqq ground state gives the same splitting as $\alpha_s = 2.2$ when the cutoff only includes the qqq $s_{1/2}$ ground state. The value of the $\Delta - N$ splitting is found to be 308 MeV before making a correction for bag radius of the Δ . The Δ and N eigenvalues are found by matrix diagonalization with elements calculated for several bag radii, $R=0.005 \text{ MeV}^{-1}$ and $R=0.0045 \text{ MeV}^{-1}$. The nucleon and Δ require different bag radii to be consistent with a given bag constant B . The higher energy of the Δ relative to the nucleon requires a larger bag (which lowers the configuration mixing energy somewhat) for the bag pressure to be in equilibrium

with the field pressure. As discussed in Ch. 5, with the neutron radius at $R_n = 0.005 \text{ MeV}^{-1} = 0.987 \text{ fm}$, the Δ^0 radius is $R_{\Delta^0} = 0.0055 \text{ MeV}^{-1} = 1.082 \text{ fm}$. We use the asymptotic dependence of the energy on bag radius to interpolate to the proper radius for the Δ , (and all other baryons).

DeGrand *et al.* (in their first fit to hadron masses and other properties), found a Δ radius of $R=0.00548 \text{ MeV}^{-1}$ compared to the nucleon radius of $R=.005 \text{ MeV}^{-1}$. The larger radius reduces the Δ mass (proportional to $1/R$ for massless u and d quarks). Their masses for the proton and Δ were 938 MeV and 1236 MeV respectively, making a 298 MeV splitting. We find almost identical results to DeGrand *et al.* for the Δ corrected to have the same bag constant as the nucleon. When the nucleon radius is $R=0.005 \text{ MeV}^{-1}$, the bag constant is $B^{1/4}=145.8 \text{ MeV}$. Keeping B constant, we find the Δ radius is $R=0.00547 \text{ MeV}^{-1}$, almost identical to DeGrand *et al.*'s result. Experimentally[1], the proton and neutron masses are 938.27 MeV and 939.56 MeV respectively, and the Δ mass is 1230 to 1234 MeV ($\approx 1232 \text{ MeV}$). We have adjusted α_s until our radius-adjusted masses match the experimental $\Delta - N$ splitting.

The trend toward smaller values of the strong coupling constant is good. For three valence ($s_{1/2}$) quarks, a value of $\alpha_s = 2.2$ is needed to reproduce the $\Delta - N$ splitting. By the same measure, a value of $\alpha_s \simeq 1.4$ is needed at our maximum cutoff. (We choose quite precise values for α_s in matching the $\Delta - N$ splitting for our series of parameter fits so that we have a consistent basis for comparison between them. However, as noted before, there is considerable uncertainty in the proper value for α_s based on the variation we see in the splitting as we make successive cutoffs.) The value of α_s depends on the energy scale μ of interactions, running asymptotically as[123]

$$\alpha_s(\mu) = \frac{4\pi}{\beta_0 \ln(\mu^2/\Lambda^2)} \left[1 - \frac{2\beta_1}{\beta_0^2} \frac{\ln[\ln(\mu^2/\Lambda^2)]}{\ln(\mu^2/\Lambda^2)} + \mathcal{O}\left(\frac{\ln^2[\ln(\mu^2/\Lambda^2)]}{\ln^3(\mu^2/\Lambda^2)}\right) \right] \quad (4.1)$$

where $\beta_0 = 11 - \frac{2}{3}n_f$, $\beta_1 = 51 - \frac{19}{3}n_f$, with n_f the number of quark flavors below the energy scale μ .

Numerous measurements[123] have been made of α_s at different scales with $\alpha_s(M_Z) = 0.117 \pm 0.005$. Using terms through second order in inverse powers of $\ln(\mu)$, we run down from measurements at slightly less than 2 GeV to the $\sim 1 \text{ GeV}$ scale of the nucleon, using three quark flavors. From this we arrive at an estimate of $\alpha_s(1 \text{ GeV}) \sim 0.5 \pm .08$. The value for α_s we determined based on matching the

$\Delta - N$ splitting is consistent with not having reached convergence for the ground state energy. Based on the trend of figure 4.3, the value needed for α_s in the MIT bag model would drop further if higher values for the cutoff were chosen. Another factor that contributes to the larger-than-measured value for α_s in our model is that we attribute all the $\Delta - N$ splitting to OGE exchange effects, whereas part of the splitting could arise from interactions of the nucleons with a pion cloud and from interactions with multiple gluons that we have not included in our model.

4.2.3 Confinement in the spherical bag and the MIT Casimir term

The process of confinement of the quarks and gluons to a finite volume gives rise to zero-point quantum effects. Usually we neglect sums over zero modes, canceling this first of many infinite quantities by matching it with a counter term. But a cavity gives rise to a finite shift in the zero-point, or Casimir, energy. This offset is calculated by considering the perturbation of the zero modes by the confining region.

Inclusion of the negative Casimir term in the MIT bag model allowed for modeling of confined particles in agreement with their observed masses. DeGrand *et al.*[54] fit the hadron spectrum quite well with $E_0 = -Z_0/R = -1.38/R$. In hindsight, the expression used for the Casimir energy, $E_C = -Z_0/R$ was not fully justified. It was added because of the need to lower the energy to fit the hadron mass spectrum, and was justified by DeGrand *et al.* as the finite part of the zero-point energy from the quarks and gluons. The problem with this term is that the contribution to a spherical cavity from the Casimir term is positive, rather than negative. It was shown by Boyer[111, 112] that the Casimir force for a spherical conducting shell is outward, instead of inward as with a parallel plate geometry. Another problem is that the MIT Casimir term with $E_0 = -Z_0/R$ (where Z_0 is positive) is unbounded from below as $R \rightarrow 0$. One could imagine fluctuations of the bag surface, with fission-like processes leading to a cavity containing no quarks. With nothing inside to keep the bag from collapsing, it could decay with an infinite gain in energy[8]. A cutoff could be introduced to prevent this, but then renormalization would directly depend on the cutoff.

We find that configuration mixing from OGE provides a natural mechanism for lowering the energy of strongly interacting particles, allowing for introduction of a Casimir term of the proper sign.

The Casimir energy[7] can be calculated as the difference in zero-point energy caused by a conductive shell or a body with dielectric or magnetic permeabilities differing from the free-space values. At short distances, quantum fluctuations of polarizable bodies give rise to attractive van der Waals forces. Retardation effects influence interactions over longer distances. In the limit of large polarizabilities, materials behave as conductors with the quantum fields excluded from the bodies[108].

In 1948, Casimir[7] calculated the force between two infinite conductive parallel plates separated by a vacuum, and found it to be attractive. The calculations involve finding the difference in number of modes inside and outside the region of interest, where the normal modes contribute $E = \sum_k \frac{1}{2} \hbar \omega_k$ to the zero-point energy of the radiation field. (Here we show powers of \hbar and c). Typically, a cutoff λ is introduced, with $E_0 \equiv \frac{1}{2} \sum \hbar \omega \exp^{-\omega/\lambda}$. Physically, conductivity tends to fall off at high frequencies, and presumably high frequencies of the order of λ and higher contribute equally to modes inside and outside the region, so the infinite terms cancel. Neglecting edge effects, for plates of area A and separation L , Casimir found the zero-point energy to be

$$E_0 = 3\pi^2 \hbar c A L \frac{1}{\lambda^4} - \frac{\pi^2}{2} \hbar c A \frac{1}{\lambda^3} - \frac{\pi^2}{720} \frac{\hbar c A}{L^3}. \quad (4.2)$$

The first two terms are divergent for short wavelengths, as $\lambda \rightarrow 0$, and are proportional to the volume and area of the region respectively. The divergent parts should cancel with the contribution of quantum fluctuations of the fields outside. The third term contributes to a net attractive force[119] that is measurable and finite,

$$F = -\frac{\pi^2}{240} \hbar c \frac{A}{L^4}. \quad (4.3)$$

Experimental agreement with this force was demonstrated in 1948[109].

Casimir suggested[110] this could provide a physical mechanism to account for the stability of the electron, with an attractive Casimir force balancing the outward classical Coulomb force of the semi-classical Abraham-Lorentz model of the electron[56]. The argument was that if the Casimir force for a spherical shell of charge with radius a was $E_0 = -C(\hbar c/2a)$, then the Coulomb force on the shell would balance if $C = e^2/\hbar c$. As an order of magnitude estimate, the parallel plate result was used, with the area A set to πa^2 , with the plates a distance a apart. This makes a Casimir energy $\Delta E \sim -0.09 \hbar c/2a$. This was suggestive of a more fundamental relation, as the

Casimir constant C with this crude approximation was within an order of magnitude of the value of the fine structure constant α .

In 1968, Boyer[111] calculated the Casimir forces on a conducting spherical shell, finding the sign of the zero-point energy to be positive rather than negative as anticipated by Casimir. He found $\Delta E \sim 0.09\hbar c/2a$, which is of about the same magnitude, but of opposite sign, as that postulated by Casimir. Thus Casimir's intriguing model of the electron was invalidated.

The MIT bag model includes contributions from quarks as well as gluons, so it is necessary to look at the zero point contributions of the Fermions as well as the vector Bosons. If the net result for the zero point energy is positive rather than negative, it also presents difficulties for the MIT bag model, in that the MIT Casimir term was introduced with a negative sign, $E_0 = -Z_0/R$.

In general, the ground state energy is renormalized by subtracting various (infinite) counter terms. As shown below, one expects that there should be contact terms proportional to polynomials of the bag radius. One is left with finite contributions including volume[49, 50, 54], and possibly surface[119] and/or a term proportional to the bag radius[107], $H' = BV + \sigma A + FR$. The volume term may be absorbed in the bag constant B .

Quantum field fluctuations in the presence of curved boundaries tend to be plagued with quadratic as well as quartic divergences in $1/\lambda$ as the cutoff is taken to zero[113, 114, 116]. In the electrodynamic case for a spherical shell calculated by Boyer, there is a cancelation of divergent contributions from internal and external fields and between TE and TM modes. The quartic divergences can be absorbed into a redefinition of the energy associated with the bag constant $\sim BV$. The quadratic divergence cannot be absorbed by any term normally used in the MIT bag model. This energy requires a counterterm of the form $\sim FR$, and there seems to be no reason not to include it in the model. No divergent contributions arise from the zero-point energy of the form $\sim \sigma A$.

In addition to the divergent pieces, finite contributions to the zero-point energy have been calculated for Fermions[118, 116] and vector Bosons[114, 115, 118, 116] in a spherical geometry. Including the quadratic divergence, each vector particle (gluon)

contributes to leading order in the asymptotic expansion

$$E_V \sim \frac{1}{\pi R} \left(-\frac{4}{3} \frac{1}{\lambda^2} + \frac{1}{8} \right), \quad (4.4)$$

and each Fermion (quark) contributes

$$E_F \sim \frac{1}{\pi R} \left(\frac{1}{3} \frac{1}{\lambda^2} - \frac{1}{48} \right). \quad (4.5)$$

Although the finite part of the quark contribution is negative, it is much smaller than the gluon contribution. Results for gluons have also been calculated in a cubical geometry using image charges[120]. The energy shift is again positive, and within a few percent of the spherical value for equal volumes. For 8 gluons (with octet color) and N quarks, the Casimir energy for a spherical volume is

$$E_0 \sim \frac{N}{\pi R} \left(\frac{1}{3} \frac{1}{\lambda^2} - \frac{1}{48} \right) + \frac{1}{\pi R} \left(-\frac{32}{3} \frac{1}{\lambda^2} + 1 \right). \quad (4.6)$$

Although the divergent terms from quarks and gluons have opposite sign, they could only cancel if $N = 32$, but N must be a multiple of three (colors). We will use $N = 9$ as we have three quark flavors in our model. Numerically, the finite part of the zero-point energy is positive, with

$$E'_0 = \frac{0.259}{R}. \quad (4.7)$$

This provides us with the basis for making a fit to a modified form of the MIT bag model, with the usual bag energy but including the new counter term F , $H' = BV + FR + \frac{259}{R}$. We find this parameterization is not successful; because of the magnitude of lowering of the ground state energy due to configuration mixing, it leads to negative values for B and unstable bags. (Adding a surface counter-term does not improve the situation because it must be negative to make B positive, and this would lead to unstable deformations of the bag surface.) With the minimal MIT prescription for the self-energy, we find the energies due to configuration mixing of the neutron at $R=.005 \text{ MeV}^{-1}$ and $R=.0045 \text{ MeV}^{-1}$ to be -581 MeV and -647 MeV respectively. Asymptotically, one expects the energy to go as $1/R$ for $R \rightarrow 0$, and as a constant for $R \rightarrow \infty$. A fit to the neutron energy of configuration mixing gives $E_{CM} \sim -15.72 - 2.826/R$ with the minimal MIT self-energy. Stability is reached only

with a positive Casimir term with coefficient greater than about 5.5. If we eliminate the new counter-terms, a fit to the neutron mass for $\alpha_s = 1.3636$ using the minimal MIT self-energy gives $B^{1/4} = 145$ MeV (making $R = .005$ MeV) and the Casimir term becomes $E_0 = 6.45/R$. With the more complete self-energy built from all vertices used in OGE diagrams below cutoff, we find the same value of B (at the same bag radius), but the Casimir term is reduced to $E_0 = 5.72/R$.

Thus with our cutoff at 1.5 GeV above the qqq ground state, we require a positive Casimir term considerably larger than the theoretical value to achieve stability for the particles. If we plot the ground state energy due to configuration mixing vs. the cutoff, we see that the ground state energy has apparently not converged (see figure 4.3). If we had included running of the coupling constant in our calculations, it would slightly diminish contributions from higher energy states. Our calculations provide no indication of when or if convergence would be reached at higher cutoffs. Perhaps it may be argued that trying to pin down the energy zero is pointless, as it can always be shifted by a trivial renormalization.

In spite of these problems, configuration mixing leads to significant lowering of the ground state energy, providing a negative contribution to the energy needed to match the hadron mass spectrum. This removes the phenomenological requirement for a Casimir term of the wrong sign.

4.3 Configuration mixing

The OGE interaction causes substantial mixing of states, especially in the qqq sector. The proton and neutron have similar compositions if one interchanges d for u quarks. However, there are small differences because of the 5 MeV difference in mass between d and u in our calculations.

The qqq state where all three quarks are in the $s_{1/2}$ ground state consists of two color singlet states. These combine to make two states, one with the symmetry of the nucleon, and one with the symmetry of the Δ . The lowest state found after configuration mixing contains none of the state with Δ symmetry, and consists of about 48% of the valence nucleon ground state. The remaining 52% of the lowest configuration-mixed state consists of a 26% contribution from the qqq basis states with two excitations to the $p_{3/2}$ level, 7% with two excitations to the $d_{5/2}$ level, and 6% with two $p_{3/2}$ and one $d_{5/2}$ excitation. There are various smaller excitations

contributing in the qqq sector. The $qqqq\bar{q}$ sector collectively accounts for less than 4% of the configuration mixing. Within this sector, the largest contribution comes from $u\bar{u}$ and $d\bar{d}$ pairs where one of the quarks is excited to a $p_{3/2}$ level. These states account for 1.9% of the mixing. These states are classified into categories and plotted in Figs 4.4 and 4.5 for the neutron. The mixing is very similar for the proton. Plots for the Δ^+ may be found in Appendix B.

The information on configuration mixing is plotted in two adjacent figures for each particle, in Parts 1 and 2. In the lower half of the figure, single quark (filled circle) and antiquark (open circle) energy levels are plotted, along with energies for the multi-quark states (diamond-star). The energy level diagrams shown from left to right correspond to categories of multi-quark states (labeled a-t and A-J for qqq states, and K-T for $qqqq\bar{q}$ states) contributing to the configuration mixing. The number of states within each category is listed below each energy level diagram. (The states contributing significant probability to each category are listed in Appendix A.) The legend to the right on the lower half of the figure identifies the single-particle energy levels. The upper half of the figure shows the probabilities summed over states for each category. Bar graphs show contributions from monopole, monopole plus dipole, ..., monopole through hexadecapole plotted directly above the energy level diagram for quarks of each category. At the top, the full monopole through hexadecapole contribution is tabulated numerically for each category.

4.3.1 *Why is less than half of the nucleon probability accounted for by three $s_{1/2}$ quarks?*

The simple textbook model[14] of a hadron assumes three quarks in the $s_{1/2}$ ground state. However, in an interacting system, the ground state is lowered by mixing in higher states, and our system is strongly interacting.

In the MIT bag, the OGE interaction is typically used to split the hadron masses, with the coupling strength α , determined by matching to the $\Delta - N$ splitting. Keeping the $\Delta - N$ splitting constant while increasing the cutoff and simultaneously decreasing α , has the effect of decreasing the amount of the three $s_{1/2}$ quark contribution. If the coupling constant is weaker, there is less mixing for any particular excited state, with the mixing decreasing in first order as α^2 . However, the number of states tends to balloon as the cutoff is raised (see Fig. 4.8).

We need a much smaller coupling ($\alpha_s = 1.3636$) to match the $\Delta - N$ splitting with our 1.5 GeV cutoff on states than is needed for three $s_{1/2}$ quarks ($\alpha_s = 2.2$). Our value is still larger than the experimental value of ($\alpha_s(1\text{GeV}) \sim 0.5$), indicating that we have not converged because we have not included enough states. The coupling would also decrease if part of the $\Delta - N$ splitting was accounted for by some other mechanism, such as through pion interactions. In this scenario, α_s would be smaller and the amount of configuration mixing would decrease.

4.3.2 *Why are excitations higher than $J = 1/2$ allowed in a spherical MIT bag?*

Often only $s_{1/2}$ and $p_{1/2}$ excitations[53, 70, 119] (sometimes with higher radial excitations) are considered in the spherical MIT bag because higher J values would involve a non-spherically symmetric field pressure that would not be balanced by a uniform bag pressure B . However, solutions for any J are easily constructed that satisfy the spherical quark boundary condition $-i\vec{\gamma} \cdot \hat{r}\psi(x) = \psi(x)$ at $r = R$ (contrary to a statement by Donoghue and Golowich, 1977[70]). The boundary condition which is of concern is $-\frac{\partial}{\partial r}\bar{\psi}(x)\psi(x) = 2B$ at $r = R$. Spherical bag solutions that satisfy the bag pressure on average and that satisfy the first boundary condition for any J may be constructed if the boundary is fixed. If it is not fixed, the boundary would move in response to differential pressure if a single state of higher J was put into the bag. But we are not faced with this situation.

In our case, the Hamiltonian has spherical symmetry, so we generate a spherically symmetric superposition of many states that contribute to the ground state. For each energy level and value of J , all m_J values contribute to different states with proper coefficients to maintain this symmetry. Thus the field pressure of the quarks may be balanced locally with the bag pressure at the surface, in agreement with both the quark and the bag pressure boundary conditions.

4.3.3 *Why are three quark states much more probable than states with an extra quark pair?*

Several factors contribute to the large mixing in the qqq sector relative to the $qqqq\bar{q}$ sector. Excited qqq states enter at a lower energy than the $qqqq\bar{q}$ states, generally have smaller energy denominators, and have more OGE transitions coupling them to the three $s_{1/2}$ quark state. In the qqq sector, states below the cutoff include quark

excitations that range up to $f_{7/2}$, or radial excitations up to $n = 3$. However, in the $qqqq\bar{q}$ sector, parity requires one quark or antiquark be excited to a $p_{1/2}$ or $p_{3/2}$ state in the $qqqq\bar{q}$ sector, and the 1.5 GeV cutoff allows no higher excitations. Coupling these states to the lowest qqq state requires that a gluon annihilate the antiquark with a like-flavor quark. In addition, there is considerable loss from the $qqqq\bar{q}$ sector seen from diagonalizing the interaction due to interference effects as compared to first order perturbative results we calculate using the same matrix elements. This will be discussed in more detail later.

4.3.4 *What enhances probabilities for states with two identical excitations?*

We find the probability for states with two quarks excited to the same energy to be much greater in general than for other states of comparable energy. About 26% of the nucleon probability is due to states with one quark left in the $s_{1/2}$ state with two quarks excited to the $p_{3/2}$ level (category f). This is the lowest energy excitation, so it has the most enhancement from a smaller energy denominator. States with two $d_{5/2}$ excitations (category n) are also enhanced. The states with two $s_{1/2}$ states (category k) may be enhanced, but their contribution is surprisingly small compared to category f. This will be examined below.

The mechanism of enhancement seems to be constructive interference due to both quark-gluon vertices being identical, along with reciprocal transitions in m_J causing the product with the elements from the spin-sum tables to add coherently. Besides maintaining constructive phases, the squared matrix elements (that vary in size) sum to a larger amplitude than the product of uncorrelated elements, even if all terms are positive. In first-order perturbation theory, these amplitudes for transitions to orthonormal states are squared and summed to get the probabilities for each category. Matrix diagonalization effectively sums perturbative results to all orders.

4.3.5 *Why do $p_{3/2}$ excitations dominate over $p_{1/2}$ excitations?*

When categories f and k are compared, we see that the contribution to the nucleon of states with two $p_{3/2}$ excitations is about 32 times larger than the contribution from states with two $p_{1/2}$ excitations. Some difference is to expected because the energy required to excite the $p_{3/2}$ level is about 2/3 of that required to excite the $p_{1/2}$ level.

(See Table 3.1). Also, category f includes 11 states, whereas category k includes 5 states. However, these factors do not explain the large difference.

The difference is primarily due to the fact that the Coulomb dipole contribution for two $s_{1/2}$ to $p_{3/2}$ transitions is large (0.4309) compared to the Coulomb dipole contribution of two $s_{1/2}$ to $p_{1/2}$ transitions (0.0651), and it is also large compared to the electric OGE terms. As shown in Appendix C, this results in a matrix element for double $s_{1/2}$ to $p_{3/2}$ transitions about 3.5 times larger than the $s_{1/2}$ to $p_{1/2}$ matrix element. Squares of these elements contribute to first order perturbation theory, so this provides a factor of about 12.5:1 that we should expect. Dipole contributions from diagonalization are in the ratio $\sim 15 : 1$, and we have more $p_{3/2}$ than $p_{1/2}$ states. The $p_{3/2}$ states also have significant quadrupole and octopole contributions, making the overall ratio of $p_{3/2}$ to $p_{1/2}$ probabilities about 33:1.

4.3.6 *Why are u pairs more probable than d , and d more probable than s pairs in our proton ground state?*

The $u\bar{u}$ vs $d\bar{d}$ part of our model prediction may seem incorrect based on two simple arguments. It is clear that $s\bar{s}$ pairs should be suppressed because the s quark is massive. But the d and u quarks do not differ enough in mass to make much difference. The two arguments are based on pion physics and on the Pauli exclusion principle. We demonstrate that constructive interference enhances probabilities for $u\bar{u}$ pairs in spite of suppression of the number of states due to the Pauli principle.

Pion physics provides a simple mechanism for dominance of \bar{d} quarks over \bar{u} quarks in the sea. The π^+ is made of a u and \bar{d} , whereas the π^- is made of a d and \bar{u} . Since there are more valence u quarks than d quarks in the proton, $d\bar{d}$ pairs are more frequently stabilized by forming a π^+ than are $u\bar{u}$ pairs stabilized by forming a π^- . Low-mass pions have been modeled with some success[54, 125] in the MIT bag. But this physics is missing from our model because of difficulties in incorporating interacting or overlapping bags. However, pions as quark-antiquark pairs have been used to dress the nucleon and Δ in the soliton bag model[127, 128]. Pions modeled as elementary particles[129] have also been introduced into the soliton bag, and have been coupled to the MIT bag to form the Cloudy Bag Model[131] to satisfy the partial conservation of axial current (PCAC).

The Pauli exclusion principle allows the s quark of an $s\bar{s}$ pair to be in any state,

$d\bar{d}$ pairs are somewhat suppressed, whereas $u\bar{u}$ pairs are suppressed more because the quarks are not able to enter the same states held by like-flavored valence quarks. Indeed, below our cutoff we have 79 orthonormal color singlet states that include $u\bar{u}$ pairs, 109 states with $d\bar{d}$ pairs, and 204 states with $s\bar{s}$ pairs.

In 1977, Field and Feynman[124] used a similar argument as a likely explanation for an apparent dominance of \bar{d} quarks over \bar{u} sea quarks inferred from electron-proton scattering at low but nonzero x , where x is the momentum fraction carried by a quark of a high-momentum hadron. They also said the number of \bar{u} and \bar{d} must become equal as $x \rightarrow 0$. However, there should be a difference between the sea created in the process of a hard collision of a lepton with a hadron and the sea associated with the ground-state nucleon. The de Broglie wavelength of a 1 GeV electron is 1 fm. When electrons are scattered off protons at much higher energies, the electrons probe individual partons (quarks or gluons). Here the Pauli principle suppresses sending the scattered quark and the quark of the quark-antiquark pair into the same state, but spectator quarks would largely be ignored.

In contrast to hard scattering, configuration mixing is dominated by low energy processes which cause coherent enhancement of interactions when a quark pair sees other quarks of the same flavor in the bag. This effect dominates over the suppression of states by the Pauli principle, causing a greater probability for $u\bar{u}$ than $d\bar{d}$ pairs in the proton. Nucleon ground state configuration mixing in the MIT bag of radius $R=0.005 \text{ MeV}^{-1} \sim 1 \text{ fm}$ is dominated by the lowest energy magnetic and electric gluon modes, with energies $2.744/R=549 \text{ MeV}$ and $4.493/R=899 \text{ MeV}$, having de Broglie wavelengths 2.25 fm and 1.38 fm respectively. A similar situation holds for low energy quark-antiquark pairs. They feel the presence of all other partons in the bag, and coherence effects become important. An antiquark does not have to be annihilated with the same quark with which it was created, although both quarks must match the antiquark flavor. This greatly increases the number of interactions available for quark-antiquark pairs when other quarks of the same flavor are present, and these interactions are responsible for the increase in probability of these states.

Many diagrams interfere in the process of creating and annihilating a pair when the pair flavor is carried by other quarks. A quark pair created by one octet color of gluon may be annihilated by another color gluon (in which case the new quark annihilating with the antiquark must be of different color than the quark left behind

from the pair). Even in first order perturbative diagrams, where a $s_{1/2}$ qqq state scatters to $qqqq\bar{q}$ and back to the same qqq state, the multipoles and type (magnetic or electric) of the two gluons participating in creation and annihilation may differ. Another possibility is that the m_J may change for the quark that emits a gluon that creates a pair without any change in the m_J value for the quark that absorbs the gluon from annihilation. All these possibilities are consistent with conservation of parity, angular momentum, and color singlicity.

Donoghue and Golowich[70] attempted a perturbative calculation of pair creation for the proton in which they included $s_{1/2}$ and $p_{1/2}$ states with various radial excitations, as well as four flavors. Their Table II lists the spin overlap of five-quark states with the proton. The table includes formulae showing effects of spin-flip vs non-spin-flip of the valence quark (and the interference term) in terms of u , d , and s pairs. Each row in the table indicates whether the scattered valence quark is in the ground state, and if it is in the same state as the sea quark. Maciel and Paton[132] made a correction for an omission of an interference term between non-spin-flip and spin-flip in the paper of Donoghue and Golowich. However, neither paper includes interference effects that depend on the flavor of the quark emitting the gluon that creates the pair. This turns out to be important because the amplitude for annihilation of the pair includes the possibility for annihilation of this quark when it is of the same flavor as the pair. Also, if a valence quark spin flips during pair creation, another quark spin can flip. The sea quark can carry the spin if another quark with the same flavor as the sea quark is annihilated. The result is that scattering probabilities depend on the flavor of the quark creating the gluon which makes a pair. Appendix D shows our symbolic results when we restrict our states to the two energy levels, $s_{1/2}$ and $p_{1/2}$, and calculate the overlap of $qqqq\bar{q}$ configurations with the proton dipole contributions. As an example of the interference effects depending on initial flavor, we compare the coefficients for dipole electric scattering from a u quark vs a d quark where the initial quark changes from energy level 1 to 3 ($s_{1/2}$ to $p_{1/2}$) creating a $d\bar{d}$ pair (with both quark and antiquark in the $s_{1/2}$ state), then scattering back by another dipole electric transition to the initial flavor of quark. The coefficient when the initial quark is a d quark is 4, whereas it is 6.8889 for an initial u quark. These interference effects are not included in Table II of Donoghue and Golowich[70] or Eq.s 2.1 of Maciel and Paton[132].

4.3.7 *Why are quark-antiquark sea probabilities much smaller than those calculated previously by perturbative methods?*

Donoghue and Golowich[70] calculated sea probabilities using $\alpha_s = 2.2$ using the spin overlap functions (with which we differ as stated above) and a gluon propagator (they modified the boundary conditions in an ad hoc manner because they got extremely large energy denominators for some modes). They only included $s_{1/2}$ and $p_{1/2}$ states for the quarks and antiquarks. Numerically their perturbative probabilities for valence, $u\bar{u}$, $d\bar{d}$, $s\bar{s}$, and $c\bar{c}$ are in ratios 1 : 0.360 : 0.271 : 0.167 : 0.020 for the proton. Their ratio for $\bar{u}/\bar{d} = 1.33$ whereas our ratio is $\bar{u}/\bar{d} = 1.23$.

Maciel and Paton[132] made a correction in the paper of Donoghue and Golowich. (We find they also did not include all interference terms.) They also used $\alpha_s = 2.2$ with only $s_{1/2}$ and $p_{1/2}$ states, but used confined perturbation theory[71, 4] like we use. (This approach does not seem to have problems with unusually large energy denominators.) They found probabilities for valence, $u\bar{u}$, $d\bar{d}$, $s\bar{s}$, and $c\bar{c}$ in the ratios 1 : 0.056 : 0.040 : 0.045 : 0.007.

To compare our results with those above, we first do a perturbative calculation using two weighted rows of our matrix corresponding to the valence neutron wave function. We did not calculate results for the c quark. Including excitations to $p_{1/2}$ or $p_{3/2}$ states with $\alpha_s = 1.3636$, we find probabilities for valence, $u\bar{u}$, $d\bar{d}$, $s\bar{s}$ in the ratios 1 : 0.078 : 0.063 : 0.025. For comparison purposes, we scale our perturbative results by α_s^2 , substituting $\alpha_s = 2.2$ instead of our $\alpha_s = 1.3636$. This would make our perturbative ratios 1 : 0.203 : 0.164 : 0.065. The contributions from $p_{3/2}$ states dominate our results, with $p_{1/2}$ states accounting for about 20% of the perturbative probability. Our ratios for including only $p_{1/2}$ states are about 1 : 0.042 : 0.034 : 0.022. Thus our perturbative results are much smaller than those of Donoghue and Golowich, but comparable to the results of Maciel and Paton.

Our configuration mixing results show much smaller contributions. There the $u\bar{u}$, $d\bar{d}$, $s\bar{s}$ probabilities are 0.017, 0.015, and 0.007. These are about 4.5 times smaller than the perturbative elements, even though the same matrix elements were used in the perturbative calculation. When viewed as a function of multipole contribution, the probabilities are decreasing rather than increasing, as more of the valence qqq sector is shifted to the states with two $p_{3/2}$ excitations. The results seem to be partly from destructive interference between transitions to the $p_{1/2}$ states from $s_{1/2}$ states

and $p_{3/2}$ states. Also much of the probability is shifting to states inaccessible by perturbation theory.

4.3.8 *Why are some energy levels unused?*

The $g_{7/2}$, $g_{9/2}$, $h_{11/2}$, and $d_{5/2}$ levels are not used in generating any configurations below our cutoff, even though single particle energy levels above them are used. This results from conservation of parity, and the requirement for conservation of angular momentum. If the cutoff were higher, combinations of states involving these levels would be seen.

4.3.9 *What about interactions of higher multipole?*

Since our highest angular momentum state in use is $f_{7/2}$, the triangle rule only allows up through hexadecapole transitions. Thus we have included all transitions consistent with our basis states.

4.3.10 *What states would enter if we continued to raise our cutoff?*

We chose a maximum cutoff 1.5 GeV above the $s_{1/2}$ qqq ground state. If the cutoff is raised further, there are states entering with two $q\bar{q}$ pairs, or $qqqqq\bar{q}\bar{q}$ states, in addition to many more excitations of the types we have considered.

If considered one parameter at a time, configuration mixing decreases for states with higher excitations by almost every measure. The mixing probabilities are dropping rapidly as functions of the gluon multipole order, the quark radial mode number, the quark angular momenta, the orbital angular momenta, and the number of particles in the state. The number of terms included in the mode sum for gluons appears adequate. As discussed in Sec. 4.3.4, there is more mixing of states where two quarks are excited to a level with higher J and thus where many μ combinations are allowed. This tends to make the graph of ground-state energy vs cutoff have periodic jumps. The size of these jumps is decreasing in general with increasing cutoff. By comparing Figs. 4.3 and 4.8, it is apparent that the jumps occur whenever the density of states is at a local maximum. The contribution of a state to the ground state configuration mixing energy decreases steadily with the energy of the state, but the increasing density of states as a function of cutoff counteracts this trend. Thus when all excitation

mechanisms are taken together, the graph of energy vs cutoff does not appear to converge by the time we reach our maximum cutoff. In figure 4.8, we plot the increasing density of states as a function of state energy (with artificial Gaussian weighting of width 100 MeV).

4.3.11 Summary

In this chapter, fits to the nucleon masses and the $\Delta - N$ splitting have allowed us to determine values for the MIT bag parameters under the assumption that the up, down, and strange quarks have masses $m_u = 0$, $m_d = 5$ MeV, and $m_s = 279$ MeV or 300 MeV respectively. We found that with our 1.5 GeV cutoff, configuration mixing in the MIT bag requires much smaller values for the strong coupling constant, $\alpha_s = 1.3636$, at $R=0.005 \text{ MeV}^{-1} \approx 1 \text{ fm}$, than was needed for the standard three valence quark bag with $\alpha_s = 2.2$ [54]. Our bag constant $B^{1/4} \approx 146 \text{ MeV}$ is almost identical to the $B^{1/4} = 145 \text{ MeV}$ value of DeGrand *et al.*. We found a positive value for the sign of the Casimir contribution to the bag energy in agreement with the calculation of Boyer[111] for a spherical geometry. This is in contrast to the negative sign calculated for the Casimir term in a plane-parallel geometry. DeGrand *et al.* introduced a negative Casimir term based on the known plane-parallel solution and their assumption that the Casimir contribution would be qualitatively similar in the spherical bag geometry. The negative offset required phenomenologically by DeGrand *et al.* is not needed with our larger basis of states since configuration mixing leads to significant lowering of the ground state energies of the particles.

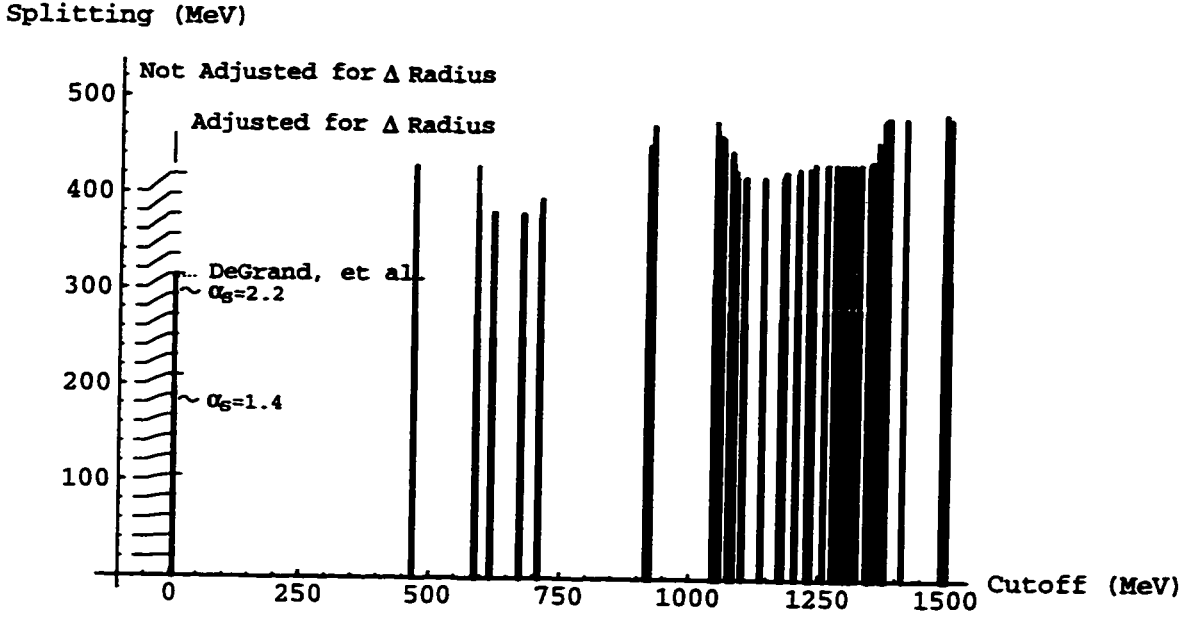


Figure 4.2: $\Delta - N$ splitting vs. energy cutoff with $\alpha_s = 2.2$ (grey) and $\alpha_s = 1.3636$ (black). The OGE interaction Hamiltonian is diagonalized for a succession of energy cutoffs set just above the thresholds where new basis states enter, continuing up to 1.5 GeV above the qqq ground state. Each vertical line corresponds to the $\Delta - N$ splitting found by taking the energy difference of the two lowest states with quantum numbers of the nucleon and Delta, found by diagonalizing over the basis states included below each cutoff. The lowest cutoff with $\alpha_s = 2.2$, where only $s_{1/2}$ quarks are included, corresponds to the results of DeGrand *et al.*, but the splitting becomes about 50% larger than it should be as the cutoff is raised to the maximum. With the strong coupling reduced to $\alpha_s = 1.3636$, the splitting approaches the correct size as the cutoff is raised and additional basis states are added beyond the qqq ground state. Note that there is about 10% uncertainty in the value for the splitting based on its variation as a function of precisely where the energy cut is made.

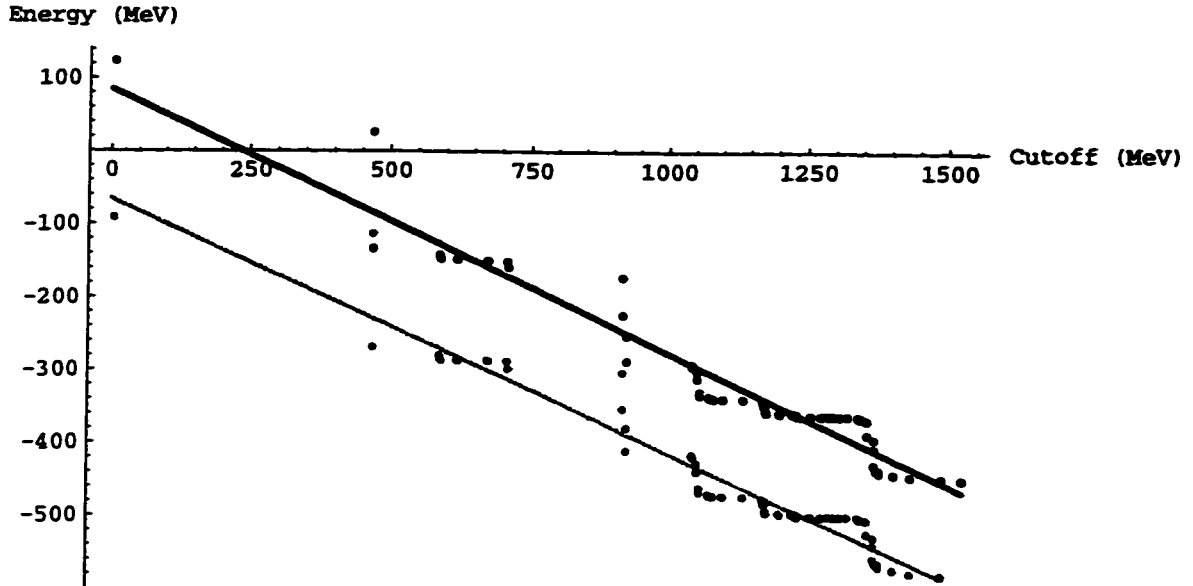


Figure 4.3: Neutron configuration mixing energy vs. cutoff with two forms for the self-energy. As the cutoff energy is increased, more basis states mix into the configuration, and the energy of configuration mixing continues to drop. This may be an indication that we have not reached convergence with our cutoffs at 1.5 GeV, or it may indicate something is missing from the model (such as contributions from gluons that we have not included in our basis). Instead, the data points appear to converge toward a line headed steadily downward. The lower (gray) data points show the configuration energy vs cutoff for the minimal MIT self-energy. The upper (black) data points show results for the self-energy where all vertices are included below cutoff. The best-fit lines have about the same slope for the full self-energy as with the minimal MIT self-energy. Inclusion of intermediate states where the quark color and spin change but the energy level doesn't change raises the configuration energy for the full self-energy. This overcomes the lowering of the configuration energy from first-order perturbative shifts where the intermediate quark energy changes. This is described further in Ch. 5. For both forms of the self-energy, the continual downward trend of the data is problematic.

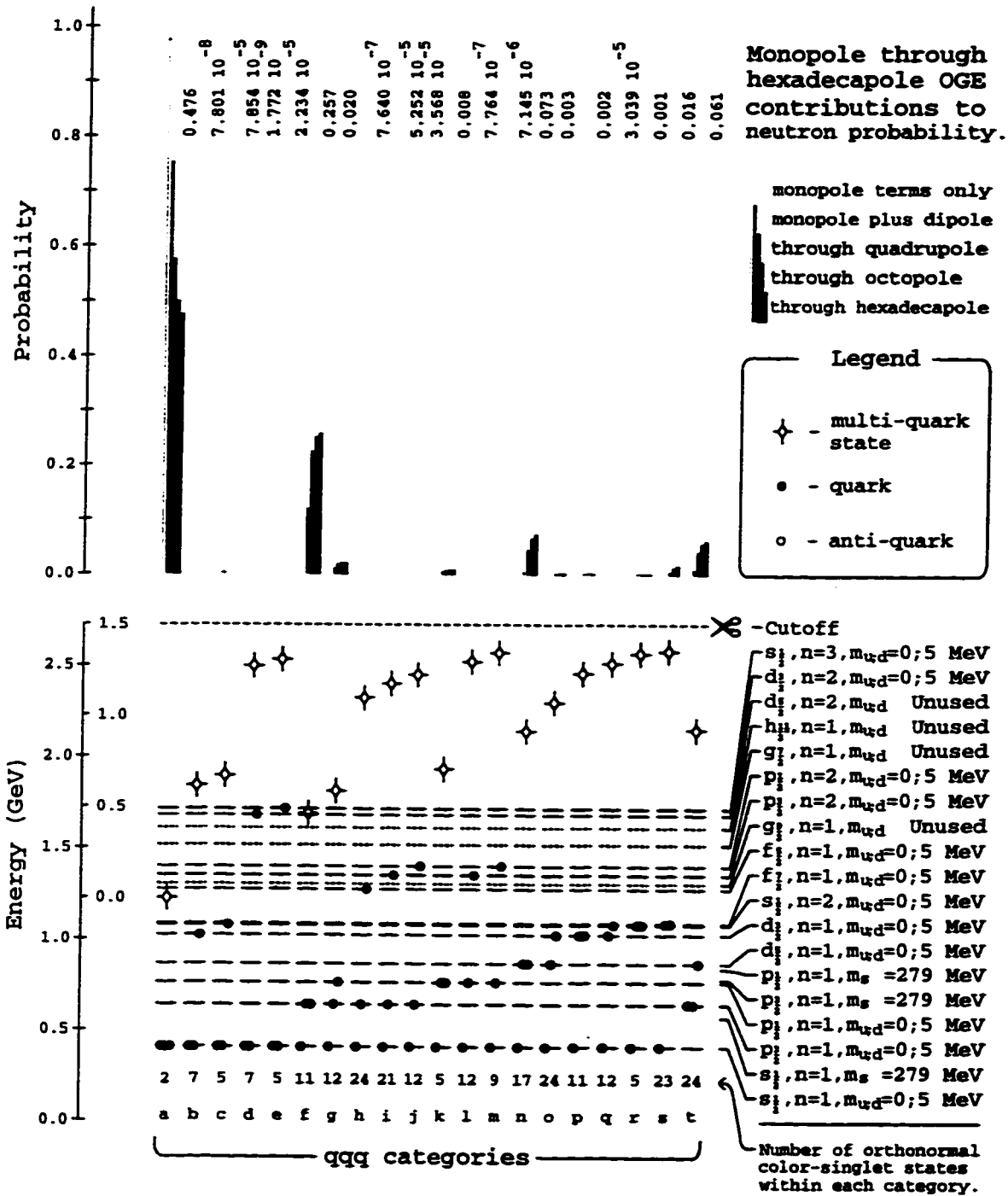


Figure 4.4: Composition of neutron ground state for $\alpha_s = 1.3636$ (Part 1 of 2). The basis states are combined into categories, with probabilities for each category shown in the upper part of the figure.

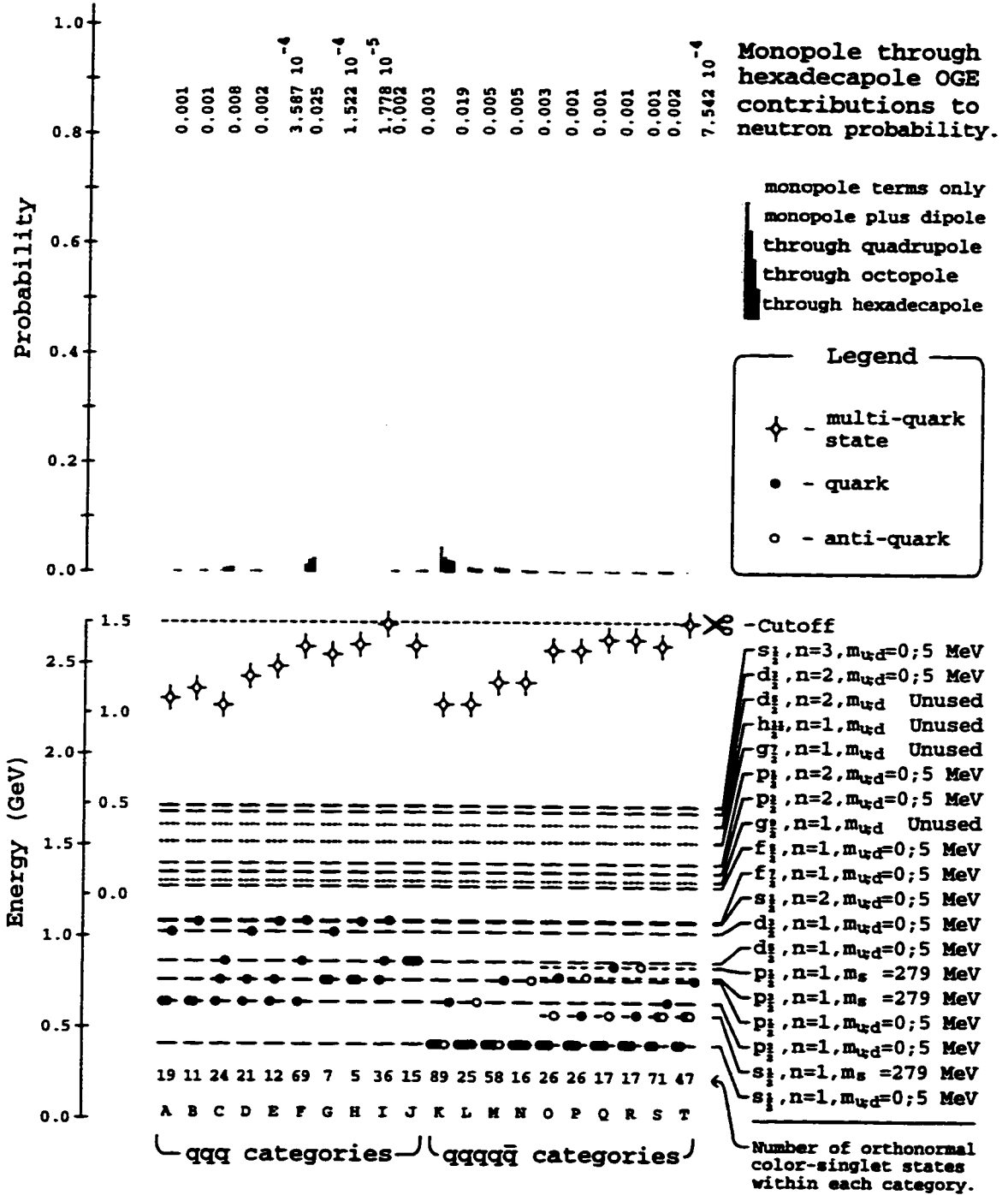


Figure 4.5: Composition of neutron ground state for $\alpha_s = 1.3636$ (Part 2 of 2). The basis states are combined into categories, with probabilities for each category shown in the upper part of the figure.

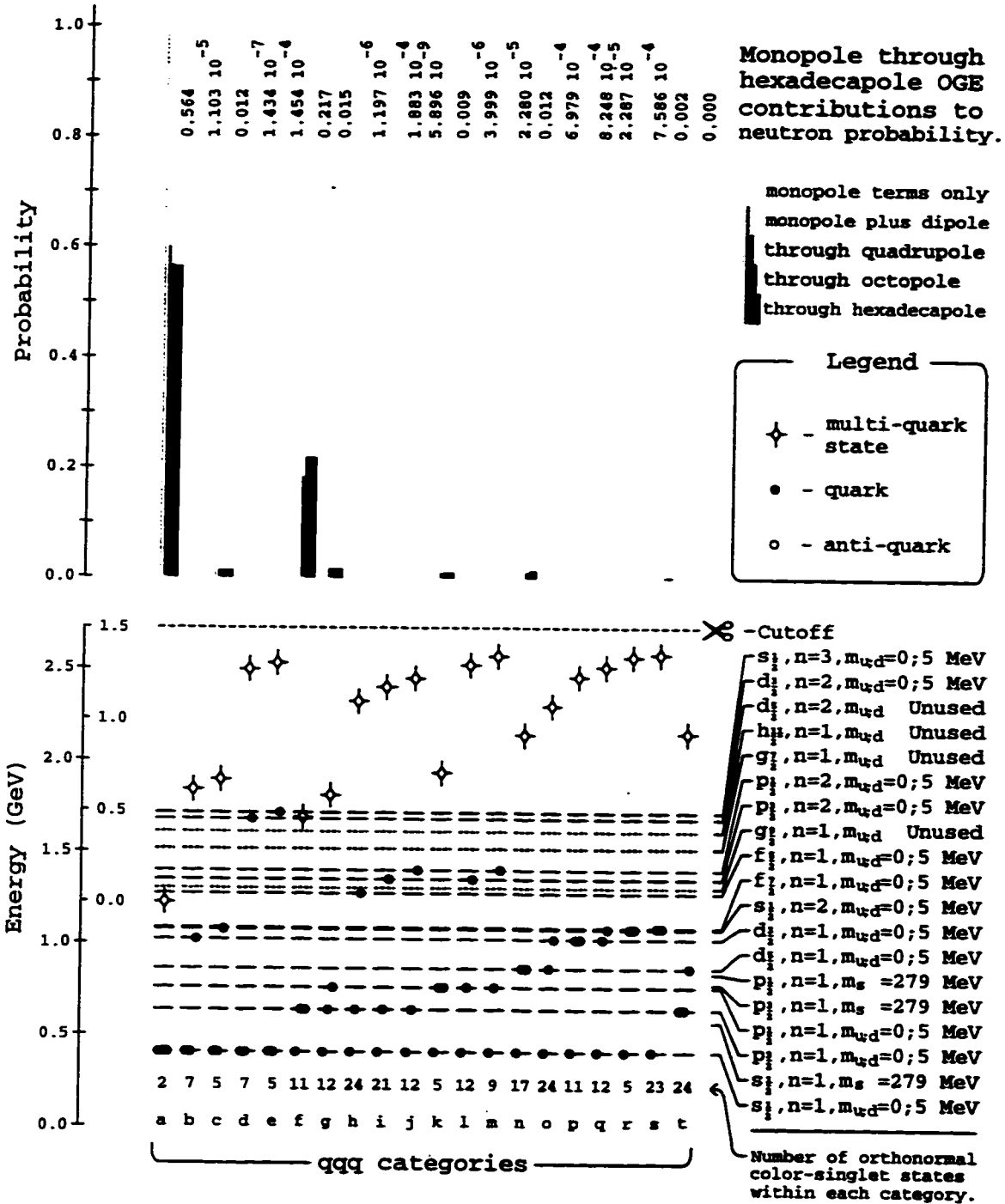


Figure 4.6: Perturbative neutron ground state for $\alpha_s = 1.3636$ (Part 1 of 2). The basis states are combined into categories, with perturbative probabilities for each category shown in the upper part of the figure.

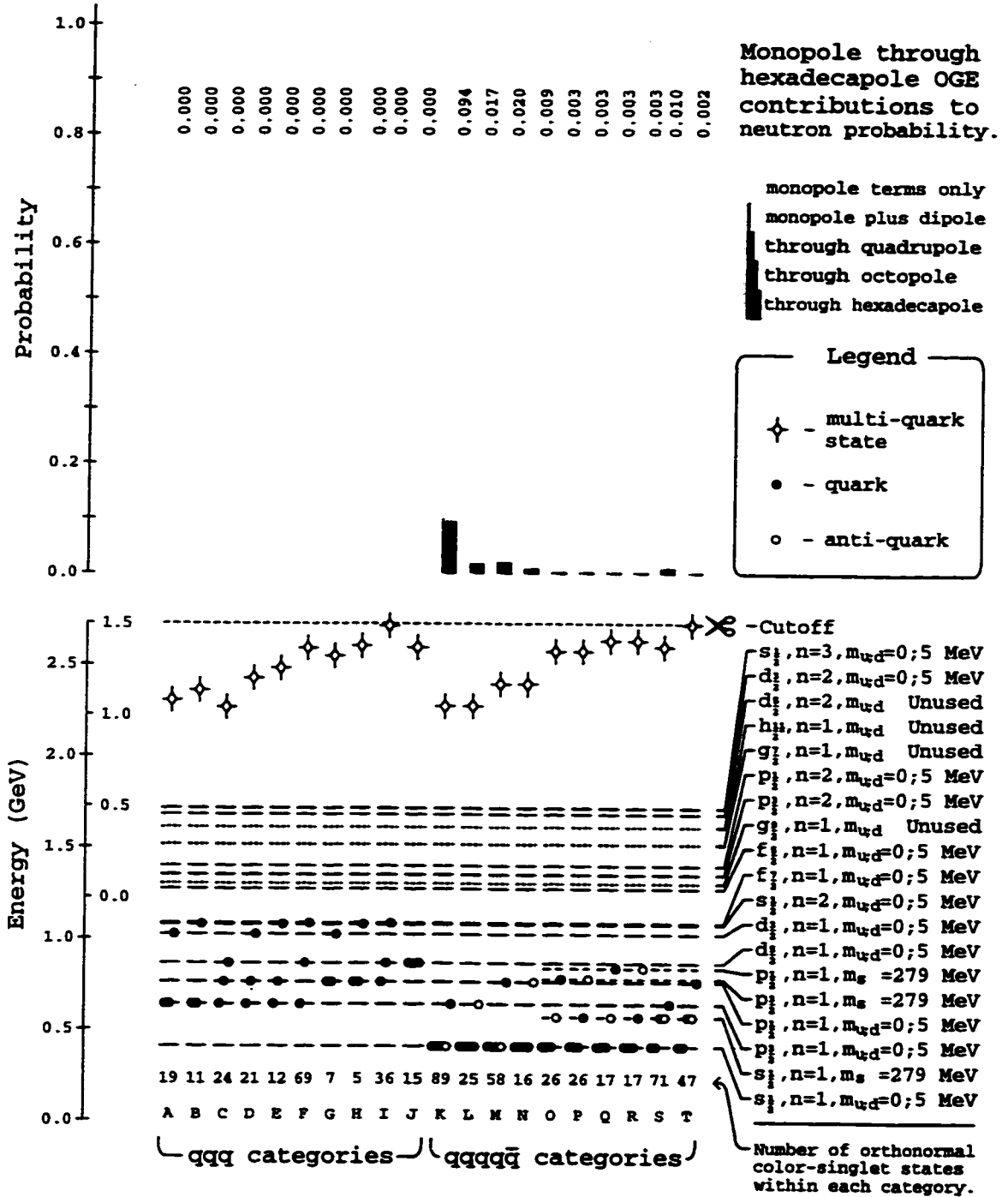


Figure 4.7: Perturbative neutron ground state for $\alpha_s = 1.3636$ (Part 2 of 2). The basis states are combined into categories, with perturbative probabilities for each category shown in the upper part of the figure.

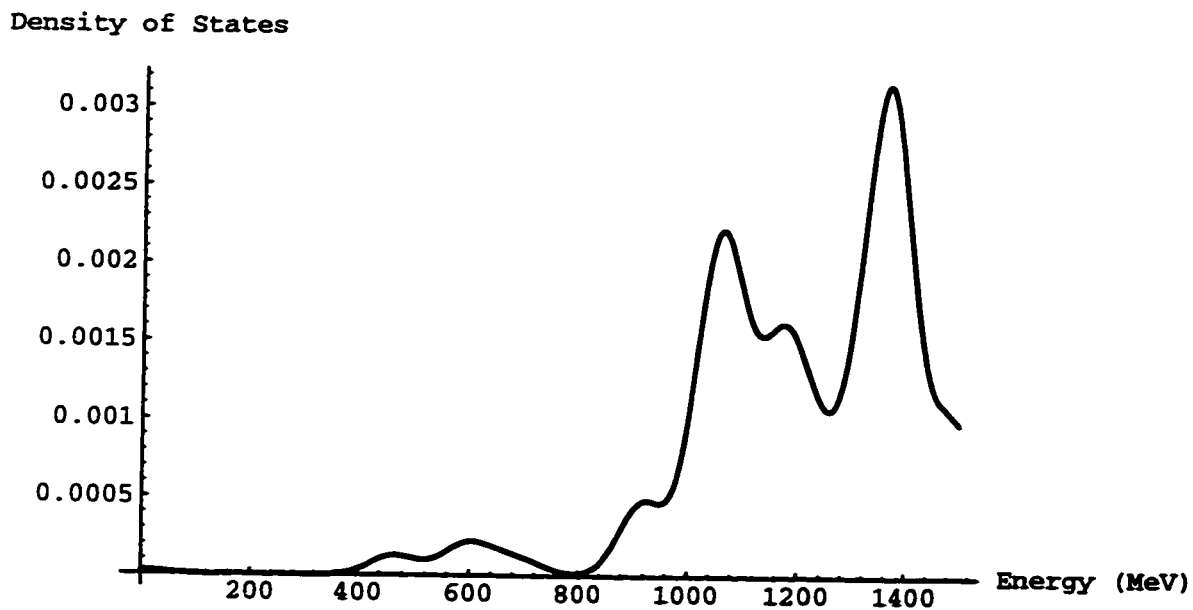


Figure 4.8: Density of color singlet basis states vs basis state energy. As the cutoff is raised, more basis states can mix into the configuration. The density of states is plotted using an arbitrary Gaussian weighting of width 100 MeV to smooth rapid variations.

Chapter 5

FITS TO THE OCTET BARYON MASSES

The MIT bag model has parameters B , Z_0 , and α_s , plus the quark current masses. Working with three quark flavors, we have kept the u quark mass at 0, but have allowed the d and s quarks to take on other values. Thus we have five parameters in our model. We initially set the d quark mass to approximately reproduce the $p - n$ mass difference. For any value of the bag constant B , we can then adjust α_s and Z_0 to reproduce the $\Delta - N$ splitting and the n mass. This leaves us with a two dimensional space where we can vary B and the strange quark mass m_s . We make three sets of calculations, altering B and m_s by about 10% in succession so that we can interpolate our results to other parameter values. For each of the three parameter sets, we calculate masses, bag radii, and other observables for the p , n , Σ^- , Σ^+ , Ξ^- , and Ξ^0 particles for two forms of the self-energy. We use these calculations to make best fits to the hadron masses for both forms of the self-energy.

5.1 Mass splitting of the neutron and proton

Isospin symmetry is broken for the proton and neutron because of the difference of u and d quark masses in the QCD Lagrangian, and also because of the electromagnetic interaction. Experimentally, the neutron is heavier than the proton by about 1.3 MeV. In our calculations, we split the u and d mass degeneracy by setting $m_u = 0$ and $m_d = 5$ MeV. We made calculations of the configuration mixing energy at several bag radii (corresponding to different values of B), with the strange mass either at $m_s = 279$ MeV or 300 MeV. (See Appendix E for tables showing results for the minimal MIT self-energy prescription and for the self-energy including all vertices used in our OGE calculations.) These values are used to calculate the equilibrium energies and bag radii for the particles at two values of B and for two values of m_s . These results are shown in Table 5.1 for the minimal MIT self-energy, and Table 5.2 for the “full” self-energy, which includes all vertices used in calculating OGE diagrams up to the cutoff. Table 5.3 shows best fits for both forms of the self-energy when B and m_s are

allowed to vary. Each choice for parameters requires recalculation of the TE and TM vertex integrals, Coulomb Green's function integrals, energy denominators for the OGE diagrams, and re-diagonalization of the interaction matrices for each particle.

The 5 MeV difference between m_d and m_u gives rise to a difference in nucleon masses of about $m_n - m_p = 2.03$ MeV at $B^{1/4} = 146$ MeV, with $R_n = 0.005$ MeV⁻¹ and $\alpha_s = 1.3636$. Maintaining the $\Delta^0 - n$ mass difference constant at 294 MeV, an increase of the bag constant to $B^{1/4} = 158$ MeV decreases the neutron radius by 10% to $R_n = 0.0045$ MeV⁻¹ and changes the nucleon mass splitting to $m_n - m_p = 2.89$ MeV.

Classically, if we modeled the proton as a uniform charge distribution in a bag with radius $R = 0.985$ fm, there would be an electromagnetic contribution to the mass of $\delta m_{em}^p \sim \frac{3}{5} e^2 / R \sim \frac{3}{5} \alpha \hbar c / R \sim \frac{3}{5} \frac{1}{137} 197 \text{ MeV fm} / (.985 \text{ fm}) \sim 0.88 \text{ MeV}$, reducing the splitting between the nucleons. However, the quark charges are point-like, and the Coulomb self-energy included in the calculation of the uniform distribution diverges for the point-like charges. We ignore the Coulomb self-energies, and calculate the Coulomb mutual interaction between quarks uniformly distributed within a sphere. For purposes of this calculation, we use the valence quark wave functions for the proton, substituting $u \leftrightarrow d$ for the neutron wave function.

$$\psi_p = \frac{1}{\sqrt{6}} [2(u \uparrow u \uparrow d \downarrow)_S - (u \uparrow u \downarrow d \uparrow)_S - (u \downarrow u \uparrow d \uparrow)_S], \quad (5.1)$$

where the subscript S denotes symmetrization.

With charge $\frac{2}{3}e$ for u and $-\frac{1}{3}e$ for d , the mutual interaction is zero for the valence quark model of the proton, since

$$E_p^C = \sum_{i < j} \int \frac{q_i q_j}{|x_i - x_j|} = \left(\frac{2}{3} \frac{2}{3} + \frac{2}{3} \left(-\frac{1}{3}\right) + \frac{2}{3} \left(-\frac{1}{3}\right) \right) \alpha \hbar c \int \frac{1}{|x - x'|} = 0. \quad (5.2)$$

For the neutron, the mutual interaction is negative, with

$$E_n^C = \left(\left(-\frac{1}{3}\right) \left(-\frac{1}{3}\right) + \frac{2}{3} \left(-\frac{1}{3}\right) + \frac{2}{3} \left(-\frac{1}{3}\right) \right) \alpha \hbar c \int \frac{1}{|x_i - x_j|} = -\frac{2}{5} \frac{\alpha \hbar c}{R}. \quad (5.3)$$

Thus for a bag radius of $R = 0.005$ MeV⁻¹, the Coulomb mutual interaction lowers the energy of the neutron by 0.584 MeV relative to the proton. A better estimate of the electromagnetic energy would include using the actual charge distribution in the Coulomb term and one-photon exchange interactions between quark states, similar to our OGE calculation.

We now estimate the one photon exchange contribution to the electromagnetic energy, where we approximate the (unconfined) photon propagator by the (confined) gluon propagator. We must also substitute $\alpha_s \langle \frac{\lambda_i}{2} \cdot \frac{\lambda_j}{2} \sigma_i \cdot \sigma_j \rangle$ by $\langle q_i \sigma_i \cdot q_j \sigma_j \rangle$. We begin by calculating the lowest order OGE contribution to the nucleon. The OGE energy shift for three $s_{1/2}$ valence quarks has equal contributions from forward and backward time ordered graphs (with energy denominators $1/(E_0 - E_n) = (-1/k)$ and gluon normalization $1/\sqrt{2k}$). The magnetic dipole vertex interaction between $s_{1/2}$ quarks is $H_I = \int_{bag} j \cdot A = I_{1,1}^k / \sqrt{2k}$ (where $k = 2.74$ for the lowest gluon mode and the lowest mode vertex integral has the value $I_{1,1}^k = 1.15$). The formula for the OGE energy shift becomes

$$\Delta E(OGE) = \sum_{i < j} \frac{\alpha_s}{R} \left(\frac{\lambda_i}{2} \cdot \frac{\lambda_j}{2} \sigma_i \cdot \sigma_j \right) \sum_k \frac{-(I_{1,1}^k)^2}{k^2}. \quad (5.4)$$

The sum over gluon modes has a value of -0.176 . For a baryon, $\langle \frac{\lambda_i}{2} \cdot \frac{\lambda_j}{2} \rangle = -\frac{2}{3}$, and $\langle \sigma_i \cdot \sigma_j \rangle = -1$ for a spin $1/2$ nucleon. Thus (ignoring higher gluon modes) the OGE energy shift for a nucleon composed of three valence quarks (with $\alpha_s = 2.2$ and $R = 0.005 \text{ MeV}^{-1}$) is

$$\Delta E(OGE) = 3 \frac{2.2}{.005} \left(-\frac{2}{3}\right) (-1) (-0.176) \text{ MeV} = -155 \text{ MeV}. \quad (5.5)$$

The factor of 3 is from the sum over quark pairs with $i < j$, and does not include self interactions (with $i = j$). This is about half the $\Delta - N$ splitting. The Δ energy is raised instead of lowered since the -1 spin expectation for the nucleon is replaced by $+1$ for the spin $3/2$ Δ . There also is a small decrease in splitting associated with the need for a larger Δ radius than nucleon radius to keep both in equilibrium with the same value for B . To first order, inclusion of self-energies offsets the N and Δ by equal amounts in the same direction.

The corresponding electromagnetic calculation differs between proton and neutron since the u and d quarks have different electromagnetic charges, in contrast to having the same form for the color interaction between different quark flavors.

With charge $\frac{2}{3}e$ for u and $-\frac{1}{3}e$ for d , the charge weighted spin expectation for the proton is

$$\frac{1}{2} \sum_{i,j} \langle q_i \sigma_i \cdot q_j \sigma_j \rangle_p =$$

$$\frac{1}{2}\alpha \left(\frac{1}{6} \left[4\left(\frac{2}{3} + \frac{2}{3} + \frac{1}{3}\right)^2 + \left(\frac{2}{3} - \frac{2}{3} - \frac{1}{3}\right)^2 + \left(-\frac{2}{3} + \frac{2}{3} - \frac{1}{3}\right)^2 \right] \right) = \frac{17}{18}\alpha. \quad (5.6)$$

The unrestricted sum over quarks i and j times $\frac{1}{2}$ includes self interactions and replaces the factor of 3 in the OGE calculation. Similarly, the valence neutron gives a contribution of

$$\frac{1}{2} \sum_{i,j} \langle q_i \sigma_i \cdot q_j \sigma_j \rangle_n = \frac{2}{3}\alpha. \quad (5.7)$$

The difference between proton and neutron for this splitting is $5/18 \alpha$. Thus the splitting due to one photon exchange ($O\gamma E$) with a confined photon propagator is approximately

$$\Delta E(O\gamma E) = \frac{5}{18} \frac{\alpha}{R} (-0.176) \text{MeV} = -0.071 \text{MeV}. \quad (5.8)$$

Bickeböllner *et al.*[126] calculated the effects of OGE with a confined and an unconfined gluon propagator in the soliton bag model. They found that confinement increases the color-magnetic energy by about 50% due to enhanced gluon field strength in the bag. If we assume a similar correction applies to our calculation of the electromagnetic one photon exchange, we need to reduce $\Delta E(O\gamma E)$ to about $2/3$ of the value calculated above. With this assumption, we combine the 0.584 MeV splitting from the Coulomb interaction and the $\frac{2}{3}(-0.071)$ MeV splitting from $O\gamma E$ interactions. Thus the electromagnetic interaction makes the proton about 0.537 MeV heavier than the neutron. Since experimentally the n is heavier than the p by 1.3 MeV, this requires an OGE splitting of about 1.8 MeV.

In contrast to a reduced splitting due to classical electromagnetic effects, Goldman *et. al*[121] argues that the nucleon mass splitting should increase due to finite electromagnetic corrections to the quark gluon vertex functions. He did not discuss what appears to be a larger contribution arising from the Coulomb interaction. He focuses on a correction to the effective strength of the strong interaction proportional to the square of electric charge that increases as one moves toward the infrared. Comparing two color singlet states with the same isospin structure, the state with more u quarks should have the mass decreased due to greater binding of u than d quarks.

The MIT bag model we use does not include important effects due to the pion cloud surrounding the nucleons. Pions should account for a portion of the nucleon masses and for some of the $\Delta - N$ splitting. Chiral perturbation theory in leading

order indicates there should be a combined QED and QCD contribution[122] of $\delta m \sim (m_d - m_u)/(m_d + m_u) m_\pi^2/m_\rho \sim (\text{a few MeV})$ to the nucleon mass splitting.

The u vs d mass difference (and electromagnetic effects) split the masses of the Σ 's and the Ξ 's as well as the nucleons. The splitting is larger for $(\Sigma^+ - \Sigma^-)$ than for the nucleons or $(\Xi^0 - \Xi^-)$ because the Σ 's differ by replacing two d for u quarks, whereas the nucleons and cascades differ by replacing one d for a u quark. We calculate the masses of these baryons using the orthonormal states generated for the nucleon, but replacing one quark mass for another. In our fits to the data, we include corrections for each particle's electromagnetic Coulomb and $O\gamma E$ contributions as outlined above.

5.2 Mass splitting of the N and Δ

In the section above, we calculated the $\Delta - N$ splitting for three $s_{1/2}$ valence quarks in order to motivate the calculation of the electromagnetic splitting between n and p . We now examine the $\Delta - N$ splitting arising from configuration mixing where more states are included in the basis. As described in the previous chapter, we adjust α_s to get the right $\Delta^0 - n$ splitting. It takes several iterations to get this correct, since the Δ^0 needs a different radius than the nucleon to be consistent with the bag constant chosen for the n , and the radius correction changes the Δ^0 energy. The $\Delta^0 - n$ splitting is plotted in Fig. 4.2 as a function of cutoff. The graph shows the splittings for all cutoffs ranging from a cutoff of 0 (with only three $s_{1/2}$ valence quarks) to the cutoff at 1.5 GeV above the three valence quark state. The graph also shows that the three quark state with $\alpha_s = 2.2$ has the same splitting as the configuration with 1.5 GeV cutoff and $\alpha_s \simeq 1.4$.

The matrix we diagonalize for configuration mixing is formed from the sum of the OGE and self-energy matrix elements proportional to α_s plus energies of each orthonormal state along the diagonal which are independent of α_s . We choose an initial value for α_s and diagonalize the matrix for the neutron at $R=0.005 \text{ MeV}^{-1}$ and repeat this for $R=0.0045 \text{ MeV}^{-1}$. The lowest two eigenvalues in each matrix correspond to the n and Δ^0 for those two radii. We assume solutions of the form

$$m_{diag} = m_0 + \frac{m_r}{R} \quad (5.9)$$

over a short range in R . We determine m_0 and m_r for the n and separately for the Δ^0 by fitting the eigenvalues at the two radii. We chose this form for the mass since

massless quark energies are proportional to $1/R$, and quarks with mass go as $1/R$ plus a constant (with $E_q = \frac{1}{R}\sqrt{x_q^2 + m_q^2 R^2}$). The eigenvalues x_q are dimensionless solutions of the Dirac equation in the bag. The OGE matrix elements have similar asymptotic behavior.

We equate the experimental neutron mass $m_n^{expt} = 938.566$ to the MIT bag energy,

$$m_{expt} = m_{diag} + \frac{4}{3}\pi R^3 B + \frac{Z}{R}. \quad (5.10)$$

We set the derivative of this equation equal to zero,

$$0 = m_r + \frac{4}{\pi}R^2 B - \frac{Z}{R^2}, \quad (5.11)$$

and solve these equations for B and Z to find the minimum energy at a given radius value.

The radius and mass of the Δ are then calculated using the same equations, but with B and Z fixed at the values determined by the n . We check to see if we have the correct $\Delta^0 - n$ splitting, adjusting α , and re-diagonalizing the matrix if the splitting is incorrect.

5.3 Octet mass splittings as functions of m_s and B and the self-energy

The s quark is much heavier than the u or d quark; it is primarily responsible for mass splittings between the nucleons and Σ 's and the Σ 's and Ξ 's. We calculate the masses for six members of the baryon octet—all cases where two valence quarks have one flavor and the third quark has a different flavor. These outer members of the octet include the nucleons (proton and neutron), Σ^+ , Σ^- , Ξ^0 , and the Ξ^- . We also calculate masses and radii for the first excitations, the Δ^+ , Σ^{*-} , Σ^{*+} , Ξ^{*-} , and Ξ^{*0} using the same values for B and Z .

We began by choosing a bag radius R_n for the neutron. Using Eq. 2.12 for the total MIT energy, we minimized the energy for the neutron to determine the bag constant B and Casimir energy. We then solve for the masses and bag radii of all the other particles using the same two equations. The proton has essentially the same radius as the neutron, since the ground state energy is only slightly lower than that of the neutron. The Σ 's and Ξ 's and all the excited states require larger bag radii

to maintain the same value for B . (B is assumed to be a property of the strongly coupled vacuum, and should remain constant.)

We choose three sets of parameter values for our calculations. The parameter sets involve orthogonal 10% variations of m_s and B . For each value of B , a different α_s is needed to retain the correct $\Delta^0 - n$ splitting. However, we also need calculations with the same α_s at different radii to determine the functional dependence of the ground state energy on radius. Thus, we calculate and diagonalize the matrix for two bag radii, for two values of the strange quark mass and with two values of α_s at each radius (See Appendix E). We repeat these calculations using two different self-energy expressions.

In our first parameter set, we assume a bag constant $B^{1/4} = 146$ MeV (which makes a neutron radius of $R = 0.005 \text{ MeV}^{-1} \simeq 0.987$ fm) and a strange quark mass $m_s = 279$ MeV. This is the same as in the first parameter set of DeGrand et al.[54]. However, we found it necessary to adjust the strong coupling α_s from 2.2 to 1.3636 in order to maintain the same $\Delta - N$ splitting with our larger set of basis states. We extend this calculation to include the Σ 's and Ξ 's. The second parameter set has a radius that is 10% smaller. Choosing $B^{1/4} = 158$ MeV, the neutron radius is $R = 0.0045 \text{ MeV}^{-1} \simeq 0.888$ fm. We keep the strange mass the same at $m_s = 279$ MeV. The third parameter set is with the original radius $R = 0.005 \text{ MeV}^{-1} \simeq 0.987$ fm, but with $m_s = 300$ MeV. From these results, we can extrapolate to combinations for the strange quark mass and bag radius where the fit to the baryon mass spectrum is optimized.

The first form for the self-energy we use corresponds to the choice by the MIT model builders[54] to include only the minimum self-energy required to satisfy the MIT bag boundary conditions. In the OGE approximation, the gluon fields satisfy Maxwell's equations for each color component. When these fields are confined within the bag, the electric and magnetic components must satisfy the boundary conditions,

$$\begin{aligned}\hat{r} \cdot \vec{E}^a &= 0, \\ \hat{r} \times \vec{B}^a &= 0,\end{aligned}\tag{5.12}$$

where a is the color index. The \vec{B} field satisfies the boundary conditions, but \vec{E} field does not, unless a portion of the self-energy terms are added in. The self-energy graphs required are those where electric-type gluons form a loop with the quark, and

the quark state remains the same throughout the process.

The second form of the self-energy we use is where we allow all intermediate spins, colors, and energy levels for the quark states within both magnetic and electric self-energy loops consistent with the Coulomb, electric and magnetic vertices used in the OGE calculations up to a given cutoff. We find similar mass splittings for both choices of self-energy, but the more complete form of the self-energy requires a smaller (positive) Casimir term.

The more complete expression for the self-energy increases the ground state energy relative to the minimal MIT prescription. At first this is surprising because from first-order perturbation theory one expects the energy to be lowered by contributions from intermediate states inside the self-energy loop that are higher in energy than the quark energy outside the loop. However this effect is small in comparison to the new self-energy terms where the quark remains at the same energy level but changes color inside the self-energy loop. There is a color factor of 2 when the quark changes to one of two other colors. In contrast to the OGE exchange diagrams, there is no minus sign due to quark exchange in normal ordering since the final state remains in normal color order. Thus the color factor of $\frac{4}{3}$ with no color change of intermediate quark state for the minimal MIT self-energy changes to $\frac{16}{3}$ with the full self-energy. There are also sums over intermediate spins which are also positive. These positive contributions to the self-energy overwhelm the negative first-order perturbative corrections to the self-energy.

In most other respects, the properties we find for the two forms of self-energy are very similar. The effects can be absorbed in renormalization of the model parameters. We find a smaller positive value for the Casimir term and also for m_s , both of which are moving in the right direction. However, it was not obvious from the outset that a new self-energy and renormalization of bag parameters including moderate changes in m_s would result in all the baryons retaining similar splittings.

5.4 Best fits to the baryon mass spectrum

We use the minimal MIT self-energy, and let m_s and B vary to determine two least-squared fits to the baryon mass spectrum. We then adjust B to reproduce the proton mean square charge radius and let m_s vary to determine a second best fit. These results are shown in table 5.3, where our two fits are compared with experimental

values[1] and with the results of DeGrand *et al.*[54]. We weight the squared errors in isospin partners by a factor of 10 over the squared errors between nucleons, Σ 's and Ξ 's.

The best fit for varying both B and m_s is with $m_s = 287.7$ MeV and $B^{1/4} = 139.3$ MeV, which makes $E_C = +6.87/R$ and $\alpha_s = 1.43$. The neutron bag radius is $R = .0053 \text{ MeV}^{-1} = 1.041 \text{ fm}$. The unweighted RMS error in fitting the twelve masses is 17.2 MeV with seven degrees of freedom. Five parameters (α_s , B , Z , m_s , and m_d) are considered to be adjustable in this model, although we have not varied m_d .

Our second fit uses $B^{1/4} = 126.6$ to fit the proton mean square charge radius, with m_s varied to fit the mass spectrum. This makes $m_s = 286.6$, $E_C = +7.97/R$ and $\alpha_s = 1.60$. The unweighted RMS error in fitting the masses is 16.3 MeV, which is actually better than where we varied both B and m_s , but the weighted fit is worse. There is a problem with the masses of the Σ 's, in that the Σ^+ is heavier than the Σ^- when we interpolate to these larger bag radii. With these parameter values, the neutron bag radius is $R = .00599 \text{ MeV}^{-1} = 1.183 \text{ fm}$.

We repeat these calculations for the self-energy built from all vertices used in OGE diagrams below the cutoff. These results are shown in Fig. 5.4. The mass fits are about the same, although using the full self-energy requires some renormalization of parameters. With the full self-energy, a smaller positive Casimir term is required, and also a smaller value for m_s is needed. Both of these trends are in the right direction.

In comparison, DeGrand *et al.*[54] had an RMS error of 26.7 MeV when considering only the hadron masses they fit (with four degrees of freedom after excluding four for setting parameters. If we calculate errors for only those baryons included in both data sets, our RMS error is 22.6 MeV for the minimal MIT self-energy and 23.1 MeV for the full self-energy, while DeGrand *et al.*'s is 37.0 MeV using valence quark wave functions and perturbation theory calculations for the hadron masses.

With the $\Delta - N$ splitting held constant, the Σ and Ξ baryons masses can be shifted higher either by increasing the strange mass, or to a lesser extent, by increasing the bag radius. However, it doesn't seem possible to bring all particle masses into full agreement simultaneously with experimental values.

In summary, we have interpolated from the baryon mass spectra calculated with three parameter sets and two self-energy prescriptions to determine values in B vs m_s space that optimizes the fit to experimental masses. Table 5.3 shows the best

fits with the minimal MIT self-energy and with the self-energy built from all vertices contributing to the OGE graphs allowed below the cutoff.

Table 5.1: Bag radii and masses for ground and first excited state baryons with several choices for the MIT bag parameters using the minimal MIT self energy. Electromagnetic corrections are included. These results are used to linearly extrapolate to other values for the strange quark mass and bag radii. The bag radius must be adjusted for each particle to achieve a consistent value for B , the bag constant.

Particle	Experiment[1]	MIT Bag With 1.5 GeV Cutoff using linear fits to particle radii based on Table E.1.						MIT Bag of DeGrand <i>et al.</i> [54]	
		$B^{1/4} = 145 \text{ MeV}$ $E_C = +6.446/R$ $m_s = 279 \text{ MeV}$ $m_u = 0 \text{ MeV}$ $m_d = 5 \text{ MeV}$ $\alpha_s = 1.3636$		$B^{1/4} = 157 \text{ MeV}$ $E_C = +5.679/R$ $m_s = 279 \text{ MeV}$ $m_u = 0 \text{ MeV}$ $m_d = 5 \text{ MeV}$ $\alpha_s = 1.2433$		$B^{1/4} = 145 \text{ MeV}$ $E_C = +6.445/R$ $m_s = 300 \text{ MeV}$ $m_u = 0 \text{ MeV}$ $m_d = 5 \text{ MeV}$ $\alpha_s = 1.3636$		$B^{1/4} = 145 \text{ MeV}$ $E_C = -1.84/R$ $m_s = 279 \text{ MeV}$ $m_u = 0 \text{ MeV}$ $m_d = 0 \text{ MeV}$ $\alpha_s = 2.2$	
	M (MeV)	R (fm)	M (MeV)	R (fm)	M (MeV)	R (fm)	M (MeV)	R (fm)	M (MeV)
n	939.6	0.987	939.6	0.888	939.6	0.987	939.6		
p	938.3	0.984	938.0	0.885	937.2	0.984	937.2	0.987	938
Σ^-	1197.4	0.983	1161.6	0.884	1157.0	0.982	1178.9		
Σ^+	1189.4	0.965	1155.0	0.866	1144.7	0.965	1167.1	0.977	1144
Ξ^-	1321.3	0.978	1324.3	0.878	1318.4	0.978	1354.0		
Ξ^0	1314.9	0.982	1319.9	0.883	1315.5	0.982	1351.0	0.969	1289
Δ^0	1233.7	1.082	1233.3	0.973	1233.3	1.082	1233.4		
Δ^+	1234.9	1.080	1233.3	0.971	1232.5	1.080	1232.5	1.081	1233
Σ^{*-}	1387.2	1.076	1378.6	0.967	1378.1	1.076	1390.9		
Σ^{*+}	1382.8	1.068	1376.2	0.959	1372.8	1.068	1385.5	1.071	1382
Ξ^{*-}	1535.0	1.069	1520.0	0.961	1519.1	1.069	1544.4		
Ξ^{*0}	1531.8	1.071	1516.0	0.963	1515.8	1.071	1541.2	1.064	1529

Table 5.2: Ground and first excited state energies and bag radii for baryons with several choices for the MIT bag parameters with the self-energy constructed from all OGE graphs contributing to diagrams below the cutoff. Electromagnetic corrections are included. These results are used to linearly extrapolate to other values for the strange quark mass and bag radii. The bag radius must be adjusted for each particle to achieve a consistent value for B , the bag constant.

Particle	Experiment[1]	MIT Bag With 1.5 GeV Cutoff using linear fits to particle radii based on Table E.2.						MIT Bag of DeGrand <i>et al.</i> [54]	
		$B^{1/4} = 145 \text{ MeV}$ $E_C = +5.72/R$ $m_s = 279 \text{ MeV}$ $m_u = 0 \text{ MeV}$ $m_d = 5 \text{ MeV}$ $\alpha_s = 1.332$		$B^{1/4} = 157 \text{ MeV}$ $E_C = +5.01/R$ $m_s = 279 \text{ MeV}$ $m_u = 0 \text{ MeV}$ $m_d = 5 \text{ MeV}$ $\alpha_s = 1.215$		$B^{1/4} = 145 \text{ MeV}$ $E_C = +5.72/R$ $m_s = 300 \text{ MeV}$ $m_u = 0 \text{ MeV}$ $m_d = 5 \text{ MeV}$ $\alpha_s = 1.332$		$B^{1/4} = 145 \text{ MeV}$ $E_C = -1.84/R$ $m_s = 279 \text{ MeV}$ $m_u = 0 \text{ MeV}$ $m_d = 0 \text{ MeV}$ $\alpha_s = 2.2$	
	M (MeV)	R (fm)	M (MeV)	R (fm)	M (MeV)	R (fm)	M (MeV)	R (fm)	M (MeV)
n	939.6	0.987	939.6	0.888	939.6	0.987	939.6		
p	938.3	0.986	936.4	0.887	936.3	0.986	936.2	0.987	938
Σ^-	1197.4	0.983	1195.1	0.884	1190.0	0.983	1214.3		
Σ^+	1189.4	0.971	1186.5	0.871	1177.5	0.971	1202.5	0.977	1144
Ξ^-	1321.3	0.984	1391.7	0.884	1385.3	0.984	1425.5		
Ξ^0	1314.9	0.988	1386.5	0.889	1381.5	0.988	1421.6	0.969	1289
Δ^0	1233.7	1.082	1232.5	0.974	1233.5	1.082	1232.6		
Δ^+	1234.9	1.081	1230.3	0.973	1231.2	1.081	1230.1	1.081	1233
Σ^{*-}	1387.2	1.076	1418.4	0.968	1418.1	1.076	1433.1		
Σ^{*+}	1382.8	1.073	1412.5	0.963	1410.8	1.073	1426.0	1.071	1382
Ξ^{*-}	1535.0	1.075	1591.5	0.966	1591.2	1.075	1620.1		
Ξ^{*0}	1531.8	1.077	1586.3	0.969	1586.9	1.077	1616.0	1.064	1529

Table 5.3: Weighted least squares fits to baryon masses with the minimal MIT self-energy. Columns 1 and 2 list the baryons and gives experimental values for the masses. Column 3 and 4 show bag radii and masses where B and m_s are allowed to vary, using linear interpolation between configuration mixing calculations. In the fit, we weight the errors in isospin splitting with a factor of ten over the errors between rows in the baryon multiplet. The unweighted RMS fit to the masses is 17.2 MeV with seven degrees of freedom. Columns 5 and 6 show results where B is set to reproduce the proton mean square charge radius and m_s is allowed to vary to fit the baryon mass spectrum. The unweighted RMS fit to the masses is 16.3 MeV with seven degrees of freedom, but extrapolation to the larger bag radius reverses the Σ masses. Column 7 and 8 show the radii and masses calculated by DeGrand *et al.* using perturbation theory with three $s_{1/2}$ valence quarks.

Particle	Experiment[1] M (MeV)	Vary B and m_s to fit masses. $B^{1/4} = 139.3$ MeV $E_C = +6.87/R$ $m_s = 287.7$ MeV $m_u = 0$ MeV $m_d = 5$ MeV $\alpha_s = 1.430$		Set B , vary m_s to fit p charge radius $B^{1/4} = 126.6$ MeV $E_C = +7.97/R$ $m_s = 286.6$ MeV $m_u = 0$ MeV $m_d = 5$ MeV $\alpha_s = 1.603$		Valence MIT DeGrand <i>et al.</i> [54] $B^{1/4} = 145$ MeV $E_C = -1.84/R$ $m_s = 279$ MeV $m_u = 0$ MeV $m_d = 0$ MeV $\alpha_s = 2.2$	
		R (fm)	M (MeV)	R (fm)	M (MeV)	R (fm)	M (MeV)
n	939.6	1.042	939.6	1.184	939.6		
p	938.3	1.039	938.1	1.181	939.3	0.987	938
Σ^-	1197.4	1.038	1171.4	1.180	1177.0		
Σ^+	1189.4	1.020	1165.8	1.162	1179.8	0.977	1144
Ξ^-	1321.3	1.034	1339.9	1.177	1346.8		
Ξ^0	1314.9	1.037	1335.3	1.179	1339.9	0.969	1289
Δ^0	1233.7	1.143	1233.3	1.298	1233.3		
Δ^+	1234.9	1.141	1233.4	1.296	1234.6	1.081	1233
Σ^{*-}	1387.2	1.137	1384.0	1.292	1384.1		
Σ^{*+}	1382.8	1.129	1382.0	1.284	1386.3	1.071	1382
Ξ^{*-}	1535.0	1.129	1530.7	1.283	1530.6		
Ξ^{*0}	1531.8	1.131	1526.6	1.285	1525.5	1.064	1529

Table 5.4: Weighted least squares fits to baryon masses with the self-energy built from all vertices contributing to OGE diagrams below cutoff. Columns 1 and 2 list the baryons and gives experimental values for the masses. Column 3 and 4 show bag radii and masses where B and m_s are allowed to vary, using linear interpolation between configuration mixing calculations. In the fit, we weight the errors in isospin splitting with a factor of ten over the errors between rows in the baryon multiplet. The unweighted RMS fit to the masses is 19.0 MeV with seven degrees of freedom. Columns 5 and 6 show results where B is set to reproduce the proton mean square charge radius and m_s is allowed to vary to fit the baryon mass spectrum. The unweighted RMS fit to the masses is 16.0 MeV with seven degrees of freedom, but the extrapolation to the larger bag reverses the Σ masses. Column 7 and 8 show the radii and masses calculated by DeGrand *et al.* using perturbation theory with three $s_{1/2}$ valence quarks.

Part- icle	Exper- iment[1]	Vary B and m_s to fit masses.		Set B , vary m_s to fit p charge radius		Valence MIT DeGrand <i>et al.</i> [54]	
		$B^{1/4} = 143.5$ MeV $E_C = +4.80/R$ $m_s = 242.9$ MeV $m_u = 0$ MeV $m_d = 5$ MeV $\alpha_s = 1.365$		$B^{1/4} = 126.7$ MeV $E_C = +5.91/R$ $m_s = 239.4$ MeV $m_u = 0$ MeV $m_d = 5$ MeV $\alpha_s = 1.577$		$B^{1/4} = 145$ MeV $E_C = -1.84/R$ $m_s = 279$ MeV $m_u = 0$ MeV $m_d = 0$ MeV $\alpha_s = 2.2$	
	M (MeV)	R (fm)	M (MeV)	R (fm)	M (MeV)	R (fm)	M (MeV)
n	939.6	1.002	939.6	1.183	939.6		
p	938.3	1.001	936.8	1.182	937.0	0.987	938
Σ^-	1197.4	0.998	1162.9	1.179	1169.0		
Σ^+	1189.4	0.986	1160.4	1.169	1174.1	0.977	1144
Ξ^-	1321.3	0.999	1334.6	1.182	1340.6		
Ξ^0	1314.9	1.003	1326.9	1.184	1330.2	0.969	1289
Δ^0	1233.7	1.098	1232.2	1.296	1230.3		
Δ^+	1234.9	1.097	1230.5	1.295	1228.9	1.081	1233
Σ^{*-}	1387.2	1.092	1393.2	1.290	1391.3		
Σ^{*+}	1382.8	1.089	1389.6	1.291	1390.4	1.071	1382
Ξ^{*-}	1535.0	1.091	1542.4	1.291	1538.1		
Ξ^{*0}	1531.8	1.093	1535.2	1.291	1529.1	1.064	1529

Chapter 6

NUCLEON OBSERVABLES

We utilize the nucleon ground state configurations that we found by matrix diagonalization to calculate various measurable nucleon properties. These observables include the charge radii, magnetic moments, the ratio of axial to vector currents (g_A/g_V), and the spin fractions carried by different flavors of quarks. We calculate these observables for values of B and m_* corresponding to the best fits to baryon masses for the minimal MIT self-energy and again using the self-energy constructed from all vertices used in OGE interactions below the 1.5 GeV cutoff.

The observables we consider are two-quark field (single particle) operators of the form,

$$\langle O \rangle = \int d^3x \bar{\psi}(x) \hat{O} \psi(x), \quad (6.1)$$

where $\psi(x)$ is a linear combination of orthonormal qqq and $qqqq\bar{q}$ states determined by matrix diagonalization. These operators are not purely diagonal. In addition to contributions weighted by the probability for each orthonormal state, there are also contributions from the operator linking different quark states to create new multi-quark states that are in the basis. If the new state has the same number of particles as the initial state, the operator must not change the parity of the particle and the m_J values must remain the same. There are also contributions if the operators link qqq amplitudes to $qqqq\bar{q}$ amplitudes by annihilating a quark and an antiquark from the $qqqq\bar{q}$ sector[70]. For $qqq \leftrightarrow qqqq\bar{q}$ transitions, the quark and antiquark that are annihilated must have the same flavor and opposite m_J values. To conserve parity, the orbital angular momenta of quark and antiquark must differ by an odd integer, since the antiquark has opposite intrinsic parity to the quark. Since the $qqqq\bar{q}$ sector includes only $s_{1/2}$, $p_{3/2}$, and $p_{1/2}$ states below the cutoff, this means either the quark or antiquark must be $p_{3/2}$ or $p_{1/2}$ while the other is $s_{1/2}$. Since the operators carry no color, they can only annihilate a pair that forms a color singlet, leaving a color singlet qqq state behind that is within the basis. Thus, the operators can not annihilate a quark-antiquark pair directly created by a gluon, as then it would have to carry octet

color. However, in contrast to perturbative calculations, the nucleon observables have small contributions from annihilation of $s\bar{s}$ pairs. The basis is complete (below the cutoff) and includes states requiring several OGE exchanges to link them to qqq states.

To calculate these $qqq \leftrightarrow qqqq\bar{q}$ cross-term contribution to two-quark field observables, we need the projection of the $qqqq\bar{q}$ states where a particular quark and antiquark form a color singlet onto $qqqq\bar{q}$ basis states that are in the same category. These are readily calculated for each type of multi-quark state using our template states. These numbers are then multiplied by the operator expectation value acting on the quark-antiquark pair and by the amplitudes for the corresponding $qqqq\bar{q}$ and qqq states determined by the eigenvectors found in diagonalizing the matrix.

6.1 Charge radii of the baryons

Electron-nucleon scattering is used to determine the charge radii of the nucleons. The charge radius can be determined from the slope of the electric or magnetic form factors as a function of Q^2 at $Q^2 = 0$. Measurements of the neutron charge radius have been based on scattering of slow neutrons on atomic electrons and by elastic and quasi-elastic electron-deuteron scattering. The neutron charge radius[133, 134, 136, 137] has been determined to be negative with $dF_{1n}/dQ^2|_{Q^2=0} = (-0.17 \pm 0.03) \cdot 10^{-2} \text{ fm}^2$. The calculations are sensitive[137, 136] to assumptions made in different treatments for ρ -exchange contributions. There are also problems with analytically continuing spectral functions and uncertainties in knowledge of the deuteron wave function. Derivation of the proton charge radius from measurements is somewhat easier, although there are still unresolved differences in the fits. For example, several fits[138, 136] to the proton charge radius give similar values, with $r_{Ep} = r_{Mp} = 0.84 \pm 0.01 \text{ fm}$ [136], or $r_{Ep} = 0.88 \pm 0.03$ and $r_{Mp} = 0.84 \pm 0.03$. One best fit to ep scattering results has determined the proton charge radius to be $0.862(12) \text{ fm}$ [144], consistent with the results above. However, an older best fit is incompatible with the stated uncertainties, with a much smaller value[145] for the proton radius at $r = 0.805(11) \text{ fm}$. In our comparisons, we list the 0.862 value, corresponding to $\langle r_p^2 \rangle = 0.743(.021)$.

In the MIT bag, the mean square charge radius is given by

$$\langle r^2 \rangle = \int_{bag} d^3r r^2 \psi^\dagger Q \psi, \quad (6.2)$$

where Q is the quark electric charge matrix. (See Table 1.1.)

The mean square charge radii for the baryons are listed in Table 6.1 for the parameter values found from best fits to the baryon masses. Our proton mean square radius found from the best fit to baryon masses where we vary B and m_s is small at $\langle r_p^2 \rangle = 0.594$. We also made a fit with a smaller value of B to give the correct value of the proton charge radius, while varying m_s to fit the masses. The charge radii are readily increased by lowering B without significant damage to the mass fits. We found very small non-diagonal contributions to $\langle r_p^2 \rangle$, with $qqq \leftrightarrow qqqq\bar{q}$ transitions contributing about 0.2%, and $qqq \leftrightarrow qq\bar{q}$ contributions of about -1%. By comparison, DeGrand *et al.*[54] found a value of $\langle r_p^2 \rangle = 0.517$ in their fit to the baryon spectrum using valence quarks. Donoghue and Golowich[70] found a value of $\langle r_p^2 \rangle = 0.64$, of which 0.12 came from their large perturbative sea amplitudes.

For a given value of B , our proton charge radius is larger than the valence MIT result. This is because about 25% of the nucleon probability involves states with two $p_{3/2}$ quark excitations, and the magnitude of the expectation for the squared radius of $p_{3/2}$ states is 17% larger than the squared radius for $s_{1/2}$ states. But the increase in size is not as large as what one might expect. We also see a positive value for the neutron charge radius. The explanation in both cases is the same. Over 80% of the probability for two $p_{3/2}$ quark excitations in the nucleon involves excitation of one u and one d quark, rather than the 2/3 ratio one might expect. This interference effect can be understood by considering the fraction of intermediate states where both excited quarks have the same m_J value in a neutron. We ignore the isospin breaking due to quark mass differences and the spin sums (which are flavor independent) and only consider the color and flavor. Since both quarks have different color, they either keep the same colors with a color factor of $-\frac{2}{3}$, or they change color with a color factor of 2 multiplied by a factor of (-1) when they are returned to normal order. Thus the probability for excitation of two d quarks to the same m_J is proportional to the square of the sum, or $\frac{64}{9}$. For a u and a d excitation of this type, the intermediate states are distinguishable because of the different flavors, with both ud and du color orderings. The probabilities are proportional to the squares of 2 and $-\frac{2}{3}$ for direct and exchange of color interactions, making a total probability proportional to $\frac{80}{9}$. This

suppresses the number of excited dd 's compared to excited ud 's. For intermediate states involving a given pair of two excited quarks with different m_J values, there are twice as many configurations where different flavors are excited as configurations where the same flavors are excited. Thus for the proton, the charge radius is decreased because of the excess number of $p_{3/2}$ d quarks. For the neutron, this means there are too few excitations of two d quarks to balance excited u quarks, and the mean square charge radius becomes positive.

Donoghue and Golowich found a small negative charge radius for the neutron, with $\langle r_n^2 \rangle = -0.007$, in comparison to the experimental value of -0.117 ± 0.002 fm. As mentioned above our result is positive, with $\langle r_n^2 \rangle = 0.013$. In our calculations, the $qqq \leftrightarrow qq\bar{q}q$ transitions were negative (at -0.00018 fm²), but negligible in comparison to the positive contribution arising from the larger fraction of u than d quarks having $p_{3/2}$ excitations.

The magnitudes of the calculated charge radii are easily modified to have larger values by choosing a smaller value for B . In column 4 of Table 6.1, we decrease B to $B^{1/4} = 126.6$ MeV to match the experimental value for the proton mean square charge radius. However, in this model, it does not seem possible to adjust parameters to make the neutron charge radius negative. The negative contribution that does arise from extra $q\bar{q}$ pairs is small in comparison to the positive contributions.

6.2 Magnetic moments

The quark magnetic moments along the z -axis are given by

$$\bar{\mu}_q = \frac{1}{2} \int_{bag} d^3r \hat{z} \cdot (\mathbf{r} \times \bar{\psi} \vec{\gamma} Q \psi), \quad (6.3)$$

If the nucleon wave function is approximated by three $s_{1/2}$ valence quarks, the non-color part is given by the symmetric direct product of mixed symmetries in spin and isospin. Thus the valence proton and neutron magnetic moments are expressed in terms of u and d magnetic moments as

$$\mu_p = (12\mu_u - 3\mu_d)/9, \text{ and } \mu_n = (12\mu_d - 3\mu_u)/9. \quad (6.4)$$

If the u and d valence quarks have equal mass, $\mu_n/\mu_p = -\frac{2}{3}$. For $s_{1/2}$ quarks, Eq. 6.3

may be integrated analytically to yield

$$\mu_u = \frac{R}{9} \frac{4\omega_u + 2m_u R - 3}{2\omega_u^2 - 2\omega_u + m_u R}, \text{ and } \mu_d = -\frac{R}{18} \frac{4\omega_d + 2m_d R - 3}{2\omega_d^2 - 2\omega_d + m_d R}. \quad (6.5)$$

The experimental value for the proton magnetic moment is $\mu_p = 2.79$ n.m., where a nuclear magneton (n.m.) is $e\hbar/(2m_p)$. The experimental value was fit quite closely by the parameter choices of Chodos *et al.*[53], with their value of $\mu_p = 2.6$ n.m., but a large bag radius is required to equal the experimental value. Close[14] shows that a bag radius of 1.5 fm is required for zero mass quarks, and a larger radius is needed if the light quarks are heavier. In the successful fit to hadron masses by DeGrand *et al.*[54], they needed a larger value for $B^{1/4}$ and thus a smaller value for the bag radius, $R=0.005 \text{ MeV}^{-1} = 0.99 \text{ fm}$. With zero-mass quarks, μ_p is proportional to R . This makes $\mu_p = 1.9$ n.m., which is significantly smaller than the experimental value. This is the most serious discrepancy of the fit given by the first parameter set of DeGrand *et al.* However, they predicted ratios of magnetic moments for other hadrons compared to the proton magnetic moment quite successfully, using the hadron radii from their fit to the hadron masses. These ratios are compared with current experimental values and with results from our calculations in Table 6.3.

Our calculations using our first best fit to the baryon masses does not improve on the results of DeGrand *et al.* for the magnetic moments. Our results are still smaller than the experimental values by a factor of 2/3. When we increase our bag radii to fit the proton mean square charge radius, our magnetic moments are closer to experimental values, but still too small. (See Table 6.2, columns 6 and 7.) The ratios of our baryon magnetic moments to proton magnetic moment are fair. The ratio we calculate for the neutron to proton magnetic moment is $\mu_n/\mu_p = -0.696$, compared to -0.684 experimentally, and $-2/3$ for the valence MIT bag. In perturbative calculation of the quark sea, Donoghue and Golowich found significant ($\sim 30\%$) contributions to the magnetic moments from quark pair creation. This increased the magnitude of the nucleon magnetic moments to within about 12% of the experimental values. We predict sea contributions that are much smaller than those of Donoghue and Golowich, with our total sea probability at about 4%. In comparison, Donoghue *et al.*[70] give perturbative probabilities of 36% for u , 27.1% for d , and 16.7% for s quarks. If we sum these probabilities and renormalize the wave function, the sea probability of Donoghue and Golowich would be 44%, or about

twelve times our sea probabilities.

We find the baryon magnetic moments are primarily given by diagonal contributions of the quark magnetic moments, weighted by the squared amplitude for each quark state. However, $qqq \leftrightarrow qqq$ transitions increase the magnitude of the moments by about 5%, and $qqq \leftrightarrow qq\bar{q}\bar{q}$ transitions add about another 1%. This does not improve the fit to experimental data because of the large amplitudes for excited $p_{3/2}$ states. The $p_{3/2}$ states with $m_J = 1/2$ have magnetic moments only about 60% of the size of $s_{1/2}$ states. (Stretched $p_{3/2}$ states have magnetic moments about 36% larger than $s_{1/2}$ states, but this is more than overcome by alignment of $s_{1/2}$ states to sum to the same m_J value for the state.)

There are several approaches to improving magnetic moments over the values given by the naive MIT model. As noted above, a larger bag radius would improve the magnetic moments. Alternatively, Donoghue and Johnson[125] introduced center of mass corrections that assumed a special form of wave packet where $\langle p^2 \rangle$ is not infinite, as is usually the case for the MIT bag. This led to fairly large corrections for the magnetic moment, raising it from 2.1 n.m. to 2.5 n.m.. However, their choice of wave packet seems to have little justification, except perhaps for pions, where the derivation of the wave packet is based on the amplitude to create a pion from the vacuum.

6.3 Axial currents and the baryon spin fraction carried by quarks

The contribution of quark spins to the spin of the nucleon may be inferred from deep inelastic scattering of polarized leptons on spin polarized targets. Results from the Electron Muon Collaboration (EMC)[139, 140], Stanford Linear Accelerator (SLAC)[141], and the Spin Muon Collaboration (SMC)[142] have been interpreted[139] as showing that valence quark spins make a very small contribution to the nucleon spin. The experiments measure asymmetries in the virtual photoabsorption cross sections, $\sigma_{1/2}$ and $\sigma_{3/2}$, where the angular momentum projection of the virtual photon plus nucleon system along the incident lepton direction is 1/2 or 3/2 respectively. These asymmetries may be expressed in terms of spin structure functions. The spin structure function of interest is

$$g_1(x) = \frac{1}{2} \sum e_i^2 (q_i^+(x) - q_i^-(x)), \quad (6.6)$$

where $q_i^+(x)$ ($q_i^-(x)$) is the momentum distribution of quark i with spin parallel (anti-parallel) to the nucleon, e_i is the quark charge, and x is the momentum fraction carried by the quark.

Ellis-Jaffe[147] and Bjorken[146] derived sum rules relating the structure functions to other observables. The Bjorken sum rule is derived using light-cone algebra for the electromagnetic and weak coupling to quark currents. Using the operator product expansion, (OPE)[38], the integrated structure function for a baryon (labeled by B) in terms of quark fields is

$$\Gamma_1^B = \int_0^1 dx g_1^B(x) = \langle B \uparrow | \sum_i \frac{1}{2} Q_i^2 \bar{\psi} \gamma_5 \gamma_\mu \psi | B \uparrow \rangle \times (1 - \alpha_s/\pi) = \frac{1}{2} \left[\frac{4}{9} \Delta u(Q^2) + \frac{1}{9} \Delta d(Q^2) + \frac{1}{9} \Delta s(Q^2) \right] \times (1 - \alpha_s/\pi), \quad (6.7)$$

where $(1 - \alpha_s/\pi)$ comes from radiative corrections[148], and α_s is also a function of Q^2 . The Bjorken sum rule states that the difference in proton and neutron structure functions integrated over all momenta is related to the ratio of axial to vector coupling constants, g_A/g_V , measurable from nucleon beta decay.

$$\Gamma(p) - \Gamma(n) = \frac{1}{6} g_A/g_V (1 - \alpha_s/\pi), \quad (6.8)$$

It is not possible to perform experiments over the full range of x , so experimental results must be extrapolated to make an estimate of Γ_1^p and Γ_1^n . The experiments have been performed at different values of Q^2 , with an average of 2 GeV² at SLAC-E142[141], 5 GeV² and 10 GeV² at SMC[142], and 10 GeV² for E80/E130[143] and EMC[139, 140]. At SMC, with $Q_0^2 = 10 \text{ GeV}^2$, Adeva *et al.* found

$$\Gamma_1^p(Q_0^2) = \int_0^1 g_1^p(x, Q_0^2) dx = 0.136 \pm 0.011 \pm 0.011, \quad (\text{SMC at } 10 \text{ GeV}^2). \quad (6.9)$$

They combined their results with those from E80/E130 and EMC, running the values in Q^2 . They found

$$\Gamma_1^p(10 \text{ GeV}^2) = 0.142 \pm 0.008 \pm 0.011 \quad (\text{Combined SMC, E80/130 and EMC}). \quad (6.10)$$

for all proton data.

There are some uncertainties in comparing the experimental results with those of quark models where $Q^2 = 0$. However, our results from configuration mixing are in reasonable agreement with the experimental values for Γ_1^p . (See Table 6.3).

We find

$$\begin{aligned}\Gamma_1^p(\sim 1 \text{ GeV}^2) &= 0.148 && \text{(Our fit varying } B \text{ and } m_s), \\ \Gamma_1^p(\sim 1 \text{ GeV}^2) &= 0.141 && \text{(Our fit matching } p \text{ charge radius).}\end{aligned}\quad (6.11)$$

Without corrections for evolution of Q^2 , our results close to experimental values for $\Gamma_1^p(10 \text{ GeV}^2)$.

To test the Bjorken sum rule, the SMC group fit Γ_1^p , Γ_1^n , and Γ_1^d at 5 GeV^2 to find,

$$\Gamma_1^p - \Gamma_1^n = 0.163 \pm 0.017 \quad (\text{n data from E142, p data from SMC at } 5 \text{ GeV}^2). \quad (6.12)$$

when using neutron data or

$$\Gamma_1^p - \Gamma_1^n = 0.204 \pm 0.029 \quad (\text{d, p data from E142, SMC at } 5 \text{ GeV}^2). \quad (6.13)$$

based on extrapolation from deuteron and proton data. They include a theoretical estimate based on the Bjorken sum rule including corrections up to third order in α_s , with

$$\Gamma_1^p - \Gamma_1^n = 0.185 \pm 0.004 \quad (\text{Theory at } Q^2 = 5 \text{ GeV}^2). \quad (6.14)$$

Higher twist effects become more important at low Q^2 , leading to about 2% effects depending on the model used.

Our results for the Bjorken sum rule are

$$\begin{aligned}\Gamma_1^p - \Gamma_1^n &= 0.147 && \text{(Our fit with minimal MIT self-energy),} \\ \Gamma_1^p - \Gamma_1^n &= 0.141 && \text{(Our fit with more complete self-energy).}\end{aligned}\quad (6.15)$$

Our values are below the 0.204 ± 0.029 experimental value for proton plus deuteron data and in agreement with the 0.163 ± 0.017 value based on neutron and proton data. If we take $\alpha_s \approx 0.5$ at the nucleon energy scale of 1 GeV , with $g_A/g_V = 1.257[1]$, the Bjorken sum rule with vertex corrections gives a value of $\Gamma_1^p - \Gamma_1^n = 0.176$, which is also slightly larger than the value we calculated.

Our value for the neutron based on configuration mixing is $\Gamma_1^n(\sim 1 \text{ GeV}^2) = 0.001$. Experimental values of $\Gamma_1^n(2 \text{ GeV}^2) = -0.022 \pm 0.011$ have been estimated from scattering of $Q^2 = 2 \text{ GeV}^2$ electrons on polarized He at E142[141], and $\Gamma_1^n(5 \text{ GeV}^2) = -0.069 \pm 0.025$ based on proton and deuteron results at $Q^2 = 5 \text{ GeV}^2$.

The Ellis-Jaffe sum rule assumed $\Delta s = 0$ and is violated by the experimental results[142]. Using current values for $\alpha_s = 0.25 \pm 0.002$ in the range of Q^2 used for the EMC experiments, the Ellis-Jaffe sum rule is[149]

$$\Gamma_1^p = 0.175 \pm 0.18 \quad (\text{Ellis-Jaffe sum rule}). \quad (6.16)$$

Comparing this with the SMC[142] results, the sum rule is violated by two standard deviations. Our results are in agreement with the Ellis-Jaffe sum rule. With $F = (\Delta u - \Delta s)/2 = 0.354$ or 0.359 , and $D = (\Delta u - 2\Delta d + \Delta s)/2 = 0.530$ or 0.537 , the Ellis-Jaffe sum rule for the proton is $\Gamma_1^p = \frac{1}{18}(9F - D)(1 - \alpha_s/\pi) = 0.148$ or 0.141 , equivalent to the values for Γ_1^p and Γ_1^n in Table 6.3.

The spin fractions we calculate for u , d , and s quarks are listed in Table 6.3 for the various particles. We find the sum of quark spins $\Delta\Sigma = \Delta u + \Delta d + \Delta s = 0.506$ or 0.461 for the neutron, and 0.532 or 0.502 for the proton. This is below the valence MIT bag model result of 0.65 and above the SMC estimate of $\Delta\Sigma = 0.22 \pm 0.10 \pm 0.10$ [142]. The spin contribution from strange quarks is negative, but negligible with $\Delta s = -0.0001$. Many fits to experimental data have utilized a significant negative strange quark contribution to the nucleon spin, with $\Delta s = -0.12 \pm 0.04 \pm 0.04$ found by the SMC collaboration[142]. Fits[150, 151] to the values of Δu , Δd , and Δs typically utilize the EMC or other experimental data in conjunction with two other equations based on weak and hyperon decays and SU(3) flavor symmetry. For example, Mulders and Pollock[150] use the formula $\Delta u - \Delta d = g_A/g_V = 1.257$, which is apparently just the SU(3) flavor-symmetric formula for the Bjorken sum rule without radiative corrections. The second formula used comes from low energy hyperon decays, with $\Delta u + \Delta d - 2\Delta s = 0.58 \pm 0.05$.

Comparing our values for the proton with these expressions, our value for $g_A/g_V = \Delta u - \Delta d = 0.884$ or 0.852 . The MIT valence value for g_A/g_V is 1.09 . Both are well below the experimental values for $g_A/g_V = 1.257$. As noted above, including a factor of $(1 - \alpha_s/\pi)$ times g_A/g_V for radiative corrections improves our result. For $\alpha_s = 0.5$, our value for g_A/g_V would be about 1.06 . We would need a value of $\alpha_s = 0.92$ to fit the experimental value. (We have been using a much larger value of the strong coupling to match the $\Delta - N$ splitting, with $\alpha_s \approx 1.4$ inside the bag.) Another approach for correcting the small value of g_A/g_V is to modify the MIT bag to be the chiral bag model. This involves matching the axial vector current at the bag surface

with a pion field outside the bag[151]. Our quark spin values are consistent with the formula for hyperon decay, with $\Delta u + \Delta d - 2\Delta s = 0.532$ to 0.502 , compared[150] to the experimental values of 0.58 ± 0.05 .

In summary, our charge radii and magnetic magnetic moments are small for the parameter fits where both B and m_s were varied. Decreasing B to match the proton mean square charge radius gave somewhat better magnetic moments, but they are still small. Our values for Γ_1^p and Γ_1^n agree with current experimental results. About 50 - 54% of the proton spin is carried by the quark spin, with the remainder accounted for by orbital angular momentum of the quarks. We have not included gluons in our basis states, so cannot make an estimate of the angular momentum they carry. The contribution from strange quarks is negligible.

Table 6.1: Mean square charge radii for baryons with several choices for the MIT bag parameters. Columns 1 and 2 list the particles and give experimental values for the mean square charge radii for the nucleons. Columns 3 and 4 give the mean square charge radii based on configuration mixing calculations using the minimal MIT self-energy. Column 3 is based on the best fit to hadron masses, varying B and m_s . Column 4 is with B chosen to reproduce the proton mean square charge radius. Column 5 lists the results of DeGrand *et al.*'s[54] perturbative calculation using three $s_{1/2}$ quarks. Column 6 is from Donoghue and Golowich's DonoghueG77 perturbative calculation with quark pair creation.

Particle	Experiment [135, 136]	Vary B and m_s to fit masses. $B^{1/4} = 139.3$ MeV $E_C = +6.87/R$ $m_s = 287.7$ MeV $m_u = 0$ MeV $m_d = 5$ MeV $\alpha_s = 1.430$	Set B , vary m_s to fit p charge radius. $B^{1/4} = 126.6$ MeV $E_C = +7.97/R$ $m_s = 286.6$ MeV $m_u = 0$ MeV $m_d = 5$ MeV $\alpha_s = 1.603$	DeGrand <i>et al.</i> [54] $B^{1/4} = 145$ MeV $E_C = -1.84/R$ $m_s = 279$ MeV $m_u = 0$ MeV $m_d = 0$ MeV $\alpha_s = 2.2$	Donoghue, <i>et al.</i> [70]
	fm ² (error)	(fm ²)	(fm ²)	(fm ²)	(fm ²)
n	-0.117(.002)	0.016	0.023	0	-0.007
p	0.743(.021)	0.594	0.743	0.533	0.64
Σ^-		-0.587	-0.738		
Σ^+		0.599	0.755		
Ξ^-		-0.553	-0.695		
Ξ^0		0.066	0.088		
Δ^0		0.012	0.019		
Δ^+		0.701	0.867		
Σ^{*-}		-0.676	-0.841		
Σ^{*+}		0.719	0.893		
Ξ^{*-}		-0.633	-0.787		
Ξ^{*0}		0.072	0.094		

Table 6.2: Magnetic moments of baryons with several choices for the MIT bag parameters using the minimal MIT self-energy. We show values for the baryon magnetic moments and also the ratio of baryon magnetic moments to proton magnetic moment. These values are based on parameters found from in the fit to particle masses by varying B and m_s and also from setting B to fit the proton charge radius and varying m_s to fit the baryon masses.

Particle	Experiment [1]		Vary B and m_s to fit masses.		Set B , vary m_s to fit p charge radius.		DeGrand, <i>et al.</i> [54]	
			$B^{1/4} = 139.3$ MeV $E_C = +6.87/R$ $m_s = 287.7$ MeV $m_u = 0$ MeV $m_d = 5$ MeV $\alpha_s = 1.430$	$\frac{\mu}{\mu_p}$	$B^{1/4} = 126.6$ MeV $E_C = +7.97/R$ $m_s = 286.6$ MeV $m_u = 0$ MeV $m_d = 5$ MeV $\alpha_s = 1.603$	$\frac{\mu}{\mu_p}$	$B^{1/4} = 145$ MeV $E_C = -1.84/R$ $m_s = 279$ MeV $m_u = 0$ MeV $m_d = 0$ MeV $\alpha_s = 2.2$	$\frac{\mu}{\mu_p}$
	$\mu(\text{nm})$	$\frac{\mu}{\mu_p}$	$\mu(\text{nm})$	$\frac{\mu}{\mu_p}$	$\mu(\text{nm})$	$\frac{\mu}{\mu_p}$	$\mu(\text{nm})$	$\frac{\mu}{\mu_p}$
n	-1.913	-0.684	-1.304	-0.696	-1.456	-0.699	-1.264	-0.667
p	2.793	1.000	1.872	1.000	2.085	1.000	1.895	1.000
Σ^-	-1.160	-0.415	-0.586	-0.313	-0.644	-0.309	-0.68	-0.36
Σ^+	2.458	0.880	1.736	0.927	1.848	0.886	1.84	0.97
Ξ^-	-0.651	-0.223	-0.377	-0.202	-0.396	-0.190	-0.44	-0.23
Ξ^0	-1.250	-0.448	-1.075	-0.574	-1.189	-0.570	-1.06	-0.56
Δ^0			-0.006	-0.003	-0.004	-0.002		
Δ^+			0.602	0.321	0.642	0.308		
Σ^{*-}			-0.556	-0.297	-0.597	-0.286		
Σ^{*+}			0.677	0.361	0.772	0.370		
Ξ^{*-}			-0.502	-0.268	-0.536	-0.257		
Ξ^{*0}			0.109	0.058	0.136	0.065		

Table 6.3: Quark spin fractions for baryon configurations with several choices for the MIT bag parameters using the minimal MIT self-energy. Spin fractions and spin structure functions are shown for the baryons based on parameters used in fitting the baryon mass spectrum by varying B and m_s , and also for B set to match the proton charge radius where m_s is varied to fit the masses.

Part- icle	Vary B and m_s to fit masses. $B^{1/4} = 139.3$ MeV $E_C = +6.87/R$ $m_s = 287.7$ MeV $m_u = 0$ MeV $m_d = 5$ MeV $\alpha_s = 1.430$				Set B , vary m_s to fit p charge radius. $B^{1/4} = 126.6$ MeV $E_C = +7.97/R$ $m_s = 286.6$ MeV $m_u = 0$ MeV $m_d = 5$ MeV $\alpha_s = 1.603$			
	Δu	Δd	Δs	Γ_1	Δu	Δd	Δs	Γ_1
n	-0.162	0.668	-0.0001	0.001	-0.153	0.614	-0.0001	0.0002
p	0.708	-0.176	-0.0002	0.148	0.677	-0.175	-0.0002	0.141
Σ^-	-0.006	0.648	-0.155	0.026	-0.008	0.606	-0.144	0.024
Σ^+	0.688	-0.023	-0.195	0.141	0.621	-0.029	-0.160	0.128
Ξ^-	0.014	-0.179	0.756	0.035	0.017	-0.169	0.705	0.034
Ξ^0	-0.164	0.057	0.688	0.005	-0.159	0.069	0.632	0.004
Δ^0	0.168	0.447	-0.0002	0.062	0.154	0.433	-0.0001	0.058
Δ^+	0.356	0.192	-0.0003	0.090	0.333	0.182	-0.0003	0.084
Σ^{*-}	0.013	0.311	0.229	0.033	0.017	0.278	0.222	0.031
Σ^{*+}	0.361	0.050	0.173	0.093	0.344	0.055	0.143	0.087
Ξ^{*-}	0.021	0.188	0.360	0.035	0.026	0.174	0.328	0.034
Ξ^{*0}	0.155	0.085	0.507	0.067	0.140	0.104	0.499	0.065

Chapter 7

CONCLUSION

We have calculated configuration mixing for quarks in the ground-state nucleon, as well as for other octet baryons. We used the spherical MIT bag model, diagonalizing the one gluon exchange (OGE) interaction linking all orthonormal color-singlet states below a cutoff of 1.5 GeV above the three quark ground state.

The basis space includes three quarks states with excitations up to $f_{7/2}$, or with radial excitations up to $n = 3$. It also includes five particle states where u , d , or s quark anti-quark pairs are created, with any single particle in a $p_{3/2}$ or $p_{1/2}$ state. Forward and backward graphs of four types contribute to the OGE interaction. We calculate the matrix elements using confined perturbation theory, including monopole through hexadecapole gluon contributions. There are Coulomb contributions, as well as transverse electric and magnetic contributions for which we do a mode sum over the first five modes. All together, there are about 10^7 OGE contributions between the 6555 normal-ordered configurations which contribute to the 859 orthonormal color-singlet basis states of the matrix we diagonalize.

A number of interesting results follow from our calculations. We find there is an enhanced probability for creation of quark pairs with the same flavor as other quarks in the bag. It is often argued that these states should be suppressed by Pauli blocking, but constructive interference effects overcome the Pauli blocking. In the qqq sector, interference effects increase the number of dissimilar flavored quarks that are both excited when two quarks are excited to the same energy level. For example, about 80% of the probability for states with two $p_{3/2}$ quark excitations that contribute to the nucleon ground state have one u and one d quark excited to the $p_{3/2}$ level, rather than the 2/3 ratio one might expect.

Configuration mixing leads to significant lowering of the ground state energy, and provides an alternative to lowering of the MIT bag energy via the Casimir term. This is significant in several respects. The Casimir term incorporates zero-point fluctuations. In the past, a slab geometry was assumed to simplify calculation of

the Casimir term for the MIT bag, with the Casimir energy given by $E_c = -Z_0/R$. However, calculations by other people for a spherical geometry indicates the Casimir term should have the opposite sign as found with a plane parallel geometry. Thus the sign of the Casimir term used to lower the bag energy is brought into question. Another problem with the form of the Casimir term traditionally used for the MIT bag is that it makes an empty bag unstable to decay, with an unbounded energy depression as the bag radius is decreased. This type of situation could arise if bag surface fluctuations pinched off a region containing no quarks.

We have made calculations for different choices for u , d , and s quark masses, and for different bag radii. This allows extrapolation to other parameter values. We also compare different prescriptions for the self energy. Since many of the initial computational steps are done symbolically, we have extended the calculations beyond the nucleons to the Σ 's and Ξ 's where two quarks have the same flavor but the third flavor is different. We fit the mass spectrum of the octet baryons by adjusting values for quark masses and the bag constant.

The strong coupling constant necessary to achieve the proper $\Delta - N$ splitting is reduced from $\alpha_s = 2.2$ used in earlier MIT bag studies to a value of about $\alpha_s = 1.4$ at the maximum cutoff. (Although the coupling runs to larger values at low energy, the value of $\alpha_s = 2.2$ is clearly too large, based on fits from scattering at higher energies.) The coupling that is required decreases as we raise the cutoff, including successively larger basis sets in the space we diagonalize. There is a substantial amount of configuration mixing, with three $s_{1/2}$ quark states accounting for about 48% of the nucleon ground state probability at the maximum cutoff. The next largest contributor is from two quarks excited to a $p_{3/2}$ level, which contribute about 26% to the probability. The four-quark plus anti-quark contribution arising from pair creation is found to be quite small, at about 4%. As a result of this, the spin contribution from strange quarks is found to be negligible. We find the fraction of proton spin attributable to quark spin is about 50 - 53%. This is less than the MIT bag result without configuration mixing, which predicts about 65%. We also agree quite well with experimental values[140, 142] for the integrated spin structure functions for the nucleons, with $\Gamma_1^p = 0.141 - 0.148$. The SMC result[142] is $\Gamma_1^p = 0.136 \pm 0.011 \pm 0.011$ at $Q^2 = 10 \text{ GeV}^2$. For the Bjorken sum rule, we find $\Gamma_1^p - \Gamma_1^n = 0.141 - 0.147$, compared to SMC and E142 for n data of $\Gamma_1^p - \Gamma_1^n = 0.163 \pm 0.017$.

BIBLIOGRAPHY

- [1] Part 1, Review of Particle Properties, Phys. Rev. **D54**, 1 (1996).
- [2] T. D. Lee, Phys. Rev. **D19**, 1802 (1979).
- [3] F. E. Close and R. R. Horgan, Nuc. Phys. **B164**, 413 (1980).
- [4] F. E. Close and S. Monaghan, Phys. Rev. **D23**, 2098 (1981).
- [5] J. Wroldsen and F. Myhrer, Z. Phys. **C25**, 59 (1984).
- [6] T. DeGrand, R. L. Jaffe, K. Johnson, and J. Kiskis, Phys. Rev. **D12**, 2060 (1975).
- [7] H. B.G. Casimir and D. Polder, Phys. Rev. **73**, 277 (1948).
- [8] L. Wilets, *Nontopological Solitons*, World Scientific, Singapore (1989).
- [9] W. Panofsky, In *Proceedings of International Symposium on High Energy Physics*, Vienna, (1968).
- [10] J. J. Thomson, *Recent Researches in Electricity and Magnetism*, Clarendon Press, Oxford (1893).
- [11] Rutherford, Phil. Mag. **21**, 669 (1911), reprinted in R. T. Beyer, *Foundations of Nuclear Physics*, Dover Publications, New York (1949).
- [12] G. Chew, in *High Energy Physics*, 1965 Les Houches Lectures, Gordon and Breach, New York (1965).
- [13] A. De Rújula *et al.*, Rev. Mod. Phys. **46**, 391 (1974).

- [14] F. E. Close, *An introduction to Quarks and Partons*, Academic Press, New York (1979).
- [15] J. D. Bjorken, In *Proceedings of 3rd International Symposium on Electron and Photon Interactions*, Stanford, California (1967).
- [16] R. P. Feynman, *Phys. Rev. Lett.* **23**, 1415 (1969).
- [17] M. Gell-Mann, *Phys. Lett.* **8**, 214 (1964).
- [18] M. Gell-Mann and Y. Ne'eman, *The Eightfold Way*, Benjamin, New York (1964).
- [19] G. Zweig, CERN Report Nos 8182/TH401 and 8419/TH412, (Unpublished) (1964), as referenced in Close, *An Introduction to Quarks and Partons*, p. 20 (1979).
- [20] Review of Particle Properties, *Phys. Rev.* **D50**, 1433 (1996).
- [21] M. Gell-Mann, *Phys. Rev.* **125**, 1067 (1962).
- [22] Y. Ne'eman, *Nucl. Phys.* **26**, 222 (1961).
- [23] R. H. Dalitz, in *Proceedings of the Thirteenth International Conference on High Energy Physics*, Berkeley University of California Press, Berkeley, 215 (1967).
- [24] J. J. J. Kokkedee, *The Quark Model*, Benjamin, New York (1969).
- [25] R. P. Feynman, *Phys. Rev.* **76**, 769 (1949).
- [26] J. Schwinger, *Phys. Rev* **82**, 914 (1951).
- [27] C. N. Yang and R. C. Mills, *Phys. Rev.* **96**, 191 (1954).
- [28] R. P. Feynman, *Photon-Hadron Interactions*, Addison-Wesley, Reading, Massachusetts (1972).
- [29] O. W. Greenberg, *Phys. Rev. Lett.* **13**, 589 (1964).

- [30] M. Y. Han and Y. Nambu, *Phys. Rev.* **139**, B1006 (1965).
- [31] E. Noether, *Nachr. Kgl. Ges. Wiss. Gottingen*, 235 (1918).
- [32] H. D. Politzer, *Phys. Reports* **C14**, 129 (1974).
- [33] P. N. Bogoliubov and D. Shirkov, *Introduction to the Theory of Quantised Fields*, Interscience, New York (1959).
- [34] G. 't Hooft, unpublished remark in *Proceedings of 1972 Marseilles Conference on Yang-Mills fields*, (1972) (quoted in footnote 3, p132 of Politzer, 1974).
- [35] H. D. Politzer, *Phys. Rev. Lett.* **30**, 1346 (1973).
- [36] D. Gross and F. Wilczek, *Phys. Rev. Lett.* **30**, 1343 (1973).
- [37] D. Gross and F. Wilczek, *Phys. Rev.* **D8**, 3633 (1973).
- [38] K. G. Wilson, *Phys. Rev.* **D10**, 2445 (1974).
- [39] J. Schwinger, *Phys. Rev.* **125**, 397 (1962); **128**, 2425 (1962).
- [40] H. B. Nielsen and P. Olesen, *Nucl. Phys.* **B61**, 45 (1973).
- [41] Y. Nambu, in *Symmetries and Quark Models*, proceedings of the International Conference on Symmetries and Quark Models, Wayne State University (1969).
- [42] S. Mandelstam, Seminar Preprint *Introduction to Quark Confinement and the Dynamics of the Strong Interaction*, Dept. of Physics, Berkeley, CA (1978).
- [43] A. A. Migdal, *Zh. Exsp. Teor. Fiz.* **69**, 810 (1975).
- [44] L. P. Kadanoff, *Rev. Mod. Phys.* **49**, 267 (1977).
- [45] P. N. Bogoliubov, *Ann. Inst. Henri Poincare* **8**, 163 (1967).
- [46] M. E. Rose, *Relativistic Electron Theory*, John Wiley and Sons, New York (1961).

- [47] J. D. Bjorken and S. D. Drell, *Relativistic Quantum Mechanics*, McGraw-Hill, New York (1964).
- [48] A. I. Akhiezer and V. B. Berestetskii, *Quantum Electrodynamics*, John Wiley and Sons, New York (1965).
- [49] A. Chodos, R. L. Jaffe, K. Johnson, C. B. Thorn, and V. F. Weisskopf, Phys. Rev. **D9**, 3471 (1974).
- [50] A. Chodos, R. L. Jaffe, K. Johnson, C. B. Thorn, and V. F. Weisskopf, Phys. Rev. **D10**, 2599 (1974).
- [51] M. Creutz, Phys. Rev. **D10**, 1749 (1974).
- [52] M. Creutz and K. S. Soh, Phys. Rev. **D12**, 443 (1975).
- [53] A. Chodos, R. L. Jaffe, K. Johnson, and C. B. Thorn, Phys. Rev. **D10**, 2599 (1974).
- [54] T. DeGrand, R. L. Jaffe, K. Johnson, and J. Kiskis, Phys. Rev. **D12**, 2060 (1975).
- [55] P. Hasenfratz and J. Kuti, Phys. Rep. **40**, 75 (1978).
- [56] J. D. Jackson, *Classical Electrodynamics*, John Wiley and Sons, New York (1975).
- [57] E. Golowich, Phys. Rev. **D12**, 2108 (1975).
- [58] J. Donoghue, E. Golowich, and B. Holstein, Phys. Rev. **D12**, 2875 (1975).
- [59] T. A. DeGrand and R. L. Jaffe, Ann. Phys. **100**, 425 (1976).
- [60] C. Rebbi, preprint MIT-CTP-551, June (1976).
- [61] J. J. Griffin and J. A. Wheeler, Phys. Rev. **108**, 311 (1957).
- [62] M. H. L. Pryce, Proc. R. Soc. London, **A195**, 62 (1948).

- [63] R. A. Krajcik and L. L. Foldy, Phys. Rev. **D10**, 1777 (1974).
- [64] R. E. Peierls and J. Yoccoz, Proc. Phys. Soc. London **A70**, 381 (1957).
- [65] E. G. Lübeck, M. C. Birse, E. M. Henley, and L. Wilets, Phys. Rev. **D33**, 234 (1987).
- [66] H. R. Fiebig and E. Hadjimichael, Phys. Rev. **D30**, 181 (1984).
- [67] K. C. Bowler and A. J. G. Hey, Phys. Lett. **B69**, 469 (1977).
- [68] K. C. Bowler and P. J. Walters, Phys. Rev. **D19**, 3330 (1979).
- [69] R. J. Jaffe, Phys. Rev. **D15**, 267 (1977); *ibid.* **D15**, 281 (1977).
- [70] J. F. Donoghue and E. Golowich, Phys. Rev. **D15**, 3421 (1977).
- [71] F. E. Close and R. R. Horgan, Nucl. Phys. **B164**, 413 (1979).
- [72] T. Hatsuda and T. Kunihiro, Nucl. Phys. **B387**, 715 (1992).
- [73] A. De Rújula, H. Georgi, and S. L. Glashow, Phys. Rev. **D12**, 147 (1975).
- [74] A. K. A. Maciel and J. E. Paton, Nucl. Phys. **B197**, 201 (1982).
- [75] M. Bickeböller, *Der Gluon-Propagator im Soliton-Bag-Modell*, Diplom Thesis, University of Bonn (1984).
- [76] P. Tang and L. Wilets, private communication (1989), as referenced in Wilets, *Nontopological Solitons*, World Scientific, Singapore (1989).
- [77] K. Ushio and H. Konashi, Phys. Lett. **B135**, 468 (1984).
- [78] K. Ushio, Phys. Lett. **B158**, 71 (1985).
- [79] K. Ushio, Z. Phys. **C30**, 115 (1986).
- [80] J. D. Bjorken, Phys. Rev. **148**, 1476 (1966).

- [81] F. Myhrer and A. W. Thomas, Phys. Rev. **D38**, 1633 (1988).
- [82] A. W. Thomas, Adv. Nucl. Phys. **13**, 1 (1984).
- [83] Y. Umino and F. Myhrer, Phys. Rev. **D39**, 3391 (1989).
- [84] N. Isgur and G. Karl, Phys. Rev. **D18**, 4187 (1978); *ibid.* **D19**, 2653 (1979).
- [85] H. Høgaasen and Myhrer, Phys. Rev. **D37**, 1950 (1988).
- [86] H. Høgaasen and Myhrer, preprint *The proton spin sum rule chiral bag prediction, an update* (Feb. 2, 1995).
- [87] R. Friedberg and T. D. Lee, Phys. Rev. **D15**, 1694 (1977); *ibid.* **D16**, 1096 (1977).
- [88] W. A. Bardeen, M. S. Chanowitz, S. D. Drell, M. Weinstein, and T. M. Yan, Phys. Rev. **D11**, 1094 (1975).
- [89] P. Tang, Thesis *Chromodielectric Model and Chiral Symmetry Breaking*, University of Washington, Seattle (1993).
- [90] G. Fai, R. Perry, and L. Wilets, Phys. Lett. **B208**, 1 (1988).
- [91] G. Krein, P. Tang, L. Wilets, and A. G. Williams, Phys. Lett. **B212**, 362 (1988); Nucl. Phys. **A523**, 548 (1991).
- [92] W. Koepf and L. Wilets, Phys. Rev. **C51**, 3445 (1995).
- [93] M. C. Birse, J. J. Rehr, and L. Wilets, Phys. Rev. **C38**, 359 (1988).
- [94] Ming Li, M. C. Birse, and L. Wilets, J. Phys. G; Nucl. Phys. **13**, 1 (1987).
- [95] L. Wilets, *Advanced Course in Theoretical Physics, Hadrons and Heavy Ions, Lecture Notes in Physics*, Springer, Berlin (1985).
- [96] L. Wilets and R. D. Puff, Phys. Rev. **C51**, 339 (1995).

- [97] H. Georgi, *Weak Interactions and Modern Particle Theory*, Addison-Wesley, New York (1984).
- [98] F. Halzen and A. D. Martin, *Quarks and Leptons: An introductory Course in Modern Particle Physics*, John Wiley and Sons, New York (1984).
- [99] L. D. Landau, *Quantum Mechanics (Non-relativistic Theory)*, Course of Theoretical Physics, Volume 3, Third Edition, Pergamon Press, Oxford (1989).
- [100] P. M. Morse and H. Feshbach, *Methods of Theoretical Physics*, McGraw-Hill, New York (1953).
- [101] M. Abramowitz and I. A. Stegun, *Handbook of Mathematical Functions, With Formulae, Graphs, and Mathematical Tables*, Tenth Printing, National Bureau of Standards, Applied Mathematics Series 55 (1972).
- [102] A. R. Edmonds, *Angular Momentum in Quantum Mechanics*, Princeton University Press, Princeton, New Jersey (1960).
- [103] Wu-Ki Tung, *Group Theory in Physics*, World Scientific, Philadelphia (1985).
- [104] J. Goldstone, Proc. Roy. Soc. **A239**, 267 (1957).
- [105] S. Coleman, *Aspects of Symmetry*, Cambridge University Press, Cambridge (1988).
- [106] W. Greiner and B. Müller, *Quantum Mechanics, Symmetries*, Springer-Verlag, Berlin (1989).
- [107] K. A. Milton, Phys. Rev. **D 22**, 1444 (1980).
- [108] L. S. Brown, and G. J. Maclay, Phys. Rev. **184**, 1272 (1969).
- [109] M. J. Sparnaay, Physics **24**, 751 (1958).
- [110] H. B. G. Casimir, Physica **19**, 846 (1956).

- [111] T. H. Boyer, Phys. Rev. **174**, 1764 (1968).
- [112] E. A. Hinds, In *Cavity Quantum Electrodynamics*, Edited by P. R. Berman, Academic Press, San Diego (1994).
- [113] R. Balian and C. Bloch, Ann. Phys. **64**, 271 (1971).
- [114] R. Balian and B. Duplantier, Ann. Phys. **104**, 300 (1977).
- [115] K. A. Milton, L. L. DeRaad, and J. Schwinger, Ann. Phys. **115**, 388 (1978).
- [116] K. A. Milton, Phys. Rev. **D 22**, 1444 (1980).
- [117] K. A. Milton, Phys. Rev. **D 22**, 1441 (1980).
- [118] C. M. Bender and P. Hays, Phys. Rev. **D 14**, 2622 (1976).
- [119] P. Hasenfratz and J Kuti, Phys. Rep **40**, 75 (1978).
- [120] C. Peterson, T. H. Hansson, and K. Johnson, Phys. Rev. **D 26**, 415 (1982).
- [121] T. Goldman, K. R. Maltman, and G. J. Stephenson Jr., Phys. Lett. **B 228**, 396 (1989).
- [122] U. van Kolck, Few-Body Systems Suppl. **9**, 444 (1995).
- [123] Part 1, Review of Particle Properties, Phys. Rev. **D50**, 1 (1994).
- [124] R. D. Field and R. P. Feynman, Phys. Rev. **D, 15**, 2590 (1977).
- [125] J. F. Donoghue and K. Johnson, Phys. Rev. **D 21**, 1975 (1980).
- [126] M. Bickeböllner, M. C. Birse, H. Marschall, and L. Wilets, Phys. Rev. **D 31**, 2892 (1985).
- [127] J.-L. Dethier and L. Wilets, Phys. Rev. **D 34**, 207 (1985).

- [128] J.-L. Dethier, *A Soliton Bag Model of the Nucleon and the Delta Dressed by a Quark-Antiquark Pion*, Doctoral Dissertation, Univ. of Washington, Seattle (1985).
- [129] L. R. Dodd and A. G. Williams, Phys. Rev. **D 37**, 1971 (1988).
- [130] L. R. Dodd and A. G. Williams, Phys. Lett. **210 B**, 10 (1988).
- [131] G. A. Miller, A. W. Thomas, and S. Th  berge, Phys. Lett. **91 B**, 192 (1980).
- [132] A. K. A. Maciel and J. E. Paton, Nuc. Phys. **B 197**, 201 (1982).
- [133] V. Krohn and G. Ringo, Phys. Rev. **D 8**, 1305 (1973).
- [134] L. Koester, W. Waschkowski, and J. Meier, Z. Phys. **A 329**, 229 (1988).
- [135] Z. Dziembowski, W. J. Metzger, and R. T. Van de Walle, Z. Phys. **C 10**, 231 (1981).
- [136] G. H  hler, *et al.*, Nucl. Phys. **B 114**, 505 (1976).
- [137] H. Leeb and C. Teichtmeister, Phys. Rev **C 48**, 1719 (1993).
- [138] F. Borkowski, *et al.*, Z. Phys. **A 275**, 29 (1975).
- [139] J. Ashman *et al.*, Phys. Lett. **B 206**, 364 (1988).
- [140] J. Ashman *et al.*, Nucl. Phys. **B 328**, 1 (1989).
- [141] P. L. Anthony *et al.*, Phys. Rev. Lett. **71**, 959 (1993).
- [142] B. Adeva *et al.*, Phys. Lett. **B 329**, 399 (1994).
- [143] G. Baum *et al.* Phys. Rev. Lett. **51**, 1135 (1983).
- [144] G. G. Simon *et al.*, Nucl. Phys. **A333**, 381 (1980).
- [145] L. N. Hand, D. G. Miller, and R. Wilson, Rev. Mod. Phys. **35**, 335 (1963).

- [146] J. D. Bjorken, Phys. Rev **148**, 1467 (1966).
- [147] J. Ellis and R. Jaffe, Phys. Rev. **D 9**, 1444 (1974).
- [148] J. Kodaira *et al.*, Phys. Rev **D 20**, 627 (1979).
- [149] R. L. Jaffe and A. Manohar, Nucl. Phys. **B 337**, 509 (1990).
- [150] P. J. Mulders and S. J. Pollock, preprint hep-ph/9412287, (1994)
- [151] H. Høgaasen and F. Myhrer, Phys. Lett **B 214**, 123 (1988).

Appendix A

NON-COLOR QUARK AND ANTI-QUARK CONFIGURATIONS CONTRIBUTING TO PROTON

Table A.1: Classification, energy, and probability of quark (non-color) configurations contributing to the proton ground state, using the MIT prescription for the quark self energy. Only states with significant probabilities are listed. The bag radius, $R=0.005$ MeV $^{-1}$. The quark masses are $m_u = 0$, $m_d = 5$ MeV, and $m_s = 279$ MeV. The No. and Cat. columns list the multi-quark number and category.

No.	Cat.	Type	States	Non-Color Configuration	Energy	Probability
1	a	1	1	$d_{1-\frac{1}{2}S_{\frac{1}{2}}} u_{1-\frac{1}{2}S_{\frac{1}{2}}} u_{1-\frac{1}{2}S_{\frac{1}{2}}}$	0.	$1.582 \cdot 10^{-1}$
2	a	2	1	$d_{1-\frac{1}{2}S_{\frac{1}{2}}} u_{1-\frac{1}{2}S_{\frac{1}{2}}} u_{1-\frac{1}{2}S_{\frac{1}{2}}}$	0.	$3.165 \cdot 10^{-1}$
27	f	1	1	$d_{1-\frac{1}{2}S_{\frac{1}{2}}} u_{1-\frac{1}{2}P_{\frac{3}{2}}} u_{1-\frac{1}{2}P_{\frac{3}{2}}}$	2.319	$1.835 \cdot 10^{-2}$
28	f	1	1	$d_{1-\frac{1}{2}S_{\frac{1}{2}}} u_{1-\frac{1}{2}P_{\frac{3}{2}}} u_{1-\frac{1}{2}P_{\frac{3}{2}}}$	2.319	$1.451 \cdot 10^{-2}$
29	f	1	1	$d_{1-\frac{1}{2}S_{\frac{1}{2}}} u_{1-\frac{1}{2}P_{\frac{3}{2}}} u_{1-\frac{1}{2}P_{\frac{3}{2}}}$	2.319	$1.514 \cdot 10^{-3}$
30	f	1	1	$d_{1-\frac{1}{2}P_{\frac{3}{2}}} u_{1-\frac{1}{2}S_{\frac{1}{2}}} u_{1-\frac{1}{2}P_{\frac{3}{2}}}$	2.321	$7.477 \cdot 10^{-2}$
31	f	1	1	$d_{1-\frac{1}{2}P_{\frac{3}{2}}} u_{1-\frac{1}{2}S_{\frac{1}{2}}} u_{1-\frac{1}{2}P_{\frac{3}{2}}}$	2.321	$4.485 \cdot 10^{-3}$
32	f	1	1	$d_{1-\frac{1}{2}P_{\frac{3}{2}}} u_{1-\frac{1}{2}S_{\frac{1}{2}}} u_{1-\frac{1}{2}P_{\frac{3}{2}}}$	2.321	$5.65 \cdot 10^{-2}$
33	f	1	1	$d_{1-\frac{1}{2}P_{\frac{3}{2}}} u_{1-\frac{1}{2}S_{\frac{1}{2}}} u_{1-\frac{1}{2}P_{\frac{3}{2}}}$	2.321	$6.597 \cdot 10^{-3}$
34	f	1	1	$d_{1-\frac{1}{2}P_{\frac{3}{2}}} u_{1-\frac{1}{2}S_{\frac{1}{2}}} u_{1-\frac{1}{2}P_{\frac{3}{2}}}$	2.321	$3.952 \cdot 10^{-2}$
35	f	1	1	$d_{1-\frac{1}{2}P_{\frac{3}{2}}} u_{1-\frac{1}{2}S_{\frac{1}{2}}} u_{1-\frac{1}{2}P_{\frac{3}{2}}}$	2.321	$4.683 \cdot 10^{-3}$
36	f	1	1	$d_{1-\frac{1}{2}P_{\frac{3}{2}}} u_{1-\frac{1}{2}S_{\frac{1}{2}}} u_{1-\frac{1}{2}P_{\frac{3}{2}}}$	2.321	$2.341 \cdot 10^{-2}$
37	f	2	1	$d_{1-\frac{1}{2}S_{\frac{1}{2}}} u_{1-\frac{1}{2}P_{\frac{3}{2}}} u_{1-\frac{1}{2}P_{\frac{3}{2}}}$	2.319	$1.322 \cdot 10^{-2}$
38	g	1	1	$d_{1-\frac{1}{2}S_{\frac{1}{2}}} u_{1-\frac{1}{2}P_{\frac{3}{2}}} u_{1-\frac{1}{2}P_{\frac{3}{2}}}$	2.919	$2.239 \cdot 10^{-3}$
39	g	1	1	$d_{1-\frac{1}{2}S_{\frac{1}{2}}} u_{1-\frac{1}{2}P_{\frac{3}{2}}} u_{1-\frac{1}{2}P_{\frac{3}{2}}}$	2.919	$6.925 \cdot 10^{-3}$
40	g	1	1	$d_{1-\frac{1}{2}S_{\frac{1}{2}}} u_{1-\frac{1}{2}P_{\frac{3}{2}}} u_{1-\frac{1}{2}P_{\frac{3}{2}}}$	2.919	$2.277 \cdot 10^{-3}$
41	g	1	1	$d_{1-\frac{1}{2}S_{\frac{1}{2}}} u_{1-\frac{1}{2}P_{\frac{3}{2}}} u_{1-\frac{1}{2}P_{\frac{3}{2}}}$	2.919	$2.319 \cdot 10^{-3}$
45	g	1	1	$d_{1-\frac{1}{2}P_{\frac{3}{2}}} u_{1-\frac{1}{2}S_{\frac{1}{2}}} u_{1-\frac{1}{2}P_{\frac{3}{2}}}$	2.921	$1.723 \cdot 10^{-3}$
46	g	1	1	$d_{1-\frac{1}{2}P_{\frac{3}{2}}} u_{1-\frac{1}{2}S_{\frac{1}{2}}} u_{1-\frac{1}{2}P_{\frac{3}{2}}}$	2.928	$1.709 \cdot 10^{-3}$
108	k	1	1	$d_{1-\frac{1}{2}P_{\frac{3}{2}}} u_{1-\frac{1}{2}S_{\frac{1}{2}}} u_{1-\frac{1}{2}P_{\frac{3}{2}}}$	3.528	$2.885 \cdot 10^{-3}$
110	k	1	1	$d_{1-\frac{1}{2}P_{\frac{3}{2}}} u_{1-\frac{1}{2}S_{\frac{1}{2}}} u_{1-\frac{1}{2}P_{\frac{3}{2}}}$	3.528	$4.376 \cdot 10^{-3}$
133	n	1	1	$d_{1-\frac{1}{2}S_{\frac{1}{2}}} u_{1-\frac{1}{2}d_{\frac{3}{2}}} u_{1-\frac{1}{2}d_{\frac{3}{2}}}$	4.564	$1.877 \cdot 10^{-3}$
134	n	1	1	$d_{1-\frac{1}{2}S_{\frac{1}{2}}} u_{1-\frac{1}{2}d_{\frac{3}{2}}} u_{1-\frac{1}{2}d_{\frac{3}{2}}}$	4.564	$3.041 \cdot 10^{-3}$
135	n	1	1	$d_{1-\frac{1}{2}S_{\frac{1}{2}}} u_{1-\frac{1}{2}d_{\frac{3}{2}}} u_{1-\frac{1}{2}d_{\frac{3}{2}}}$	4.564	$2.373 \cdot 10^{-3}$
138	n	1	1	$d_{1-\frac{1}{2}d_{\frac{3}{2}}} u_{1-\frac{1}{2}S_{\frac{1}{2}}} u_{1-\frac{1}{2}d_{\frac{3}{2}}}$	4.566	$1.498 \cdot 10^{-2}$
140	n	1	1	$d_{1-\frac{1}{2}d_{\frac{3}{2}}} u_{1-\frac{1}{2}S_{\frac{1}{2}}} u_{1-\frac{1}{2}d_{\frac{3}{2}}}$	4.566	$1.279 \cdot 10^{-2}$
142	n	1	1	$d_{1-\frac{1}{2}d_{\frac{3}{2}}} u_{1-\frac{1}{2}S_{\frac{1}{2}}} u_{1-\frac{1}{2}d_{\frac{3}{2}}}$	4.566	$1.072 \cdot 10^{-2}$
144	n	1	1	$d_{1-\frac{1}{2}d_{\frac{3}{2}}} u_{1-\frac{1}{2}S_{\frac{1}{2}}} u_{1-\frac{1}{2}d_{\frac{3}{2}}}$	4.566	$8.803 \cdot 10^{-3}$

Table A.2: Classification, energy, and probability of quark (non-color) configurations contributing to the proton ground state, using the MIT prescription for the quark self energy. Only states with significant probabilities are listed. The bag radius is $R=.005 \text{ MeV}^{-1}$. The quark masses are $m_u = 0$, $m_d = 5 \text{ MeV}$, and $m_s = 279 \text{ MeV}$. The No. and Cat. columns list the multi-quark number and category.

No.	Cat.	Type	States	Non-Color Configuration	Energy	Probability
146	n	1	1	$d_{1-\frac{1}{2}d_{\frac{1}{2}}} u_{1-\frac{1}{2}s_{\frac{1}{2}}} u_{1-\frac{1}{2}d_{\frac{1}{2}}}$	4.566	$7.036 \cdot 10^{-3}$
148	n	1	1	$d_{1-\frac{1}{2}d_{\frac{1}{2}}} u_{1-\frac{1}{2}s_{\frac{1}{2}}} u_{1-\frac{1}{2}d_{\frac{1}{2}}}$	4.566	$5.434 \cdot 10^{-3}$
149	n	2	1	$d_{1-\frac{1}{2}s_{\frac{1}{2}}} u_{1-\frac{1}{2}d_{\frac{1}{2}}} u_{1-\frac{1}{2}d_{\frac{1}{2}}}$	4.564	$1.719 \cdot 10^{-3}$
209	s	1	1	$d_{1-\frac{1}{2}f_{\frac{1}{2}}} u_{1-\frac{1}{2}s_{\frac{1}{2}}} u_{1-\frac{1}{2}f_{\frac{1}{2}}}$	6.77	$2.544 \cdot 10^{-3}$
211	s	1	1	$d_{1-\frac{1}{2}f_{\frac{1}{2}}} u_{1-\frac{1}{2}s_{\frac{1}{2}}} u_{1-\frac{1}{2}f_{\frac{1}{2}}}$	6.77	$2.289 \cdot 10^{-3}$
213	s	1	1	$d_{1-\frac{1}{2}f_{\frac{1}{2}}} u_{1-\frac{1}{2}s_{\frac{1}{2}}} u_{1-\frac{1}{2}f_{\frac{1}{2}}}$	6.77	$2.045 \cdot 10^{-3}$
215	s	1	1	$d_{1-\frac{1}{2}f_{\frac{1}{2}}} u_{1-\frac{1}{2}s_{\frac{1}{2}}} u_{1-\frac{1}{2}f_{\frac{1}{2}}}$	6.77	$1.811 \cdot 10^{-3}$
217	s	1	1	$d_{1-\frac{1}{2}f_{\frac{1}{2}}} u_{1-\frac{1}{2}s_{\frac{1}{2}}} u_{1-\frac{1}{2}f_{\frac{1}{2}}}$	6.77	$1.589 \cdot 10^{-3}$
219	s	1	1	$d_{1-\frac{1}{2}f_{\frac{1}{2}}} u_{1-\frac{1}{2}s_{\frac{1}{2}}} u_{1-\frac{1}{2}f_{\frac{1}{2}}}$	6.77	$1.379 \cdot 10^{-3}$
221	s	1	1	$d_{1-\frac{1}{2}f_{\frac{1}{2}}} u_{1-\frac{1}{2}s_{\frac{1}{2}}} u_{1-\frac{1}{2}f_{\frac{1}{2}}}$	6.77	$1.181 \cdot 10^{-3}$
225	t	1	1	$d_{1-\frac{1}{2}p_{\frac{1}{2}}} u_{1-\frac{1}{2}p_{\frac{1}{2}}} u_{1-\frac{1}{2}d_{\frac{1}{2}}}$	4.603	$4.896 \cdot 10^{-3}$
226	t	1	1	$d_{1-\frac{1}{2}p_{\frac{1}{2}}} u_{1-\frac{1}{2}p_{\frac{1}{2}}} u_{1-\frac{1}{2}d_{\frac{1}{2}}}$	4.603	$3.982 \cdot 10^{-3}$
227	t	1	1	$d_{1-\frac{1}{2}p_{\frac{1}{2}}} u_{1-\frac{1}{2}p_{\frac{1}{2}}} u_{1-\frac{1}{2}d_{\frac{1}{2}}}$	4.603	$1.461 \cdot 10^{-3}$
228	t	1	1	$d_{1-\frac{1}{2}p_{\frac{1}{2}}} u_{1-\frac{1}{2}p_{\frac{1}{2}}} u_{1-\frac{1}{2}d_{\frac{1}{2}}}$	4.603	$1.032 \cdot 10^{-3}$
230	t	1	1	$d_{1-\frac{1}{2}p_{\frac{1}{2}}} u_{1-\frac{1}{2}p_{\frac{1}{2}}} u_{1-\frac{1}{2}d_{\frac{1}{2}}}$	4.603	$3.586 \cdot 10^{-3}$
231	t	1	1	$d_{1-\frac{1}{2}p_{\frac{1}{2}}} u_{1-\frac{1}{2}p_{\frac{1}{2}}} u_{1-\frac{1}{2}d_{\frac{1}{2}}}$	4.603	$3.187 \cdot 10^{-3}$
234	t	1	1	$d_{1-\frac{1}{2}p_{\frac{1}{2}}} u_{1-\frac{1}{2}p_{\frac{1}{2}}} u_{1-\frac{1}{2}d_{\frac{1}{2}}}$	4.603	$1.761 \cdot 10^{-3}$
235	t	1	1	$d_{1-\frac{1}{2}p_{\frac{1}{2}}} u_{1-\frac{1}{2}p_{\frac{1}{2}}} u_{1-\frac{1}{2}d_{\frac{1}{2}}}$	4.603	$4.301 \cdot 10^{-3}$
239	t	1	1	$d_{1-\frac{1}{2}p_{\frac{1}{2}}} u_{1-\frac{1}{2}p_{\frac{1}{2}}} u_{1-\frac{1}{2}d_{\frac{1}{2}}}$	4.603	$4.29 \cdot 10^{-3}$
240	t	1	1	$d_{1-\frac{1}{2}d_{\frac{1}{2}}} u_{1-\frac{1}{2}p_{\frac{1}{2}}} u_{1-\frac{1}{2}p_{\frac{1}{2}}}$	4.604	$7.234 \cdot 10^{-3}$
241	t	1	1	$d_{1-\frac{1}{2}d_{\frac{1}{2}}} u_{1-\frac{1}{2}p_{\frac{1}{2}}} u_{1-\frac{1}{2}p_{\frac{1}{2}}}$	4.604	$2.307 \cdot 10^{-3}$
243	t	1	1	$d_{1-\frac{1}{2}d_{\frac{1}{2}}} u_{1-\frac{1}{2}p_{\frac{1}{2}}} u_{1-\frac{1}{2}p_{\frac{1}{2}}}$	4.604	$3.948 \cdot 10^{-3}$
244	t	1	1	$d_{1-\frac{1}{2}d_{\frac{1}{2}}} u_{1-\frac{1}{2}p_{\frac{1}{2}}} u_{1-\frac{1}{2}p_{\frac{1}{2}}}$	4.604	$1.157 \cdot 10^{-3}$
245	t	1	1	$d_{1-\frac{1}{2}d_{\frac{1}{2}}} u_{1-\frac{1}{2}p_{\frac{1}{2}}} u_{1-\frac{1}{2}p_{\frac{1}{2}}}$	4.604	$1.429 \cdot 10^{-3}$
246	t	2	1	$d_{1-\frac{1}{2}d_{\frac{1}{2}}} u_{1-\frac{1}{2}p_{\frac{1}{2}}} u_{1-\frac{1}{2}p_{\frac{1}{2}}}$	4.604	$8.576 \cdot 10^{-3}$
247	t	2	1	$d_{1-\frac{1}{2}d_{\frac{1}{2}}} u_{1-\frac{1}{2}p_{\frac{1}{2}}} u_{1-\frac{1}{2}p_{\frac{1}{2}}}$	4.604	$3.52 \cdot 10^{-3}$
248	t	2	1	$d_{1-\frac{1}{2}d_{\frac{1}{2}}} u_{1-\frac{1}{2}p_{\frac{1}{2}}} u_{1-\frac{1}{2}p_{\frac{1}{2}}}$	4.604	$1.741 \cdot 10^{-3}$
279	C	1	1	$d_{1-\frac{1}{2}p_{\frac{1}{2}}} u_{1-\frac{1}{2}p_{\frac{1}{2}}} u_{1-\frac{1}{2}d_{\frac{1}{2}}}$	5.202	$1.695 \cdot 10^{-3}$

Table A.3: Classification, energy, and probability of quark (non-color) configurations contributing to the proton ground state, using the MIT prescription for the quark self energy. Only states with significant probabilities are listed. The bag radius is $R=.005 \text{ MeV}^{-1}$. The quark masses are $m_u = 0$, $m_d = 5 \text{ MeV}$, and $m_s = 279 \text{ MeV}$. The No. and Cat. columns list the multi-quark number and category.

No.	Cat.	Type	States	Non-Color Configuration	Energy	Probability
281	C	1	1	$d_{1-\frac{1}{2}p_{\frac{1}{2}}} u_{1-\frac{1}{2}p_{\frac{1}{2}}} u_{1-\frac{1}{2}d_{\frac{1}{2}}}$	5.202	$1.027 * 10^{-3}$
382	F	1	1	$d_{1-\frac{1}{2}f_{\frac{1}{2}}} u_{1-\frac{1}{2}p_{\frac{1}{2}}} u_{1-\frac{1}{2}d_{\frac{1}{2}}}$	6.828	$2.848 * 10^{-3}$
384	F	1	1	$d_{1-\frac{1}{2}f_{\frac{1}{2}}} u_{1-\frac{1}{2}p_{\frac{1}{2}}} u_{1-\frac{1}{2}d_{\frac{1}{2}}}$	6.828	$1.687 * 10^{-3}$
386	F	1	1	$d_{1-\frac{1}{2}f_{\frac{1}{2}}} u_{1-\frac{1}{2}p_{\frac{1}{2}}} u_{1-\frac{1}{2}d_{\frac{1}{2}}}$	6.828	$1.097 * 10^{-3}$
390	F	1	1	$d_{1-\frac{1}{2}f_{\frac{1}{2}}} u_{1-\frac{1}{2}p_{\frac{1}{2}}} u_{1-\frac{1}{2}d_{\frac{1}{2}}}$	6.828	$1.008 * 10^{-3}$
469	K	3	3	$d_{1-\frac{1}{2}s_{\frac{1}{2}}} u_{1-\frac{1}{2}s_{\frac{1}{2}}} u_{1-\frac{1}{2}s_{\frac{1}{2}}} u_{1-\frac{1}{2}p_{\frac{1}{2}}} \bar{u}_{1-\frac{1}{2}s_{\frac{1}{2}}}$	5.269	$2.116 * 10^{-3}$
482	K	4	2	$d_{1-\frac{1}{2}s_{\frac{1}{2}}} u_{1-\frac{1}{2}p_{\frac{1}{2}}} u_{1-\frac{1}{2}s_{\frac{1}{2}}} u_{1-\frac{1}{2}s_{\frac{1}{2}}} \bar{u}_{1-\frac{1}{2}s_{\frac{1}{2}}}$	5.269	$1.084 * 10^{-3}$
491	K	4	2	$u_{1-\frac{1}{2}s_{\frac{1}{2}}} u_{1-\frac{1}{2}p_{\frac{1}{2}}} d_{1-\frac{1}{2}s_{\frac{1}{2}}} d_{1-\frac{1}{2}s_{\frac{1}{2}}} \bar{d}_{1-\frac{1}{2}s_{\frac{1}{2}}}$	5.245	$2.662 * 10^{-3}$
503	K	4	2	$d_{1-\frac{1}{2}s_{\frac{1}{2}}} d_{1-\frac{1}{2}p_{\frac{1}{2}}} u_{1-\frac{1}{2}s_{\frac{1}{2}}} u_{1-\frac{1}{2}s_{\frac{1}{2}}} \bar{d}_{1-\frac{1}{2}s_{\frac{1}{2}}}$	5.247	$1.088 * 10^{-3}$
506	K	5	1	$d_{1-\frac{1}{2}p_{\frac{1}{2}}} u_{1-\frac{1}{2}s_{\frac{1}{2}}} u_{1-\frac{1}{2}s_{\frac{1}{2}}} u_{1-\frac{1}{2}s_{\frac{1}{2}}} \bar{u}_{1-\frac{1}{2}s_{\frac{1}{2}}}$	5.271	$1.225 * 10^{-3}$

Appendix B

**GROUND STATE CONFIGURATION MIXING FOR
THE DELTA**

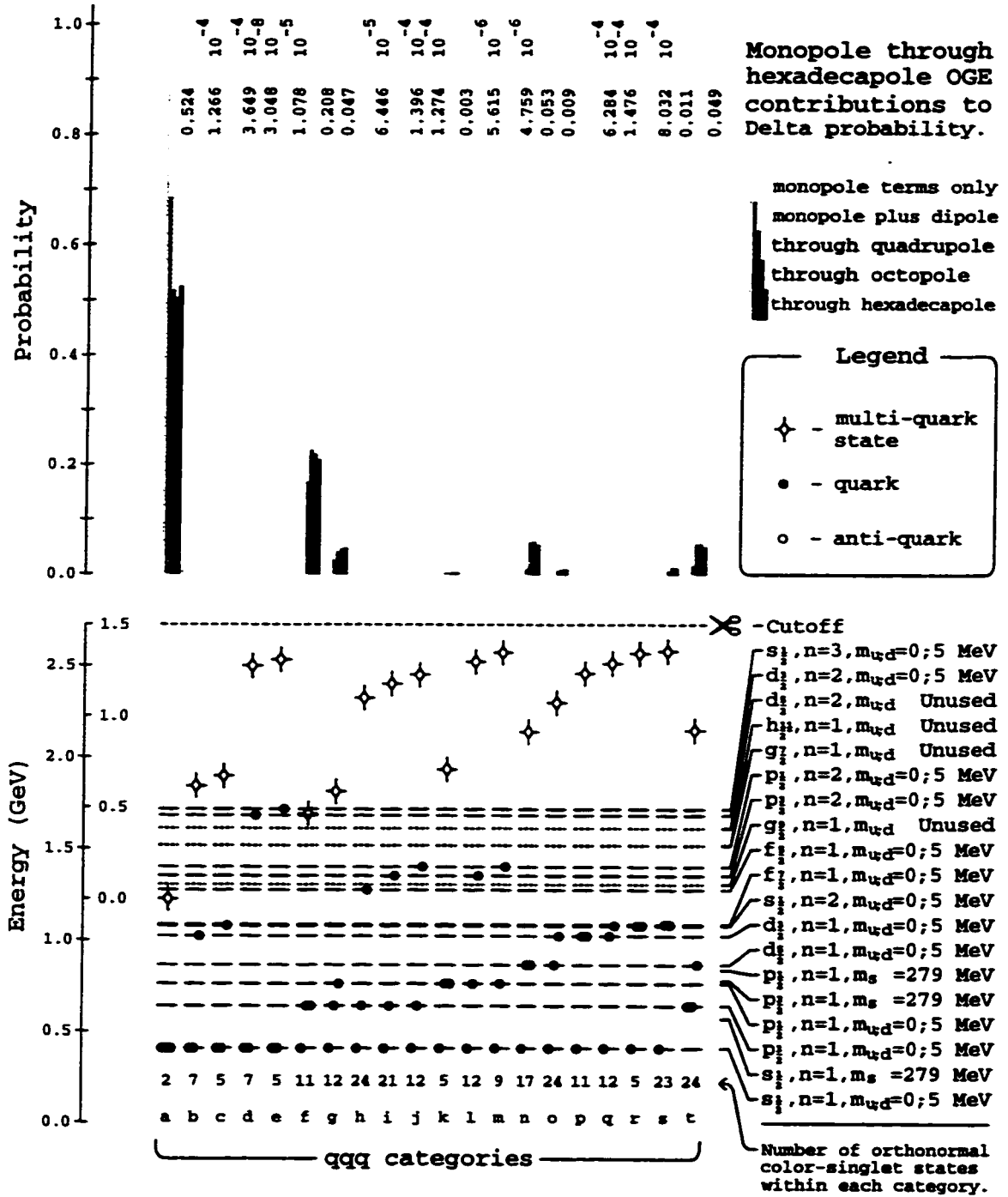


Figure B.1: Composition of Δ^+ ground state for $\alpha_s = 1.3636$ (Part 1 of 2). The basis states are combined into categories, with probabilities for each category shown in the upper part of the figure.

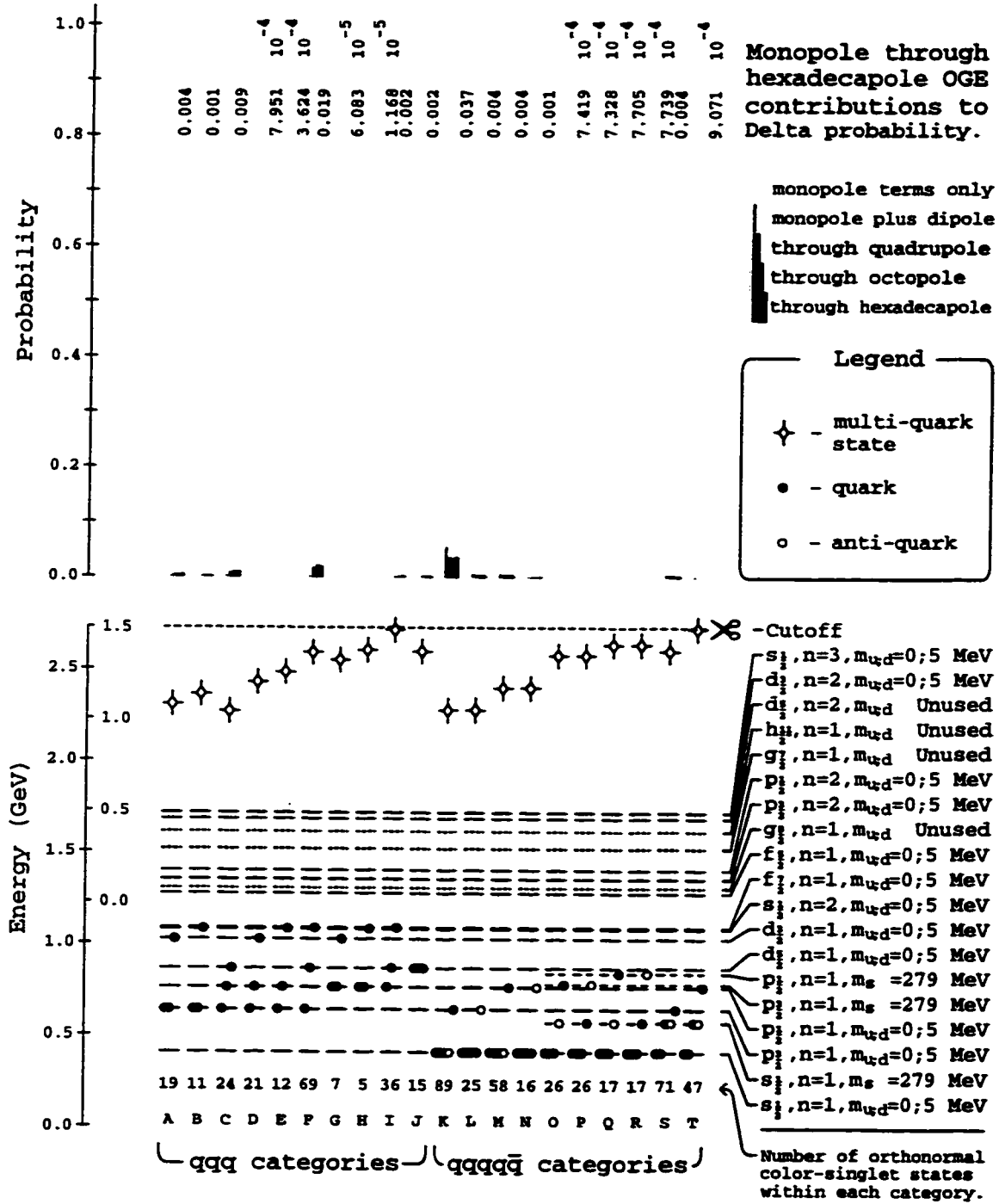


Figure B.2: Composition of Δ^+ ground state for $\alpha_s = 1.3636$ (Part 2 of 2). The basis states are combined into categories, with probabilities for each category shown in the upper part of the figure.

Appendix C

EXAMPLES OF MATRIX ELEMENT CALCULATIONS

We illustrate the procedures used in calculating matrix elements by considering several OGE graphs involving quark transitions between $s_{1/2}$ and $p_{3/2}$ or $p_{1/2}$ states. Our results agree with examples provided by Close and Monaghan[4] who also worked in Coulomb gauge using techniques similar to ours, and with the examples of Wroldsen and Myhrer[5], as corrected by Umino and Myhrer[83], using colored electric and magnetic fields in Lorentz gauge to calculate the OGE matrix elements.

Let V_{mn}^k represent the quark-gluon vertex elements for quark transitions between the energy levels m and n with gluon eigenvalue k . We label quark states $s_{1/2}$, $p_{3/2}$, $p_{1/2}$, \dots as 1, 2, 3, \dots . We will use notation where M, D, Q, O, and S stand for monopole, dipole, quadrupole, octopole, and hexadecapole, and e, m, and c stand for electric, magnetic, and Coulomb Green's function terms.

For purposes of comparison with previous calculations[4, 5, 83], we first calculate $\Delta E'_{ij}$ with energy denominators using the initial energy of quarks i and j as the zero of energy. In this case, it is the sum of energies 1 and 3. Following this, we calculate ΔE^0_{ij} , the OGE element between quarks i and j with spectator quarks, assuming for purposes of this example that the spectator is a $m=0$ quark in the $s_{1/2}$ state. Here the zero of energy in the energy denominators is set at the energy of three $s_{1/2}$ quarks.

We take as a first example the dipole transitions of quark i making transitions from level 1 ($\omega_1 = 2.043$) to 3 ($\omega_3 = 3.812$) and quark j making a transition from level 3 to 1. Orbital angular momentum changes by one unit, so the quark parity changes and the quark gluon vertex elements are of electric dipole type, with electric gluon eigenvalues $k_{e1} = 4.493$, $k_{e2} = 7.735$, \dots . Summing over forward and backward graphs and (the first five) gluon modes, we have

$$\begin{aligned} \Delta E'^D_{ij}[1, 3, 3, 1] &= \frac{\alpha_s}{R} \langle \vec{\sigma}_1 \cdot \vec{\sigma}_2 \rangle \langle \lambda_1 \cdot \lambda_2 \rangle \left[\sum_k \frac{1}{2k_e} (D_{ef1331}^k + D_{eb1331}^k) + D_{c1331} \right] = \\ &\frac{\alpha_s}{R} \langle \vec{\sigma}_1 \cdot \vec{\sigma}_2 \rangle \langle \lambda_1 \cdot \lambda_2 \rangle \left[\sum_{k_d} \frac{1}{2k_e} \left(\frac{V_{13}^k V_{31}^k}{k_e + \omega_3 - \omega_1} + \frac{V_{13}^k V_{31}^k}{k_e - \omega_3 + \omega_1} \right) + \right. \end{aligned}$$

$$\int_{bag} j_{13}^0(x) G_D(x, x') j_{31}^0(x') \Big] \quad (C.1)$$

With $V_{13}^1 = -1.284$, the first five electric modes contribute

$$\begin{aligned} D_{ef1331}^k + D_{eb1331}^k = \\ \frac{\alpha_s}{R} \langle \vec{\sigma}_1 \cdot \vec{\sigma}_2 \rangle \langle \lambda_1 \cdot \lambda_2 \rangle \frac{(-1.284)(1.284)}{(4.493)^2 - (3.812 - 2.043)^2} + (\text{higher modes}) = \\ \frac{\alpha_s}{R} \langle \vec{\sigma}_1 \cdot \vec{\sigma}_2 \rangle \langle \lambda_1 \cdot \lambda_2 \rangle (-0.0967 - 0.00015 - 0.0000045 - 0.0000006 - 0.0000001) \end{aligned} \quad (C.2)$$

The Coulomb greens function is integrated with the quark currents using $r_>$, $r_<$ variables over the bag volume. Its value is

$$D_{c1331} = \frac{\alpha_s}{R} \langle \vec{\sigma}_1 \cdot \vec{\sigma}_2 \rangle \langle \lambda_1 \cdot \lambda_2 \rangle (0.0651). \quad (C.3)$$

Factoring out spin and color factors, these results sum to -0.032 in agreement (up to a phase) with the Coulomb gauge calculation of Close and Monaghan[4]. Working in Lorentz gauge with electric and magnetic fields, Wroldsen and Myhrer calculated dipole electric and dipole magnetic terms of -0.115 and 0.083 times α_s/R and spin and color sums. These sum to -0.032 , which is identical to our results.

In doing our ground state calculations for ΔE_{ij}^0 , all energy denominators are calculated with the energy zero given by the state with three quarks in the $s_{1/2}$ state, in contrast to the calculations above for $\Delta E_{ij}'$, which used an energy zero equal to the sum of the two initial quark energies. Now each energy denominator is the difference of the intermediate state energy including spectators and the $s_{1/2}$ qqq energy zero. With the same diagram as above, assuming that there is single $m = 0$ $s_{1/2}$ spectator,

$$\begin{aligned} \Delta E_{ij}^{0D}[1, 3, 3, 1] = \frac{\alpha_s}{R} \langle \vec{\sigma}_1 \cdot \vec{\sigma}_2 \rangle \langle \lambda_1 \cdot \lambda_2 \rangle \left[\frac{1}{2} (D_{ef1331}^k + D_{eb1331}^k) + D_{c1331} \right] = \\ \frac{\alpha_s}{R} \langle \vec{\sigma}_1 \cdot \vec{\sigma}_2 \rangle \langle \lambda_1 \cdot \lambda_2 \rangle \left[\frac{1}{2} \left(\sum_{k_e} \frac{V_{13}^k V_{31}^k}{k_e + 2\omega_3 - 2\omega_1} + \sum_{k_e} \frac{V_{13}^k V_{31}^k}{k_e} \right) + \right. \\ \left. \int_{bag} j_{13}^0(x) G_D(x, x') j_{31}^0(x') \right] \end{aligned} \quad (C.4)$$

The Coulomb contribution remains as before, so

$$\begin{aligned} \Delta E_{ij}^{0D}[1, 3, 3, 1] = \frac{\alpha_s}{R} \langle \vec{\sigma}_1 \cdot \vec{\sigma}_2 \rangle \langle \lambda_1 \cdot \lambda_2 \rangle * \\ [(-0.0637 - 0.00012 - 0.0000038 - 0.0000005 - 0.0000012) + (0.0651)] = \\ \frac{\alpha_s}{R} \langle \vec{\sigma}_1 \cdot \vec{\sigma}_2 \rangle \langle \lambda_1 \cdot \lambda_2 \rangle (-0.00118). \end{aligned} \quad (C.5)$$

This dipole element turns out to be quite small because of the cancelation between the transverse and Coulomb contributions. As can be seen from this example, the choice of energy zero in the energy denominator can have a significant effect on the matrix element.

Now we examine the matrix elements responsible for excitation of two $p_{1/2}$ states from two initial $s_{1/2}$ states, with a $m = 0$ $s_{1/2}$ spectator. This is of interest because of the small contribution to the nucleon ground state of pairs of excited $p_{1/2}$ states (less than 1%) compared to $p_{3/2}$ states (about 25%). For double $p_{1/2}$ excitations,

$$\begin{aligned} \Delta E_{ij}^{0D}[1, 2, 1, 2] &= \frac{\alpha_s}{R} \langle \vec{\sigma}_1^{[\frac{1}{2}, \frac{3}{2}]} \cdot \vec{\sigma}_2^{[\frac{1}{2}, \frac{3}{2}]} \rangle \langle \lambda_1 \cdot \lambda_2 \rangle \left[\frac{1}{2} (D_{ef1212}^k + D_{eb1212}^k) + D_{c1212} \right] = \\ &\quad \frac{\alpha_s}{R} \langle \vec{\sigma}_1^{[\frac{1}{2}, \frac{3}{2}]} \cdot \vec{\sigma}_2^{[\frac{1}{2}, \frac{3}{2}]} \rangle \langle \lambda_1 \cdot \lambda_2 \rangle * \\ &\quad \left[\frac{1}{2} \left(\sum_{k_e} \frac{(V_{12}^k)^2}{k_e + \omega_2 - \omega_1} + \sum_{k_e} \frac{(V_{12}^k)^2}{k_e + \omega_2 - \omega_1} \right) + \int_{bag} j_{12}^0(x) G_D(x, x') j_{12}^0(x') \right] = \\ &\quad \frac{\alpha_s}{R} \langle \vec{\sigma}_1^{[\frac{1}{2}, \frac{3}{2}]} \cdot \vec{\sigma}_2^{[\frac{1}{2}, \frac{3}{2}]} \rangle \langle \lambda_1 \cdot \lambda_2 \rangle * \\ &\quad [(0.0068 + 0.000042 + 0.0000036 + 0.0000007 + 0.00000020) + (0.4309)] = \\ &\quad \frac{\alpha_s}{R} \langle \vec{\sigma}_1^{[\frac{1}{2}, \frac{3}{2}]} \cdot \vec{\sigma}_2^{[\frac{1}{2}, \frac{3}{2}]} \rangle \langle \lambda_1 \cdot \lambda_2 \rangle (0.4377) \quad .(C.6) \end{aligned}$$

If we ignore the details of the spin sums, we see the matrix element for $s_{1/2}$ to $p_{3/2}$ is about 3.5 times larger than the $s_{1/2}$ to $p_{1/2}$ matrix element. Squares of these elements contribute to first order perturbation theory, so this provides a factor of about 12.5:1 that we should expect. Dipole contributions from diagonalization are in the ratio $\sim 15 : 1$, and we have more $p_{3/2}$ than $p_{1/2}$ states. The $p_{3/2}$ states also have significant quadrupole and octopole contributions, making the overall ratio of $p_{3/2}$ to $p_{1/2}$ probabilities about 32:1.

Appendix D

PERTURBATIVE DIPOLE OVERLAP BETWEEN VALENCE PROTON STATE AND FIVE PARTICLE STATES INVOLVING ONE $P_{1/2}$ EXCITATION SHOWING INTERFERENCE EFFECTS.

Here notation is such that (for example) $Ded13\bar{d}d11$ represents the dipole electric (forward + backward + Coulomb) term where a d quark changes from energy level 1 ($s_{1/2}$) to 3 ($p_{1/2}$) and emits a gluon to form a $d\bar{d}$ pair with both quark and antiquark at energy level 1.

$$\begin{aligned}
 P[qqq \rightarrow qqqq\bar{q}] := & \\
 & \alpha_s^2 (4 * Ded13\bar{d}d11^2 + 4 * Ded13\bar{s}s11^2 + \\
 & 2.88889 * Ded13\bar{u}u11^2 + 6.88889 * Deu13\bar{d}d11^2 + \\
 & 8 * Deu13\bar{s}s11^2 + 13.55556 * Deu13\bar{u}u11^2 - \\
 & 1.33333 * Ded13\bar{d}d11 * Dmd11\bar{d}d13 + \\
 & 4 * Dmd11\bar{d}d13^2 + 3.33333 * Dmd11\bar{d}d31^2 + \\
 & 4 * Dmd11\bar{s}s13^2 + 4 * Dmd11\bar{s}s31^2 - \\
 & 0.88889 * Deu13Uu11 * Dmd11\bar{u}u13 + \\
 & 4 * Dmd11\bar{u}u13^2 + 2.88889 * Dmd11\bar{u}u31^2 - \\
 & 0.88889 * Ded13\bar{d}d11 * Dmu11\bar{d}d13 + \\
 & 5.33333 * Dmd11\bar{d}d13 * Dmu11\bar{d}d13 + \\
 & 6.66667 * Dmu11\bar{d}d13^2 + \\
 & 4.44444 * Dmd11\bar{d}d31 * Dmu11\bar{d}d31 + \\
 & 4.66667 * Dmu11\bar{d}d31^2 + \\
 & 5.33333 * Dmd11\bar{s}s13 * Dmu11\bar{s}s13 + \\
 & 6.66667 * Dmu11\bar{s}s13^2 +
 \end{aligned}$$

$$\begin{aligned}
& 5.33333 * Dmd11\bar{s}s31 * Dmu11\bar{s}s31 + \\
& \quad 6.66667 * Dmu11\bar{s}s31^2 - \\
& 2.22222 * Deu13\bar{u}u11 * Dmu11\bar{u}u13 + \\
& 5.33333 * Dmd11\bar{u}u13 * Dmu11\bar{u}u13 + \\
& \quad 6.66667 * Dmu11\bar{u}u13^2 + \\
& 8 * Dmd11\bar{u}u31 * Dmu11\bar{u}u31 + \\
& \quad 11.33333 * Dmu11\bar{u}u31^2) \tag{D.1}
\end{aligned}$$

Appendix E

CONFIGURATION MIXING FOR DIFFERENT PARAMETER SETS AND SEVERAL SELF-ENERGY PRESCRIPTIONS

Table E.1: Configuration mixing energy for ground and first excited state energies for baryons with several choices for the MIT parameters, using the minimal MIT self-energy prescription. We determine the dependence of particle energies on the bag radius, then determine the B and Casimir parameters required for the neutron to be in stable equilibrium. This is repeated for both bag radii. The bag radius is then adjusted for each particle to achieve a consistent value for B and the particle masses are determined as shown in table 5.1.

Particle	$R = 0.987$ $m_s = 279 \text{ MeV}$ $m_u = 0 \text{ MeV}$ $m_d = 5 \text{ MeV}$ $\alpha_s = 1.3636$	$R = 0.888$ $m_s = 279 \text{ MeV}$ $m_u = 0 \text{ MeV}$ $m_d = 5 \text{ MeV}$ $\alpha_s = 1.3636$	$R = 0.987$ $m_s = 300 \text{ MeV}$ $m_u = 0 \text{ MeV}$ $m_d = 5 \text{ MeV}$ $\alpha_s = 1.3636$	$R = 0.987$ $m_s = 279 \text{ MeV}$ $m_u = 0 \text{ MeV}$ $m_d = 5 \text{ MeV}$ $\alpha_s = 1.2433$	$R = 0.888$ $m_s = 279 \text{ MeV}$ $m_u = 0 \text{ MeV}$ $m_d = 5 \text{ MeV}$ $\alpha_s = 1.2433$
	(MeV)	(MeV)	(MeV)	(MeV)	(MeV)
n	-580.596	-646.525	-580.412	-496.767	-553.408
p	-582.640	-649.418	-583.302	-498.807	-556.287
Σ^-	-359.718	-426.971	-342.214	-279.152	-337.222
Σ^+	-365.046	-437.568	-352.754	-284.431	-347.930
Ξ^-	-196.759	-265.551	-166.891	-115.729	-175.514
Ξ^0	-200.224	-267.702	-168.970	-119.237	-177.474
Δ^0	-272.219	-303.790	-271.877	-219.317	-245.076
Δ^+	-273.416	-305.919	-274.004	-220.505	-247.224
Σ^{*-}	-129.947	-164.029	-117.448	-75.306	-103.634
Σ^{*+}	-133.864	-170.913	-124.368	-79.259	-110.740
Ξ^{*-}	9.766	-26.921	34.301	66.419	35.364
Ξ^{*0}	7.325	-28.483	32.747	63.911	33.851

Table E.2: Configuration mixing energy for ground and first excited state energies for baryons with several choices for the MIT parameters, with the self-energy built from all vertices contributing to OGE graphs below the cutoff. We determine the dependence of particle energies on the bag radius, then determine the B and Casimir parameters required for the neutron to be in stable equilibrium. This is repeated for both bag radii. The bag radius is then adjusted for each particle to achieve a consistent value for B, and the particle masses are determined as shown in table 5.2.

Particle	$R = 0.987$ $m_s = 279 \text{ MeV}$ $m_u = 0 \text{ MeV}$ $m_d = 5 \text{ MeV}$ $\alpha_s = 1.3323$	$R = 0.888$ $m_s = 279 \text{ MeV}$ $m_u = 0 \text{ MeV}$ $m_d = 5 \text{ MeV}$ $\alpha_s = 1.3323$	$R = 0.987$ $m_s = 300 \text{ MeV}$ $m_u = 0 \text{ MeV}$ $m_d = 5 \text{ MeV}$ $\alpha_s = 1.3323$	$R = 0.987$ $m_s = 279 \text{ MeV}$ $m_u = 0 \text{ MeV}$ $m_d = 5 \text{ MeV}$ $\alpha_s = 1.215$	$R = 0.888$ $m_s = 279 \text{ MeV}$ $m_u = 0 \text{ MeV}$ $m_d = 5 \text{ MeV}$ $\alpha_s = 1.215$
	(MeV)	(MeV)	(MeV)	(MeV)	(MeV)
n	-435.648	-485.581	-435.667	-362.616	-404.441
p	-439.307	-489.491	-439.567	-366.161	-408.271
Σ^-	-181.320	-232.490	-162.109	-112.049	-155.255
Σ^+	-188.894	-243.682	-172.936	-119.482	-166.578
Ξ^-	15.469	-35.381	49.268	83.280	40.220
Ξ^0	11.288	-38.373	46.329	79.084	37.464
Δ^0	-128.017	-143.550	-127.916	-84.904	-95.708
Δ^+	-130.923	-146.769	-131.114	-87.674	-98.853
Σ^{*-}	54.914	37.018	69.587	98.791	85.489
Σ^{*+}	48.601	29.220	62.083	92.526	77.379
Ξ^{*-}	227.680	209.133	256.282	272.185	258.138
Ξ^{*0}	224.305	206.788	253.948	268.770	255.903

VITA

William Donald Hazelton graduated from Walla Walla College in June, 1977 with Bachelor of Science degrees in Physics and Mathematics. He worked with his parents, Lloyd and Carolyn Hazelton, operating a machine shop in Walla Walla, Washington. In August, 1997, he graduated from the University of Washington with a Doctor of Philosophy Degree in Physics.